

Exocometary physics: material release and tails

Théo Vrignaud¹, Dennis Bodewits^{2†}, Jake Hanlon^{*3†},
Matthew M. Knight^{4†}, Tim D. Pearce^{5†}, Daryl Zeligman^{6,7†},
Dimitri Veras^{8,9,10†}, Geraint H. Jones^{3,11†}

¹Institut d'Astrophysique de Paris, CNRS, UMR 7095, Sorbonne
Université, 98bis boulevard Arago, 75014 Paris, France.

²Department of Physics, Auburn University, Edmund C. Leach Science
Center, Auburn, 36849, AL, USA.

³Mullard Space Science Laboratory, University College London,
Holmbury St. Mary, Dorking, RH5 6NT, Surrey, United Kingdom*.

⁴Physics Department, United States Naval Academy, 572C Holloway Rd,
Annapolis, 21402, MD, USA.

⁵Department of Physics, University of Warwick, Coventry, B5 4TF, UK.

⁶Department of Physics and Astronomy, Michigan State University, ,
East Lansing, 48824, MI, USA.

⁷NSF Astronomy and Astrophysics Postdoctoral Fellow.

⁸Centre for Exoplanets and Habitability, University of Warwick,
Coventry, B5 4TF, UK.

⁹Centre for Space Domain Awareness, University of Warwick, Coventry,
B5 4TF, UK.

¹⁰Department of Physics, University of Warwick, Coventry, B5 4TF, UK.

¹¹European Space Technology Centre (ESTEC), European Space Agency,
Keplerlaan 1, 2200 AG Noordwijk, Netherlands.

*Corresponding author.

Contributing authors: vrignaud@iap.fr; dennis@auburn.edu;
jake.hanlon.23@ucl.ac.uk *; knight@usna.edu; tim.pearce@warwick.ac.uk;
dzs@msu.edu; dimitri.veras@aya.yale.edu; geraint.jones@esa.int;

†These authors contributed equally to this work.

Abstract

Despite decades of observations, the physical processes governing mass loss from small bodies beyond our Solar System remain poorly constrained. These “exocomets” are often treated as analogs of Solar System comet, yet the stellar environments they inhabit spans a wide range in terms of luminosity, stellar wind intensity, and evolutionary stage, leading to potentially very diverse physical behaviors. Within our Solar System, small bodies lose gas and dust through a range of mechanisms, including sublimation, desorption, impacts, and/or sputtering. Once released, the composition and dynamics of the ejecta are then altered by additional processes, such as dust sublimation, ionization, and radiation pressure. In extrasolar systems, these mechanisms unfold under vastly different radiative and plasma conditions, leading to a rich diversity of mass-loss pathways and observable signatures.

This work reviews our understanding of the mechanisms driving mass loss from small bodies and the subsequent evolution of ejecta in diverse stellar environments. We compare the physical and chemical mechanisms that drive gas and dust production, such as sublimation, thermal and photon desorption, and investigate how they scale with stellar luminosity, temperature, and activity. We then examine the processes that modify the composition of the ejecta (e.g., dust sublimation, dissociation, or ionisation) and its dynamics (e.g., radiation pressure or stellar winds). To illustrate how these processes vary across different stellar environments, we use four well-studied planetary systems as case studies: the Sun, β Pictoris, AU Microscopii, and WD 1145+017. By exploring how cometary tails behave under such diverse conditions, this work provides a physical framework for interpreting exocometary activity and sheds light on why A-type stars, such as the famous β -Pictoris, are over-represented in the population of exocomet-hosting stars.

1 Introduction

Small bodies in the Solar System, such as comets and asteroids, are relics from the era of planet formation. When their orbits are altered, they can redistribute water, noble gases, and organic materials across a wide range of heliocentric distances (Rubin et al., 2019). In our Solar System, these objects can be studied directly through telescopic observations and spacecraft missions, providing detailed insights into their composition and evolution. Beyond our Solar System, however, small bodies are typically studied indirectly. Observations around other stars often capture the collective properties of multiple bodies rather than the unique characteristics of single objects (Strøm et al., 2020). When small bodies release gas and dust into space, whether by sublimation, thermal desorption, or other processes, this “activity” offers a window into their chemical composition. Yet even within the Solar System, sublimation represents only one pathway for mass loss. Thermal and photon desorption, plasma sputtering, micrometeoroid impacts, and electrostatic lofting also shape the evolution of airless bodies and asteroids. Linking these ejecta back to the physical properties of the parent body requires an understanding of storage and release mechanisms, the physical

and chemical processes that alter these materials, and an accurate interpretation of their excitation to determine relative abundances (e.g., the recent review by [Bodewits et al., 2024](#)).

Solar System small bodies experience a wide range of physical environments that shape their behavior. For example, many comets sublimate as they approach the Sun, forming characteristic gas and dust tails. Some objects, like the near-Sun asteroid (3200) Phaethon, reach surface temperatures exceeding 1000 K (see the review by [Jones et al., 2018](#)), leading to the thermal desorption of refractory elements such as alkali metals ([Zhang et al., 2023a](#)). In contrast, more distant objects remain too cold for significant sublimation; for example, water and CO₂, typically sublimate only within 2.5 au and 13 au of the Sun, respectively (e.g., [Meech and Svoren, 2004](#)). Around other stars, small bodies may encounter even more extreme conditions. For example, exocomets around β Pictoris (β Pic) pass close to a hot A-type star, exposing them to intense radiation and high temperatures, while potential exocomets orbiting AU Microscopii (hereafter AU Mic), a highly variable M-dwarf, endure intense stellar winds. These diverse environments add complexity to exocometary behavior and evolution.

This work reviews the physical processes governing mass loss and tail formation for small bodies and explores how these processes vary across different stellar environments. We compare Solar System comets with exocomets, examining the mechanisms driving gas and dust ejection, their dependence on surface composition, and the physical factors altering the ejected material. We also discuss observational constraints, including differences between absorption and emission features, and how these processes serve as diagnostics of local environments. To illustrate these key concepts, four case-study stars are used throughout this work: the Sun, β Pic, AU Mic, and WD 1145+017, each hosting a unique planetary system (see the stellar properties in [Table 1](#)). These stars provide a framework for assessing whether Solar System comets can serve as valid analogs for exocomets.

Star	Distance (pc)	Mass [M_{\odot}]	Radius [R_{\odot}]	T_{eff} [K]	Luminosity [L_{\odot}]	Age [Gyr]	Planets
AU Mic	9.7	0.6	0.82	3665	0.10	0.023	b, c, d, e?
Sun		1.00	1.00	5770	1.00	4.57	
Beta Pic	19.3	1.75	1.51	8052	8.7	0.020	b, c
WD 1145+017	142	0.63	0.012	15020	0.02 ^a	0.22	b ^b

Table 1: Properties of the four stars chosen as case-studies.

[a] The progenitor of WD 1145+017 was an A-type star, which lived 550 ± 100 Myr before becoming a white dwarf ([Izquierdo et al., 2021](#)).

[b] As of 2025, the dust activity around WD1145+017 has completely ceased, suggesting that planet b has likely been destroyed ([Aungwerojwit et al., 2024a](#)).

References:

AU Mic: [Donati et al. \(2023\)](#);

Sun: [Prša et al. \(2016\)](#); [Bonanno et al. \(2002\)](#);

β Pic: [Crifo et al. \(1997\)](#); [Miret-Roig et al. \(2020\)](#); [Gray et al. \(2006\)](#);

WD1145+017: [Gaia Collaboration et al. \(2018\)](#); [Izquierdo et al. \(2021\)](#); [Farihi et al. \(2017\)](#);

Planet	Semi-major axis	Period	Mass	Radius	T_{eq}
AU Mic b	0.065 au	8.5 d	$10.2^{+3.9}_{-2.7} M_{\oplus}$	$3.96 \pm 0.15 R_{\oplus}$	600 K
AU Mic d ^a	0.085 au	12.7 d	$1.0 \pm 0.5 M_{\oplus}$	$1.02 \pm 0.14 R_{\oplus}$	520 K
AU Mic c	0.11 au	18.9 d	$14.2^{+4.8}_{-3.5} M_{\oplus}$	$2.52 \pm 0.25 R_{\oplus}$	450 K
AU Mic e ^b	0.16 au	33.4 d	$35.2^{+6.7}_{-5.4} M_{\oplus}$		380 K
β Pic c	2.7 au	3.3 yr	$8.2 \pm 0.8 M_J$	$1.1 \pm 0.1 R_J$	1300 K
β Pic b	10.0 au	23.6 yr	$11.7 \pm 2.3 M_J$	$1.5 \pm 0.2 R_J$	1600 K
WD 1145+017 b	0.0054 au	4.5 h	$\sim 1.6 \times 10^{-5} M_{\oplus}$	$\sim 0.03 R_{\oplus}$	1100 K

Table 2: Known planets in the WD1145+017, AU Mic and β Pic systems.

[a] AU Mic d was detected through TTV; the parameters provided here correspond to the favored solution in Wittrock et al. (2023).

[b] AU Mic e has not been confirmed.

References:

AU Mic: Donati et al. (2023); Wittrock et al. (2023);

β Pic: Nowak et al. (2020); Feng et al. (2022); Bonnefoy et al. (2014);

WD1145+017: Vanderburg et al. (2015); Rappaport et al. (2016);

To model the influence of the Sun, β Pic, AU Mic and WD 1145+017 on nearby small bodies, we adopt the following spectral energy distributions (also shown in Fig. 1):

- **AU Mic:** We use the spectrum from Feinstein et al. (2022), reconstructed by combining observations and synthetic models. This spectrum corresponds to a quiescent stellar activity.
- **The Sun:** We use the Solar Spectral Irradiance Reference Spectra for Whole Heliosphere Interval (Woods et al., 2009), measured in March 2008 during a period of moderately low solar activity. This spectrum spans the wavelength range from 1 to 24 000 Å.
- **β Pic:** For the photosphere, we use a synthetic spectrum from the PHOENIX library (Husser et al., 2013), with $T_{\text{eff}} = 8000$ K, $\log(g) = 4.5$, $[\text{Fe}/\text{H}] = 0$, and $[\alpha/\text{H}] = 0$. This spectrum was convolved with the rotational velocity of the star, 130 km s^{-1} . At wavelength shorter than 1300 Å, we adopt the synthetic spectrum of Wu et al. (2025), which includes chromospheric and coronal emission. This spectrum, calculated with CLOUDY (Ferland et al., 2013), This model, computed with CLOUDY (Ferland et al., 2013), is calibrated to reproduce the observed flux in the C III and O VI emission lines.
- **WD1145+017:** A spectrum provided by Le Bourdais et al. (2024) is adopted, incorporating absorption lines from metallic species in the white dwarf’s polluted photosphere.

These spectral models will help evaluate the environmental effects on cometary activity across different stellar systems, guiding our understanding of how small bodies evolve under diverse radiative conditions, how these environments shape detectable spectral features, and how those features can be linked to the physical and chemical properties of the small bodies.

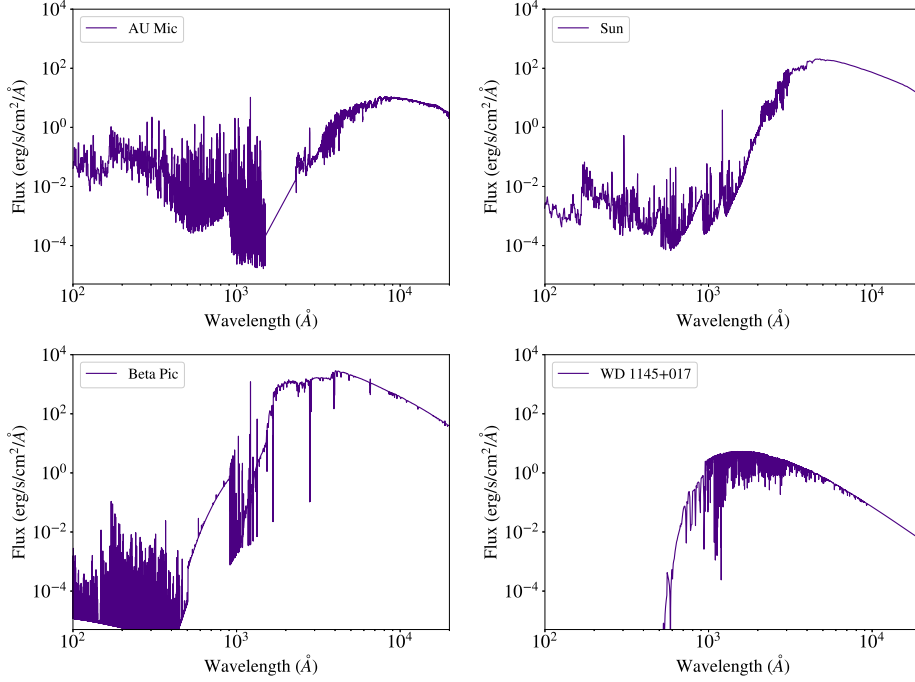


Fig. 1: Spectral energy distribution used for our case study stars. The fluxes are all provided for distances of 1 au.

2 Mass loss processes

2.1 Diversity in the Solar System

Activity among Solar-System bodies spans a remarkable range of environments and mechanisms, from volatile sublimation in icy comets to impact vaporization and sputtering on airless surfaces (see Fig. 2). Table 3 summarizes the principal drivers of mass loss and the conditions under which they dominate. The Sun loses about $3 \times 10^9 \text{ kg s}^{-1}$ through radiation and the solar wind (Pitjeva et al., 2021). Atoms and molecules in Earth’s exosphere can reach escape velocity and are lost to space (e.g., Howe et al., 2020). Owing to its lower gravity, Mars lost most of its water over time (e.g., Pollack et al., 1987) and continues to release hydrogen produced by the photodissociation of H_2O (Mayyasi et al., 2023). Mercury, the Moon, and Phaethon exhibit ongoing mass loss, as evidenced by the detection of sodium and potassium in their exospheres, likely driven by photon-induced desorption or sputtering (Wurz et al., 2022, see also Table 3). Comets, volatile-rich remnants from the era of planet formation, release gases as their ices sublimate when heated by the Sun, dragging refractory particles along to form characteristic tails. Asteroids lose mass through electrostatic lofting, as well as in collisions that eject fragments or, in extreme cases, disrupt the entire body (see Section 2.4).



Fig. 2: Example of mass loss in Solar System objects.

Upper left: Sodium tail of Mercury, observed through a narrowband filter centered on the Na D lines around 589 nm. (Credit: Andrea Alessandrini). Mercury’s sodium tail is produced from a variety of processes, including photon and thermal desorption, meteoroid impact, and ion sputtering.

Upper right: HST/WFC3 captured multiple tails emerging from the asteroid Dimorphos after impact with the DART spacecraft (Credits: NASA, ESA, STScI, Jian-Yang Li (PSI); Joseph DePasquale).

Lower left: Gas and dust tails of C/2020 F3 (NEOWISE), driven by the sublimation of volatiles (Credits: Kiss Péter, 2020).

Lower right: Sodium tail of (3200) Phaethon (Zhang et al., 2023b), produced from the thermal desorption of Na atoms at the surface of the asteroid.

The mechanisms driving mass loss in small bodies can generally be categorized into macroscopic processes – such as collisions, tidal breakups, rotational instability, or thermal fracturing – which shape the long-term evolution of minor bodies (Jewitt et al., 2014), and microscopic effects – including sublimation, plasma sputtering, micrometeoroid impacts, and photon- or thermally-driven desorption – which act on shorter timescales but are equally important for the gradual alteration of surfaces

(e.g., see the review by [Wurz et al., 2022](#)). In the inner Solar System, volatile sublimation is by far the most efficient mechanism for material release ([Rickman, 2010](#); [Cochran et al., 2015](#); [Bockelée-Morvan and Biver, 2017](#), see also Table 3). However, whether this remains true for small bodies orbiting stars of different spectral types or at different evolutionary stages is still uncertain. Since the efficiency of each mass-loss process depends on the local radiation field and plasma environment, the dominant mechanism ultimately varies with both orbital distance and stellar type.

In the Solar System, mass loss processes can often be inferred directly from observational evidence. For example, the recurring activity of main-belt comets implied sublimation driven activity (e.g., [Hsieh and Jewitt, 2006](#)) well before it was directly detected ([Kelley et al., 2023](#)). In contrast, non-recurrent activity coupled with unusual morphology identified a natural impact event on asteroid (596) Scheila (cf. [Bodewits et al., 2011](#)). For small bodies beyond the Solar System, however, disentangling these mechanisms is much more challenging. The following subsections therefore review the various processes that may trigger mass loss from minor bodies. This broad perspective is essential for identifying better Solar System analogs for exocomets and understanding how their activity is influenced by both internal properties and external environments. The various processes driving material release for solar system objects are summarized in Fig. 6.

Object	Release mechanism(s)	Material	Rate (kg/s)	References
Phaethon	Thermal desorption	Na	0.02	1
Mercury	Thermal desorption, photon desorption, sputtering, micrometeroid impact	H, He, K, Al, Fe, Na, Ca, Mg ...	0.01	2
Moon	photon desorption, sputtering, micrometeroid impact, electrostatic lofting	H ₂ O, Na ...	0.001	3
Asteroids	Impact, rotational spin up, electrostatic lofting	Dust	Variable	4
Ganymede	Thermal desorption, sublimation, sputtering micrometeroid impact	OH, H ₂ O, H ₂ , O O ₂ , O ₃	30	5
Comets ^a	Sublimation	H ₂ O, CO ₂ , CO, Na, Fe, Ni, dust ...	Up to 10 ⁶ (Hale-Bopp)	6

Table 3: Examples of mass loss processes in a variety of Solar System objects. References: [1] [Zhang et al. \(2023b\)](#), [2] [McClintock et al. \(2018\)](#), [3] [Stern \(1999\)](#), [4] [Jewitt \(2012\)](#), [5] [Galli et al. \(2022\)](#), [6] [Biver et al. \(2022\)](#).

[a] So far, over 100 species have been observed in comets. See [Biver et al. \(2022\)](#) for a complete review.

2.2 Processes linked to the sublimation of volatiles

2.2.1 Volatile release

Sublimation is the primary mechanism driving activity in most classical comets. As comets approach the sun, rising temperatures trigger the sublimation of various ices. The primary cometary volatiles that contribute to the outgassing are known to be H₂O, followed by CO₂ and CO (the relative abundances of CO and CO₂ can vary by more than an order of magnitude, [Harrington Pinto et al., 2022](#)). The volatility of an ice is set predominantly by the latent heat of sublimation. The latent heats for sublimation of H₂O, CO₂, and CO are around 51, 26, and 8 kJ mol⁻¹ respectively (see for instance the NIST database, [Kramida et al., 2023](#)). Therefore, these three primary drivers of activity represent high, medium, and low volatility species. In the Solar System, the sublimation fronts of these materials are located at ~ 2.5 au (H₂O), 13 au (CO₂), and 120 au (CO; see Table 1 of [Meech and Svoren, 2004](#)). However, in other planetary systems, these ice lines shift depending on the luminosity of the host star. [Fig. 3](#) and [4](#) show the location of sublimation fronts for various volatiles around different stars, including main sequence stars ([Fig. 3](#)) and white dwarfs ([Fig. 4](#)). The position of an ice line varies significantly with stellar type. Around M and K dwarfs, the sublimation line of H₂O is located within 1 au, whereas it shifts to ~ 8 au around an A5V star (such as β Pic), and 25 au around an even hotter B8V star. These differences have profound implications for comet activity, as comets orbiting hotter stars would begin outgassing volatiles at much greater distances. In extreme cases, such as of OB stars, the extreme sublimation rate of volatiles could even lead to the complete disruption of the cometary nucleus before it can reach periastron (see the discussion, [Sect. 5.5](#)).

The velocity of the gas outflow is typically given by the ambient sound speed, $c_s = \sqrt{\gamma k_B T / (\mu m_u)}$ ([Probstein, 1969](#)), where T is the temperature of the outgassing material, γ is the adiabatic index of the outflow, μm_u is the mass of the species, and k_B is the Boltzmann constant. In the Solar System, typical temperatures in the inner comae are in the range $10^1 - 10^3$ K ([Rodgers et al., 2004](#)), and generally rise with increasing distance to the nucleus.

Different from most other volatilization mechanisms, sublimation is not confined to the surface; it can also occur in the interior, depending on the thermal conductivity of the nucleus and the duration or intensity of heat exposure ([Huebner et al., 2006](#)). Gases released from the deeper layers of the nucleus may migrate toward the surface and, depending on the thermal environment, refreeze in subsurface layers when the comet moves away from the Sun ([Parhi and Prrialnik, 2025](#); [Luspay-Kuti et al., 2022](#); [Filacchione et al., 2016](#)). This internal sublimation and redeposition process highlights the complexity of volatile storage and release in comets. Consequently, the chemical composition of gases in the coma may not directly reflect the original abundances of ices present in the nucleus (see [Brasser and Wang, 2015](#); [Seligman et al., 2022](#)).

In white dwarf planetary systems ([Fig. 4](#)), volatile-rich bodies deliver material to the stellar photosphere, where their presence is detected through atmospheric contamination ([Farihi et al., 2013](#); [Raddi et al., 2015](#); [Gentile Fusillo et al., 2017](#); [Xu et al., 2017](#); [Hoskin et al., 2020](#)). However, unlike in the Solar System, these deposited

volatiles are observed as individual elements rather than molecules, because the bonds holding the latter together are broken apart by the immense gravity of the white dwarf. Hence, the original composition of accreted material has to be reconstructed from the elemental composition of the deposited metals, which mix with the native photospheric elements (a combination of hydrogen and helium). For instance, the ice fraction of the comets can be inferred from the excess oxygen content (Farihi et al., 2013), which is likely produced from the sublimation of H₂O, CO, and CO₂ (the most common oxygen-bearing molecules, Fig. 4). In the case of a prominent nitrogen signature (Xu et al., 2017), the key molecules sublimated are likely HCN and NH₃.

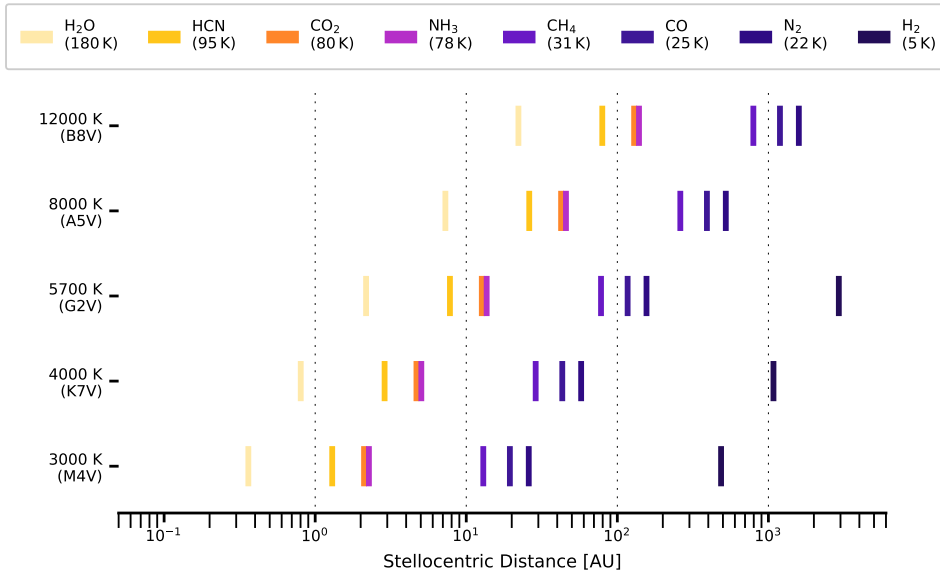


Fig. 3: Location of the sublimation fronts of a variety of volatiles for 5 stars, spanning a wide range of effective temperatures. The values are from Table 1 in Meech and Svoren (2004), and scaled to each star assuming the sublimation distance of each molecule scales with $L_*^{0.5} \propto T_{\text{eff}}^2 R_*$, where L_* , T_{eff} and R_* are the stellar luminosity, effective temperature and radius, respectively.

2.2.2 Dust release

In many cases, detecting dust in a coma or tail is a far easier way to identify cometary activity than directly observing volatile escape. The sublimation of volatiles (see Section 2.2.1) is the primary mechanism driving dust ejection from cometary nuclei. The rate and onset distance of dust production vary depending on the comet’s composition, thermal properties, and active surface fraction. Generally, the closer a comet is to the Sun, the greater its dust production, as increased insolation leads to the sublimation of a larger range of volatile species. Empirical correlations exist between water

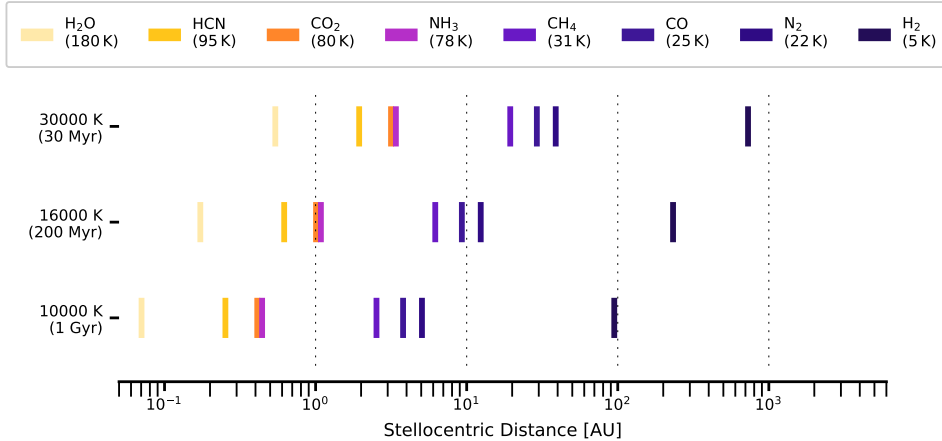


Fig. 4: Same as Fig. 3 but for three white dwarfs with different ages (known as “cooling ages” in the white dwarf community). Again, values were derived from Meech and Svoren (2004), scaling the sublimation distance with $L_{\star}^{0.5}$. The age-luminosity relationship of white dwarfs was taken from Veras et al. (2022) (Eq. 9). The second row ($T_{\text{eff}} = 16\,000$ K) corresponds to WD 1145+017.

production rates and a comet’s visible brightness, as dust reflects sunlight (Jorda et al., 2008).

Robotic surveys are enabling comet discoveries at increasingly large distances from the Sun discoveries, and pre-discovery observations in their archival data allow us to study the activity evolutions even farther out (Meech et al., 2017). For example, C/2017 K2 (Pan-STARRS) was detected with sustained activity at 23.75 au pre-perihelion (Hui et al., 2018), well beyond the expected limit for CO₂ sublimation, providing strong evidence for CO-driven activity (Meech et al., 2017). The large discovery distances of C/2017 K2 and a handful of other long-period comets (e.g. C/2014 UN271, Farnham et al. (2021); C/2019 E3 Hui et al. (2024)) suggest that CO sublimation may play a more significant role in cometary activity at large distances than previously assumed. JWST observations of long period comet C/2024 E1 at 7 au pre-perihelion revealed that its activity was driven by CO₂, and detected no emission from H₂O or CO (Snodgrass et al., 2025). The exact mechanisms governing cometary activity beyond 10 au remain uncertain, and future observations of distant comets and Centaurs will be essential to further constrain these processes (e.g., Faggi et al., 2024; Pinto et al., 2023).

The Rosetta mission to comet 67P/Churyumov–Gerasimenko provided an unprecedented view of cometary volatile release, revealing complex associations between different gases and shedding light on the mechanisms governing cometary activity. Unlike previous flyby missions, Rosetta remained in close proximity to 67P for over two years, which made possible a temporally resolved chemical analysis of the comet’s coma (Combi et al., 2020). The mission confirmed that H₂O and CO₂ outgassing originate from distinct regions of the nucleus, supporting the idea that

minor species are embedded in separate ice matrices within the nucleus (Luspay-Kuti et al., 2015). Seasonal variations played a significant role in altering volatile production rates, with different molecules correlating with H₂O or CO₂ depending on the comet’s orbital position (see Section 2.3.1). These findings were complemented by ground-based observations, which, while unable to directly detect CO₂ due to atmospheric absorption, used ethane (C₂H₆) as a proxy for CO₂ sublimation (Saki et al., 2024).

Since cometary nuclei vary in shape, activity, and rotation state, a range of coma features such as fans, shells, and jets can form (e.g., Farnham, 2009). Modeling dust grain dynamics in a cometary coma is particularly challenging, as it requires accounting for a wide range of gas-dust interactions and particle collisions (e.g., Combi, 2002; Tenishev et al., 2011). Once dust is released from the nucleus, the motion of the smallest dust particles is initially governed by drag forces from sublimated volatiles, whereas larger grains are mostly affected by radiation pressure. Once in the coma, dust-dust collisions can alter the properties of the ejected grains. Continuing with 67P as a Solar System example, modeling by Planes et al. (2024) found that grain erosion, fragmentation, and grain density (physical density rather than number density) increases with the number of collisions, whilst larger grain speeds (150 m s⁻¹) prevent the coagulation of grains. Consequently, collisions between dust grains in the coma can determine the properties of dust grains later detected in the tail.

As demonstrated by 67P, dust production is a highly dynamic process, influenced by a combination of sporadic events on the nucleus surface, grain-grain interactions in the coma, and varying external forces. As a result, modeling the dust production rate of an exocomet may be challenging, and simplifications have to be made. Lecavelier Des Etangs (1999) proposed the production of dust is dependent on the luminosity L_* of the host star and the stellocentric distance r of an exocomet, such that:

$$P(r) = P_0 \left(\frac{r_0}{r}\right)^2 \left(\frac{L_*}{L_\odot}\right) \quad (1)$$

where P_0 is the dust production rate at $r_0 = 1$ au (which depends on the comet size and composition), and L_\odot the solar luminosity. The dependence on luminosity implies comet-like objects orbiting smaller and less luminous stars such as the M-dwarf AU Microscopii could struggle to form well defined comae and dust tails.

This approach was implemented by (Bodman and Quillen, 2016), which analyzed photometric variations in the KIC 8462852 light curve. The study concluded a family of comets could explain the unusual dips in flux. This approach also assumes dust production ceases when an exocomet is beyond a distance $r_{\text{crit}} = 3\sqrt{L_*/L_\odot}$. The ability of a minor body to eject dust is essential to produce asymmetric photometric variations that are identifiable as exocomets. Since dust production varies with stellar luminosity, our ability to photometrically detect exocomets could be confined to stars with suitable luminosities. This is discussed later in Sect. 5.

Universally modeling the size distribution of ejected cometary dust is also a difficult task. Influential work developed by Lecavelier Des Etangs (1999) modeled asymmetric

photometric variations by assuming a size distribution which followed:

$$\frac{dn}{ds} = \frac{(1 - s_0/s)^m}{s^n}, \quad (2)$$

$$m = \frac{n(s_p - s_0)}{s_0}, \quad (3)$$

where s is the radius of a dust grain and n its number density. This description is based on observations of cometary grains in the solar system (Hanner, 1983). The values of s_0 (minimum grain size) and s_p (peak size distribution) are found to vary in time, with dust distribution peaking at smaller sizes for smaller heliocentric distances (Newburn and Spinrad, 1985). For comet 67/P, the value of α was also found to increase sharply after perihelion Fulle et al. (2004). These temporal variations are not fully understood; they may result from changes in the nucleus region exposed to stellar irradiation (Fulle et al., 2004), or to the fragmentation of dust grains in the inner coma at short heliocentric distances (Gronkowski, 2009).

Models considered by Lecavelier Des Etangs (1999) are summarized in Table 4. In a slightly different way, Bodman and Quillen (2016) decided to adopt a power law distribution coupled with an exponential cut-off for small particles outlined by Fink and Rubin (2012). In this case, the size distribution took the form

$$\frac{dn}{ds} \propto \left(\frac{s_p \alpha}{s}\right)^\alpha \exp\left(-\frac{s_p \alpha}{s}\right) \quad (4)$$

where $s_p = 0.50 \mu\text{m}$ and $\alpha = 4.0$. The two approaches produce similar distributions (see Fig. 5), with the main difference being Bodman and Quillen (2016) using fewer parameters than Lecavelier Des Etangs (1999). Since the absorption cross-section of a dust grain is dependent on its size (see Sect. 3.1), considering realistic grain size distributions is crucial to the interpretation of asymmetric transit events in the light curve of nearby stars, and link the observed events to the properties, e.g. dust production rate, of the transiting exocomets.

Periastron [au]	S_p [μm]	S_0 [μm]	n
q < 0.50	0.20	0.05	4.2
q < 0.50	0.25	0.10	4.2
q > 0.50	0.50	0.10	4.2

Table 4: Parameters used by Lecavelier Des Etangs (1999).

Finally, we note that volatile sublimation is not the only mechanism responsible for dust release. For instance, dust can also be ejected through electrostatic lofting. On airless bodies, the day side can become positively charged as incident solar photons remove electrons from the surface, while electrons in the solar wind accumulate preferentially on the night side, creating a localized electric field. This process results in negatively charged dust grains that are repelled by the surface and lofted into space.

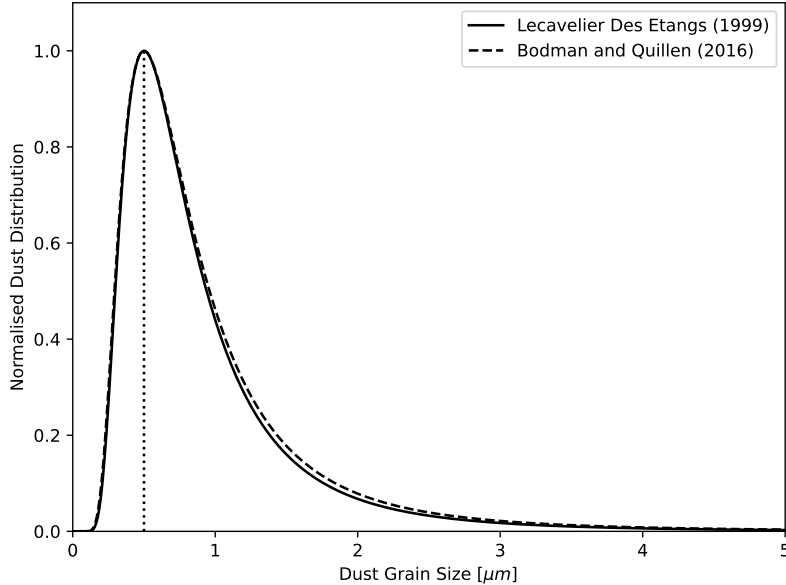


Fig. 5: Comparison of the distribution models used by [Lecavelier Des Etangs \(1999\)](#) and [Bodman and Quillen \(2016\)](#). In this example, $s_p = 0.50 \mu\text{m}$, $s_0 = 0.10 \mu\text{m}$, $n = 4.2$, and $\alpha = 4$.

Electrostatic lofting has been proposed as a contributing factor to dust activity on near-Earth asteroid Bennu ([Hartzell et al., 2022](#)), Phaethon ([Kimura et al., 2022](#)), and 67P itself ([Nordheim et al., 2015](#)), demonstrating that dust ejection is not solely reliant on volatile sublimation.

2.3 Other microscopic processes

While volatile sublimation is the main mechanism that leads comets to lose gas and dust, other processes play important roles in the mass loss of rocky bodies, such as asteroids, terrestrial planets and moons, whose surfaces are largely devolatilized. Different from sublimation, which can release materials from great depth, the following processes only affect the topmost layers. The impact of these processes on exocomets (or, more generally, exo-small bodies) has never been studied. However, they could represent important drivers of activity for objects exposed to different stellar environments than the Sun.

2.3.1 Thermal desorption

Thermal desorption refers to the release of species that are adsorbed onto or trapped within another material as a result of heating. Unlike sublimation, thermal desorption does not involve breaking chemical bonds but instead overcomes physical adsorption forces or diffusive barriers between the matrix and the molecule or atom being released ([Collings et al., 2004](#)). Volatile species commonly released through thermal desorption

include H, He, Ar, Ne, H₂, O₂, N₂, H₂O, OH, and CO₂, as observed on the Moon (Stern, 1999) and Mercury (Killen et al., 2007; Wurz et al., 2022). Some of these species, such as H₂O and CO₂, can freeze out on the night side of these bodies and are subsequently released at dawn due to solar heating.

Another example of a body experiencing thermal desorption is (3200) Phaethon, which experiences surface temperatures up to 1000 K near perihelion (at 0.14 au, see Masiero et al., 2021). At such temperatures, the thermal desorption of Na atoms becomes efficient, leading to a peak loss rate of 5.5×10^{23} atoms s⁻¹ (Zhang et al., 2023a). The sodium is sequestered beneath a devolatilized surface layer about 0.1 m thick that acts as a diffusive barrier. If this barrier were disrupted or absent, the sodium production rate could increase by six orders of magnitude, potentially generating enough pressure to lift dust from the surface (Masiero et al., 2021). By contrast, on Mercury (perihelion 0.31 au), the release of sodium atoms by thermal desorption is marginal and limited to the subsolar point (Wurz et al., 2022). This illustrates the strong sensitivity of thermal desorption to stellocentric distance and, more generally, to the incoming radiative flux. As a result, thermal desorption is expected to play an even more prominent role around stars hotter and more luminous than the Sun, leading asteroids and refractory grains to rapidly lose atoms as they approach their host stars.

Thermal desorption processes are also linked to matrices found on comets (e.g., clathrates), where H₂O and CO₂ ices serve as storage reservoirs for minor species. Observations have shown correlations between the release of minor volatiles (e.g., C₂H₆, CH₃OH, HCN, ...), and major volatile species (H₂O and CO₂) in cometary comae (Dello Russo et al., 2016; Luspay-Kuti et al., 2018; Saki et al., 2024). Such correlations are consistent with laboratory results (Collings et al., 2004; Kruczkiewicz et al., 2024). It has also been suggested that amorphous water ice in the nuclei of distant comets may phase transition into crystalline ice, releasing minor species and driving activity (cf. Jewitt, 2009; Guilbert-Lepoutre, 2012). Although amorphous ice is thermodynamically unstable, at low temperatures its crystallization timescale is longer than the age of the Solar System; only when the ice is heated above ~ 100 K does crystallization proceed efficiently (Jewitt, 2009). This temperature-dependent phase transition is exothermic, and the energy released can drive additional activity at distances beyond which water-ice sublimation is expected. Consequently, there might be multiple ‘snow lines’ for a given species: one where the species itself sublimates, and others where trapped volatiles are released as the matrix holding them either undergoes a phase transition or sublimates.

2.3.2 Photon and electron desorption

Photon-stimulated desorption (PSD; also known as photodesorption or photosputtering) is a low-energy process capable of releasing atoms and molecules from a surface when sufficient UV flux is present. In our Solar System, PSD plays a significant role in the release of sodium (Na) and potassium (K) from airless bodies such as Mercury and the Moon (Yakshinskiy and Madey, 1999), while on icy moons like Europa and Enceladus, it contributes to the ejection of water molecules and their fragments (e.g., Plainaki et al., 2010; Plainaki et al., 2012).

In PSD, a photon is absorbed by an atom or molecule adsorbed on a surface, promoting it into an unbound excited state. The photon energies involved ($4 - 10$ eV, corresponding to $3000 - 1200$ Å, Wurz et al., 2022), are typically insufficient to break chemical bonds within minerals, restricting PSD to species that are already loosely bound to the surface. The required photon energy depends on the bonding strength of the adsorbed species: water molecules are held to surfaces by weak hydrogen bonds or van der Waals forces (Fillion et al., 2022), while alkalis such as Na and K are often strongly bound to metallic or oxide surfaces, requiring higher energies for desorption (Yakshinskiy and Madey, 2000). PSD yields vary significantly between species, ranging from $\approx 10^{-3}$ photon $^{-1}$ for H₂O to $\approx 10^{-4}$ photon $^{-1}$ for Na and K, and are probably even lower for heavier atoms like Ni and Fe. The yield also depends on surface composition, temperature, and photon flux intensity (Bahr and Baragiola, 2012; Fillion et al., 2022).

The efficiency of PSD scales with the incident photon flux, making Mercury’s PSD rates higher than those of the Moon. The same scaling implies stronger PSD around hotter stars with elevated UV flux, or during stellar flares, which can temporarily enhance PSD rates by up to an order of magnitude (Welsh et al., 2006). However, PSD can be attenuated by the presence of gas above the solid surface, which absorbs UV photons. For example, water vapor has strong absorption cross-sections between 50 and 175 nm (Phillips et al., 1977; Parkinson and Yoshino, 2003), and when production rates typically exceed 10^{27} molecules s $^{-1}$ (30 kg s $^{-1}$) for a \sim km-wide nucleus, the resulting coma becomes optically thick to UV photons within several kilometers above the surface (e.g., Bodewits et al., 2016, for 67P). PSD yields for H₂O are approximately an order of magnitude higher than for D₂O, potentially leading to isotopic fractionation over time (Fillion et al., 2022). This phenomenon may influence the interpretation of isotopic ratios.

Electron-stimulated desorption (ESD) is a process very similar to PSD, but involves impact by low-energy electrons instead of photons. This process has been proposed to explain part of the release of Na and K from Mercury; however, disentangling the impacts of ESD and PSD is difficult, due to the close similarity between the two processes (Wurz et al., 2022). The cross-sections for ESD and PSD are of similar magnitude; for instance, the cross-section of Na is typically 10^{-20} cm $^{-2}$ for PSD and 10^{-19} cm $^{-2}$ for ESD (Wurz et al., 2022). In the Solar System, the UV photon flux is usually much higher than the electron flux, making PSD the dominant desorption process (Killen et al., 2007). As with PSD, ESD can be suppressed by collisions with ambient gas, as inelastic interactions with molecules such as H₂O rapidly degrade electron energies (Cravens and Korosmezey, 1986; Itikawa and Mason, 2005).

Thermal, photon, and electron desorption processes thus provide efficient, non-sublimative mechanisms for mass release from refractory surfaces. In the solar system, these processes lead to the formation of tenuous tails around bodies like Mercury, the Moon or Phaethon, which would however be too faint to produce detectable signatures in the solar spectrum if viewed from an extrasolar perspective. Nevertheless, their strong dependence on stellar radiation and particle flux implies that, in exocometary systems orbiting luminous or active stars, these mechanisms may rival or even exceed classical volatile sublimation as sources of transient gas and dust.

2.3.3 Sputtering

The surfaces of airless bodies can lose material through sputtering, which is the momentum transfer from a projectile (typically ions) to molecules or atoms of a solid. In our Solar System, sputtering contributes to the formation of tenuous atmospheres around the icy moons of Jupiter and Saturn (Plainaki et al., 2010; Plainaki et al., 2012; Galli et al., 2022), along with photon-desorption. Mercury has a rather weak magnetosphere, resulting in localized sputtering at magnetic poles releasing O, Si, Ca and Fe, among other species (Killen et al., 2007). Earth’s Moon, which spends most of its time outside Earth’s magnetosphere, also loses H, O, Ca, Na, and Fe atoms through sputtering (Wurz et al., 2022; Vorburget et al., 2012; Poppe et al., 2016). Sputtering occurs through two main mechanisms: nuclear-elastic collisions between the incoming ion and atoms/molecules, known as knock-on sputtering, and electronic sputtering, where a particle is released through the electronic excitation of a dissociative state, similar to photon/electron desorption (Johnson, 2013; Sigmund, 1981).

Sputtering yields depend heavily on the nature of the collision partners and the energy of the incident ions. For water ice, ions with energies below 1 keV/amu (typical of solar wind velocities) predominantly induce nuclear (knock-on) sputtering, resulting in the release of water molecules and their fragments (Shi et al., 1995; Famá et al., 2008). At higher ion energies, electronic sputtering becomes more effective as electronic excitations dominate the energy deposition processes (Johnson, 2013). Conversely, for refractory materials and metals, knock-on sputtering is generally the primary mechanism due to their denser and more robust atomic structures, which favor momentum transfer during collisions (Johnson and Baragiola, 1991; Cassidy and Johnson, 2005).

A third type of sputtering is potential sputtering, which occurs when highly charged ions eject material from a surface through the release of Coulomb potential energy. Unlike nuclear and electronic sputtering, this mechanism relies on the ion’s high charge state rather than its kinetic energy (Bodewits, 2010). As highly charged ions approach or impact a surface, they undergo rapid neutralization as electrons transfer from the surface to the ions. This neutralization process releases significant energy, capable of disrupting the surface and ejecting particles. Consequently, ions with higher charge states in the solar wind can significantly increase the sputtering yield (Tielens, 2005). Overall, the energy of the incident ion plays a critical role in determining sputtering efficiency. At low energies, the projectile may not have sufficient momentum to cause substantial material ejection. At extremely high energies, the ion may penetrate too deeply into the material, depositing most of its energy below the surface and reducing the effective sputtering yield (Johnson, 2013). Optimal sputtering occurs at intermediate energy ranges where surface interactions dominate. Solar wind disturbances, such as Coronal Mass Ejections, can temporarily enhance sputtering rates by introducing higher fluxes, or particles with higher charges (Killen et al., 2012; Killen et al., 2012). In fact, comparing sputtering yields under different solar wind conditions, and at different heliocentric distances, could provide insights into the role of sputtering processes around different host stars. In this context, the Moon, Mercury, and Sun-grazing asteroids could serve as excellent analogs to explore the effects of stellar winds on airless bodies (Wurz et al., 2022; Poppe et al., 2016).

2.3.4 Micrometeorite impacts

The impacts of micrometeorites on unprotected planet surfaces drive numerous processes, including exospheric generation, impact gardening, surface contamination, and electrostatic effects (Szalay et al., 2018). One key outcome is the formation of impact plumes, which consist of surface materials fragmented into particles ranging from macroscopic debris to atoms and molecules. These plumes contribute significantly to the exosphere, particularly through the release of low-volatile and refractory species (Stern, 1999; Killen, 2016; Janches et al., 2021). During periods of low solar activity, micrometeorite impacts may dominate particle release processes across an entire planetary surface, especially at night, when other mechanisms, such as solar wind sputtering and PSD, are absent (Cassidy et al., 2021; Pokorný et al., 2018; Nie et al., 2024). The high impact speeds of micrometeorites result in substantial vaporization of surface materials (Collette et al., 2014).

The energy involved in micrometeorite impacts is substantial, producing vapor clouds at temperature ranging from 2500 to 5000 K (Eichhorn, 1978), and perhaps as hot as 15000 K (Cassidy et al., 2021), far exceeding typical surface temperatures. At Mercury, for example, the temperature of the impact plumes can reach up to 10 times higher than the surface temperature on the day side (Killen, 2016). The volume of material vaporized during impacts depends on the mass, density, and velocity of the projectile, as well as the composition of the surface material (Collette et al., 2014).

Recent findings by Nie et al. (2024) further support this by showing that micrometeorite impacts are responsible for approximately 70% of the Moon’s exosphere, as determined from isotopic analyses of lunar soil samples. The remaining 30% of the exosphere is maintained by solar wind sputtering, emphasizing the crucial role of impact vaporization in sustaining tenuous atmospheres around airless bodies.

2.4 Macroscopic processes

In young and compact extrasolar systems, macroscopic processes, such as tidal disruptions or collisions between planetesimals, can also play a major role in shaping the circumstellar environment. These processes can generate substantial amounts of dust and gas, leading to the formation of detectable, comet-like tails.

Since the Sun is much older than any of our other case-study systems, a direct comparison of the macroscopic processes presently observed as mass-loss mechanisms is not particularly helpful. Collisions are infrequent in the current solar system, but there is evidence from the cratering record of past higher rates. As the planets accreted ~ 4.5 Gyr ago, the cratering rate declined. This was likely followed by a period of enhanced bombardment between ~ 3.5 and 4.0-4.2 Gyr, known as the Late Heavy Bombardment (Wetherill, 1975). Although there is some debate about the details of the Late Heavy Bombardment, including if there was ever a minimum prior to a later spike (see, e.g., the review by Bottke and Norman, 2017), the modern cratering rates on the Moon, Mars, and Mercury are unarguably lower than in the early solar system (cf. Strom et al., 2005, 2015).

Despite today’s lower cratering rate, collisions are still relatively common in the asteroid belt, with several asteroid families apparently having formed within the last

million years (see review by [Nesvorný et al., 2015](#)). The importance of collisions in sculpting the asteroid population has been well-established for decades, primarily driven by asteroids’ size-frequency distribution (cf. [Bottke et al., 2005](#), and references therein). Regular monitoring of Jupiter, Saturn, and the Moon has occasionally revealed evidence of impacts by asteroids and/or comets, with the impact of D/1993 F2 (Shoemaker-Levy 9) into Jupiter the prime example (cf. [Weaver et al., 1994](#); [Hammel et al., 1995](#)). Several main-belt asteroids have also been observed to release material as a direct consequence of recent impacts ([Jewitt, 2012](#)).

Some extrasolar systems show evidence for a much stronger collisional activity. As discussed in [Mustill et al. \(submitted\)](#) and [Bannister et al. \(2025\)](#), the widespread detection of dusty debris discs around mature stars necessitates ongoing, destructive collisions in planetesimal belts (e.g. [Wyatt, 2008](#); [Hughes et al., 2018](#); [Pearce, 2024](#)). This is because the collisional lifetimes of detected grains are much shorter than the stellar ages, and these grains are typically located in discs ~ 100 s of au from their stars, so they are thought to be released via planetesimal collisions rather than from sublimating comets. Further evidence for extrasolar collisions comes from observed-dust quantities around stars decreasing with stellar age, which is consistent with the picture that planetesimal belts collisionally erode over time (e.g. [Wyatt et al., 2007](#); [Löhne et al., 2008](#); [Matrà et al., 2025](#)). Short-term spikes in dust production are also seen around some stars, which are thought to signify collisions between large asteroids (e.g. [Su et al., 2019](#)), and resolved images of some debris discs show tail-like structures thought to arise from a single impact event (e.g. [Jackson et al., 2014](#); [Jones et al., 2023](#); [Rebollido et al., 2024](#)).

Besides collisions, minor bodies can also be disrupted through tidal interactions with stars and massive planets. In the solar system, there is evidence for tidal disruptions of comets due to close approaches to the Sun and Jupiter. The aforementioned comet Shoemaker-Levy 9 was conclusively shown to have disrupted in 1992 during a close approach to Jupiter, 2 years before its eventual impact into the planet ([Sekanina et al., 1994](#); [Asphaug and Benz, 1996](#)). The Kreutz group of sungrazing comets (see Section 5.1) are thought to have been produced by ongoing, hierarchical fragmentation driven in part by tidal forces near the Sun (see review by [Marsden, 2005](#)). Extrasolar systems also show tidal disruption; the most-convincing indications come from white-dwarf stars, where there is evidence of disintegrating comet-sized bodies inside the star’s tidal-disruption radius (e.g. [Jura, 2003](#); [Vanderburg et al., 2015](#)). The disintegration of these small bodies lead to the formation of tail structures, which produce asymmetric transit events in the stellar light curve (e.g., [Gänsicke et al., 2016](#)).

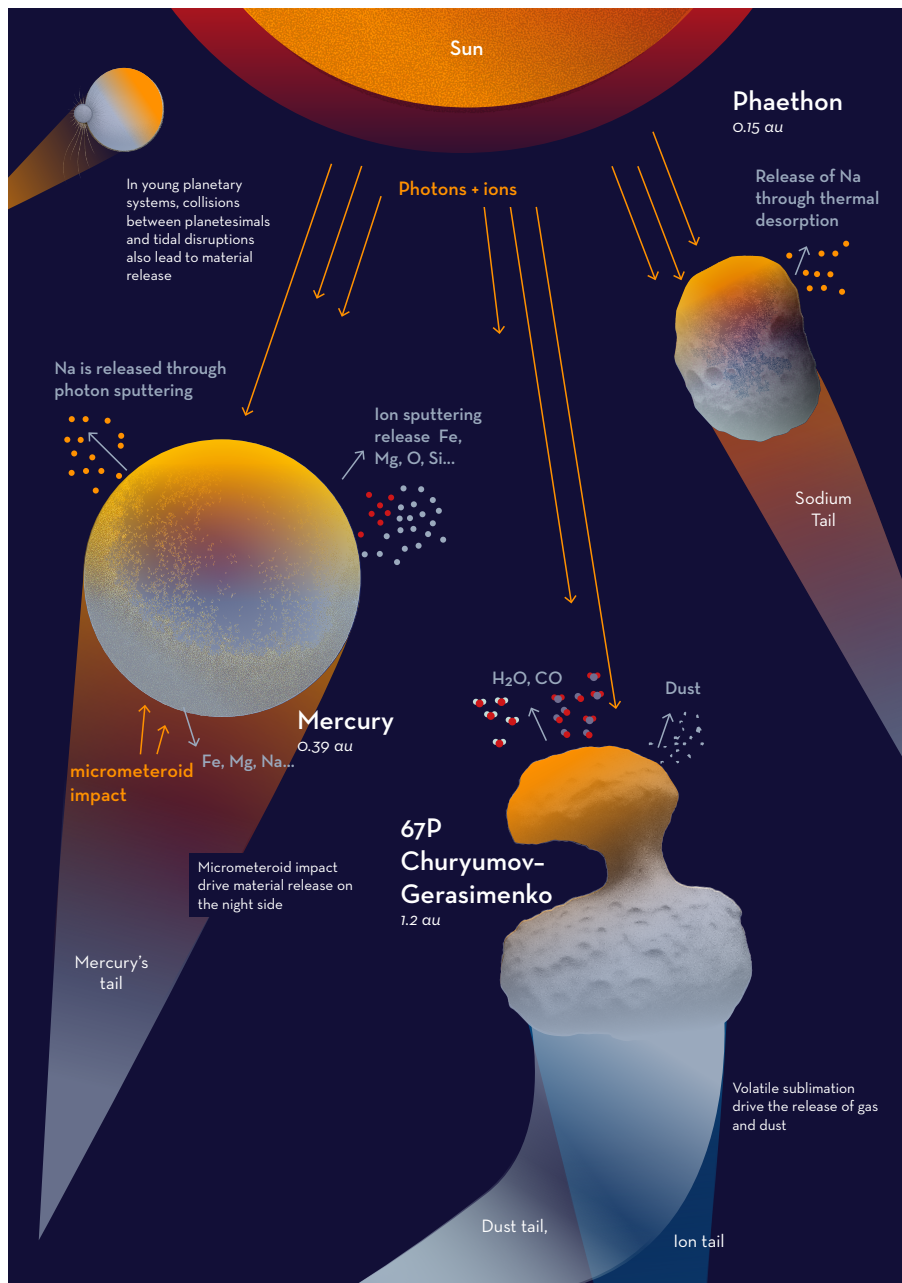


Fig. 6: Summary of the various physical processes that trigger material release from Solar System objects. Depending on the nature of the object (e.g. rocky asteroid, terrestrial planet, or comet) and its heliocentric distance, different mechanisms dominate the mass-loss process.

3 Production of secondary species

This section investigates the various processes that alter the composition, excitation and ionisation states of the material released by comets or exocomets, and how these processes scale across different stellar environments.

3.1 Dust grain sublimation

When dust grains are released from cometary nuclei, they become directly exposed to stellar radiation. This can trigger their sublimation, which is the process by which minerals (e.g. Mg_2SiO_4 , forsterite) transition from solid to gas phase. For most minerals, this transition is accompanied by the breaking of chemical bonds (e.g., [Steinmeyer et al., 2023](#)); as a result, the sublimation products are generally atoms (e.g. Mg, Si, O) or simpler molecules (e.g. SiO). This process likely occurs in the β Pic system, leading to the release of extreme amounts of refractory atoms and ions by exocomets ([Beust et al., 1990](#)). The goal of this section is to investigate the stellar conditions under which dust sublimation becomes efficient, considering the physical properties of the grains, such as their size and composition.

The sublimation rate of a dust grain is directly linked to its temperature, which in turn is controlled by the energy equilibrium of the grain (see for instance [Kimura et al., 2002](#)). Taking into account the flux received from the star, the flux emitted by the grain, and the energy used in sublimation, this energy equilibrium is written:

$$\Omega \int \sigma_{\text{abs}}(s, \lambda) I_{\star}(\lambda) d\lambda = 4\pi \int \sigma_{\text{abs}}(s, \lambda) B(\lambda, T) d\lambda - \frac{dm}{dt}(s, T)L, \quad (5)$$

where σ_{abs} is the absorption cross-section of the dust grain (which depends on its radius s and on the wavelength λ), I_{\star} is the stellar specific intensity ($\text{J/s/cm}^2/\text{\AA}/\text{sr}$), B is the Planck function (assuming that the dust grain radiates like a black-body; same unit as I_{\star}), T is the grain temperature, and L is the dust latent heat of sublimation. The solid angle covered by the star (Ω) is linked to the stellar distance, d , through:

$$\Omega = 2\pi \left(1 - \sqrt{1 - (R_{\star}/d)^2}\right), \quad (6)$$

and the mass loss $\frac{dm}{dt}$ is given by:

$$\frac{dm}{dt} = -4\pi s^2 \alpha \sqrt{\frac{m_{\text{gas}}}{2\pi k_B T}} p(T), \quad (7)$$

where $p(T)$ is the vapor pressure of the released gas, m_{gas} is the molecular mass of the sublimated molecule, k_B is the Boltzmann constant, and α is a correction factor < 1 . The vapor pressure $p(T)$ can be obtained from Clausius-Clapeyron's law:

$$p(T) = p_{\infty} \exp\left(-\frac{m_{\text{gas}}L}{k_B T}\right), \quad (8)$$

where p_∞ is the vapor pressure at infinite temperature. More complex $p - T$ relationships are also used (e.g. [Lamy, 1974](#), for water ice).

Equation 5 can be solved numerically to extract the equilibrium temperature T of the grain, which in turn provides the mass loss rate (Eq. 7). For large grains ($s \geq 1 \mu\text{m}$), the cross section σ_{abs} is rather uniform throughout the UV/visible spectrum; as a result, the energy balance of the grain can be simply written as (neglecting the energy lost in sublimation):

$$\Omega\pi s^2\sigma T_{\text{eff}}^4 = 4\pi^2 s^2\sigma T^4, \quad (9)$$

with σ the Stefan-Boltzmann constant and T_{eff} the stellar effective temperature. This yields:

$$T = T_{\text{eff}} \left(\frac{\Omega}{4\pi} \right)^{\frac{1}{4}}. \quad (10)$$

In this case, the sublimation rate of dust grains is similar to the sublimation rate of material directly at the surface of the nucleus (Sect. 2.2.1). For smaller grains, however, the absorption cross section may vary by several orders of magnitude from visible to infrared wavelengths, leading to equilibrium temperatures that are very different from that of a macroscopic object, and thus to different sublimation rates. In this case, the exact resolution of Eq. 5 becomes mandatory, using cross sections derived from the Mie theory.

To illustrate the typical sublimation rate of dust in various stellar environments, Fig. 7 provides the sublimation timescale (defined as $m/\frac{dm}{dt}$) of a $0.5 \mu\text{m}$ dust grain around our four case-study stars (AU Mic, the Sun, β Pic, and WD 1145+017; see the radius and temperature properties in Table 1), for various compositions (olivine, pyroxene) and stellocentric distances. The grain cross sections were taken from [Budaj et al. \(2015\)](#), and the temperature-pressure relationships from [van Lieshout et al. \(2014\)](#) (forsterite, enstatite, alumina, amorphous carbon), [Kimura et al. \(2002\)](#) (olivine, pyroxene), and [Lamy \(1974\)](#) (water ice). The grain radius, $0.5 \mu\text{m}$, corresponds to the peak of the size distributions discussed in Sect. 2.2.2.

The ability of a given star to sublimate dust depends heavily on its effective temperature. For a $0.5 \mu\text{m}$ olivine grain orbiting β Pic, the distance for which the sublimation time is 1 day is located around 0.18 au. Around the Sun and AU Mic, this limit falls down to ~ 0.06 and ~ 0.015 au respectively. Due to its small radius, dust sublimation around WD 1145+017 occurs within a very small region (~ 0.03 au, about a solar radii). More detailed studies of dust sublimation around polluted white dwarfs can be found in [Shestakova et al. \(2022\)](#) and [Steckloff et al. \(2021\)](#).

The sublimation rate also depends on the grain composition. While some minerals are sublimated at rather large stellocentric distances (e.g. olivines), others appear to be more resistant (e.g. enstatite). In general, a dust grain will be more resistant to sublimation when its cross section in the UV/visible (where the stellar flux is absorbed) is higher than in the IR (where the energy is re-emitted).

In a similar way, Fig 8 provides the sublimation distance (here defined as the stellar distance at which the sublimation timescale is 1 day), as a function of the grain radius. Although slight variations of the sublimation distance with grain size are observed, the main trend is that β Pic is generally much more efficient at sublimating grains

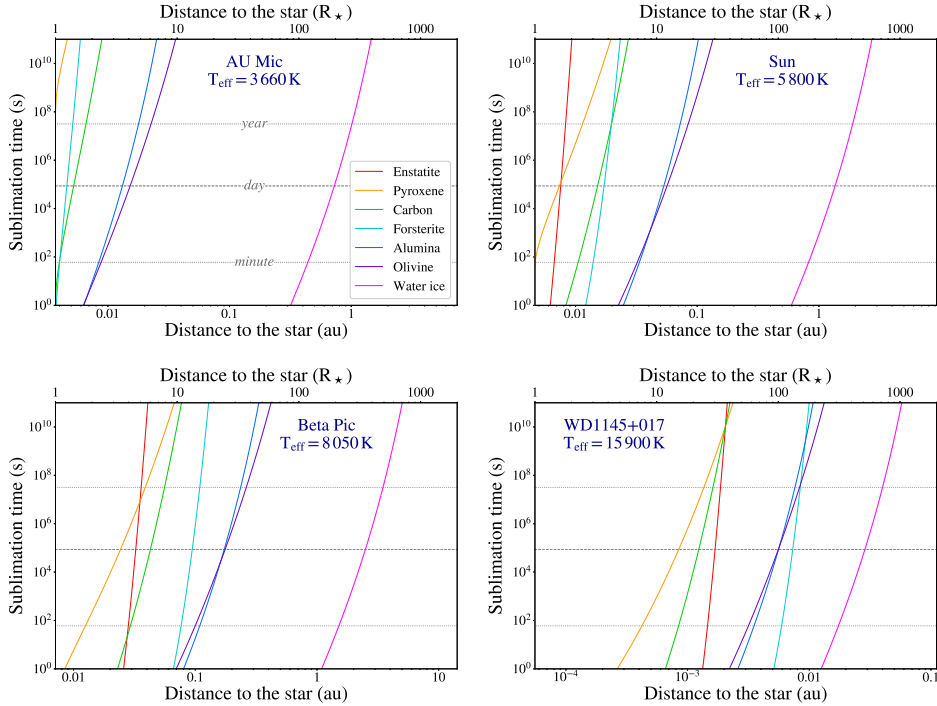


Fig. 7: Sublimation timescale of a $0.5 \mu\text{m}$ dust grain with various compositions around four different stars, as a function of the distance to the star. Dotted lines indicate a one-minute, one-day, and one-year times. Distances are expressed in stellar radii (upper axis; same scale for all stars) and au (lower axis; specific to each star).

(below $\sim 0.1 - 0.5$ au, depending on the grain size) than the Sun or AU Mic. This is consistent with the observation of large amounts of refractory ions (e.g. Fe^+ , Ca^+ ...) in the tails of β Pic exocomets.

We emphasize that the calculations presented here are simplistic, and only provide an approximate description of the behavior of dust grains around stars. In reality, dust grains may have inhomogeneous compositions (with various minerals taking various crystalline forms), and are likely not spherical (as assumed in the calculations of the cross-sections), resulting in potentially large variations in their sublimation rates and distances. For instance, [Protopapa et al. \(2018\)](#) showed that the sublimation rate of icy grains strongly varies with their size and purity. Grain porosity is also expected to influence the sublimation rate, although very few studies on this aspect are available (e.g., [Kossacki, 2021](#)). Finally, it should be noted that young, dense dust discs may be optically thick, thereby reducing sublimation rates and shifting the sublimation lines closer to the star.

The sublimation of dust grains produced by exocomets is related to the problem of ‘hot dust’, which is detected around one-fifth of main-sequence stars (e.g. [Ertel et al., 2016](#); [Kirchschlager et al., 2017](#); [Absil et al., 2021](#)). This dust is composed of

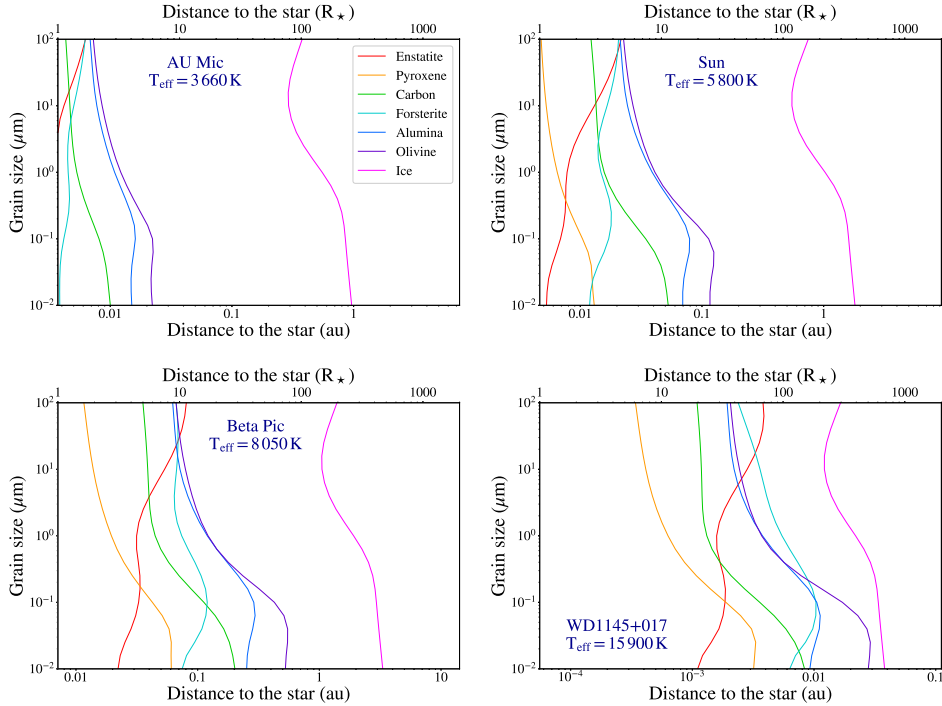


Fig. 8: Distance from the host star at which the sublimation timescale of a dust grain is 1 day, depending on the grain radius and composition. For all figures, the distance range is set to $[1, 2000] R_{\star}$.

sub-micron-size dust grains at a temperature above 1500 K (Defrère et al., 2012), and can be detected in the near infrared using optical long-baseline interferometry. The nature of this dust is a mystery. These grains should rapidly sublimate or blow away under radiation pressure, and so far all attempts to dynamically explain hot dust have failed to completely reproduce the phenomenon (e.g. van Lieshout et al., 2014; Rieke et al., 2016; Sezestre et al., 2019; Kimura et al., 2020; Pearce et al., 2020). This dust is most likely associated with exocomets, because some hot dust is variable which is best explained by stochastic cometary infall (Ertel et al., 2016), and there is a tentative relation between hot-dust detections and circumstellar gas indicative of cometary activity (Rebollido, 2020). However, cometary supply alone is unlikely to fully explain hot exozodiacal dust, or exozodis. Although star-grazing comets are promising candidates, the required comet inflow rates and dust ejecta size distributions conflict with current cometary and planetary system models. Additional dust-trapping mechanisms may work alongside cometary input to produce hot exozodis, but comets alone are insufficient to explain this phenomenon (Pearce et al., 2022).

3.2 Dissociation and ionization of molecules

Molecules released from cometary nuclei—such as H_2O and CO —may dissociate into lighter molecules (e.g., OH) or atoms (O , H), or they may undergo photoionization (e.g., forming H_2O^+), depending on the stellar flux they’re exposed to. These processes are frequently observed in Solar System comets (cf. [Feldman et al., 2004](#); [Fortenberry et al., 2021](#)), and they are likely even more pronounced in the β Pic system due to its star’s higher UV flux.

The dissociation rate of a molecule (e.g., H_2O) released by a comet can be calculated from its dissociation cross-section and the spectrum of its host star. This writes:

$$dP_{\text{dis}} = \Omega \int_0^\infty \frac{\lambda}{hc} I_\star(\lambda) \sigma_{\text{dis}}(\lambda) d\lambda dt, \quad (11)$$

where dP_{dis} is the dissociation probability within a time dt , Ω is the solid angle covered by the host star (which depends on the distance between the particle and the star; Eq. 6), $I(\lambda)$ is the specific intensity of the stellar disc ($\text{J/s/cm}^2/\text{\AA}/\text{sr}$), h is the Planck constant, c is the speed of light, and σ_{dis} is the dissociation cross-section. For a given molecule, different sets of dissociation products are possible (e.g., $\text{H}_2\text{O} \rightarrow \text{H}_2 + \text{O}$; $\text{H}_2\text{O} \rightarrow \text{H} + \text{OH}$, ...; cf. [Combi et al. 2004](#)). Similarly, the ionization rate can be written:

$$dP_{\text{ph}} = \Omega \int_0^\infty \frac{\lambda}{hc} I_\star(\lambda) \sigma_{\text{ph}}(\lambda) d\lambda dt, \quad (12)$$

where dP_{ph} is the photo-ionization probability within a time dt and σ_{ph} the photo-ionization cross-section.

As an example, Table 5 provides the typical dissociation and ionization times of key molecules (H_2O , HCN , CO_2 , ...) at 0.2 au from our four case study stars (corresponding to the typical transit distance of β Pic exocomets, [Kiefer et al., 2014](#); [Lecavelier des Etangs et al., 2022](#)). Calculations were performed using the spectral distribution provided in Sect. 1, and cross-sections from the Phidrates database ([Huebner et al., 1992a](#)). While around the Sun all molecules are able to survive $\sim 1 - 10$ hours, around β Pic they are rapidly dissociated, particularly H_2O , HCN , and OH (lifetime ~ 1 s). As a result, it is little surprise that none of these species has been directly detected in β Pic exocomets so far - only CO has been observed in the stable disc ([Roberge et al., 2000](#); [Dent et al., 2014](#)). The ionization timescale is generally higher than the dissociation timescale, although it can be dominant for specific species, like CO or C_2 .

More generally, Fig. 9 presents typical lifetimes for the studied molecules as a function of the stellar effective temperature, again at a distance of 0.2 au. These dissociation timescales were calculated using synthetic spectra from the PHOENIX library ([Husser et al., 2013](#)), and again cross-sections from the Phidrates database. Since the PHOENIX spectra are purely photospheric, the dissociation timescales obtained are very likely overestimated, in particular for cool stars which should exhibit strong coronal and chromospheric emission. Nonetheless, Fig. 9 shows that stars hotter than ~ 7000 K should rapidly dissociate most molecules ($\tau_{\text{dissoc}} \ll 1$ day), whereas around cooler stars they can survive significantly longer (as also shown in Table 5). These short lifetimes of the most prominent fragment species observed in Solar System comets (such as OH , CN , C_2 , etc; [Feldman et al. \(2004\)](#)) could explain why they have not been detected in exocometary systems yet.

Species	Process	WD 1145+017	AU Mic	Sun	Beta Pic
OH	Dissociation	2.8×10^1	1.4×10^3	1.8×10^3	1.3×10^0
	Ionization	7.5×10^3	4.5×10^3	1.2×10^5	5.5×10^3
HCN	”	2.8×10^1	1.1×10^3	2.8×10^3	2.2×10^1
	”	9.8×10^2	2.4×10^3	5.3×10^4	7.0×10^2
H ₂ O	”	4.4×10^1	2.1×10^3	4.0×10^3	1.5×10^0
	”	8.8×10^2	3.6×10^3	7.6×10^4	1.1×10^3
CN ^a	”	2.7×10^1	5.6×10^2	7.6×10^3	6.3×10^1
	”	-	-	-	-
CO ₂	”	3.5×10^1	1.7×10^3	2.1×10^4	1.0×10^2
	”	1.1×10^3	2.0×10^3	4.0×10^4	7.1×10^2
C ₂	”	3.5×10^2	1.5×10^4	2.4×10^5	6.4×10^3
	”	2.2×10^2	1.4×10^3	2.6×10^4	2.4×10^2
CO	”	4.1×10^2	5.7×10^3	6.7×10^4	6.3×10^2
	”	1.6×10^3	2.9×10^3	6.5×10^4	1.1×10^3

Table 5: Photo-dissociation and ionization timescales (in s) of common molecules around our four case-study stars, calculated at a stellocentric distance of 0.2 au.

Notes. [a] Photo-ionization cross section for CN are not included in the Phidrates database.

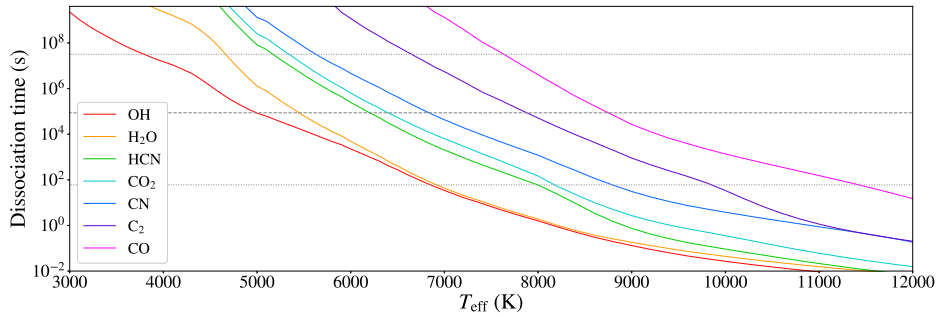


Fig. 9: Lifetimes (combining photo-dissociation and ionization) of various molecules at 0.2 au from their host star, depending on the stellar effective temperature. Dotted horizontal lines are identical to Fig. 7. Calculations were performed with synthetic spectra from the PHOENIX library, which are purely photospheric; as a result, these values should be considered as upper limits only.

3.3 Ionization of atoms and ions

3.3.1 Photo-ionization

Around hot stars, efficient dust sublimation (Sect. 3.1) and molecular dissociation (Sect. 3.2) should lead to the production of large amounts of neutral atomic species, including O, C, and Fe. Depending on their ionization energies and on the intensity and distribution of the stellar flux, these species can be subsequently photo-ionized. The ionization rate of a given species can be calculated using its ionization cross section and the stellar luminosity, in a similar way as for molecules (Eq. 12).

As an example, Fig. 10 shows typical ionization times of various atomic and ionized species around our four case-study stars, at a stellocentric distance of 0.2 au. The calculations were performed using ionization cross sections from the Phidrates database, as was done for photo-dissociation, and the spectral distributions adopted in Sect. 1. The largest differences between the four stars occur for neutral atoms: around the Sun and AU Mic the photo-ionization timescales of Na, Fe, or Si are rather long ($\sim 10^4$ s, corresponding to a few days at 1 au), and they drop below 60 s around β Pic, due to a much stronger photospheric continuum below 2000 Å. This explains why refractory species observed around β Pic are almost always ionized (for instance, signatures in Fe I or Na I are rare and extremely shallow; Welsh and Montgomery, 2016; Hoeijmakers et al., 2025), while neutral atoms such as Fe, Ni, and Na are commonly observed in the exospheres and tails of Solar System objects, even though they eventually become ionized, too (Manfroid et al., 2021; Fulle et al., 2007).

For species with ionization threshold shorter than the Ly- α limit (10.2 eV \sim 1216 Å), the difference in photo-ionization times is less important. Thanks to their relatively strong EUV fluxes, the Sun and AU Mic are able to photo-ionize species such as C, C⁺, H, or Fe⁺, in 1 – 10 days. These ionization rates should be sufficient to produce substantial quantities of highly charged ions within a single periastron, at least for star-grazing comets (e.g., Kreutz family; Bryans and Pesnell 2012). In the solar system, observing such species is however difficult, because they are rapidly removed by radiation pressure and solar wind. Still, emission from C⁺ and C²⁺ was detected in the tails of the near-Sun comets C/2002 X5 (Kudo-Fujikawa) and 96P/Machholz at 0.19 and 0.12 au from the Sun, respectively (Povich et al., 2003; Raymond et al., 2022), as well as C⁺, C²⁺, O⁺ and O²⁺ in the distant tail of C/1996 B2 (Hyakutake) (Gloeckler et al., 2000), and O³⁺ in the far tail of C/2006 P1 (McNaught) (Neugebauer et al., 2007). These species are very likely produced by photoionization (see table 3 of Raymond et al., 2022).

Similarly, β Pic appears to be able to rapidly photoionise singly charged ions, such as Ca⁺, Fe⁺ or Si⁺, owing to its strong chromospheric flux in the 500 - 900 Å region (Wu et al., 2025). In particular, the lifetime of Al⁺ at 0.2 au is about 80 days, which is of the same order at the timescale of a cometary periastron. Therefore, photo-ionization could explain the presence of Al²⁺ in β Pic exocomets, along with collisional ionization (Beust and Tagger, 1993, see Sect. 4.2.4).

Fig. 11 also provides the ionization timescales of the studied species as a function of the stellar effective temperature, using photospheric models from the PHOENIX

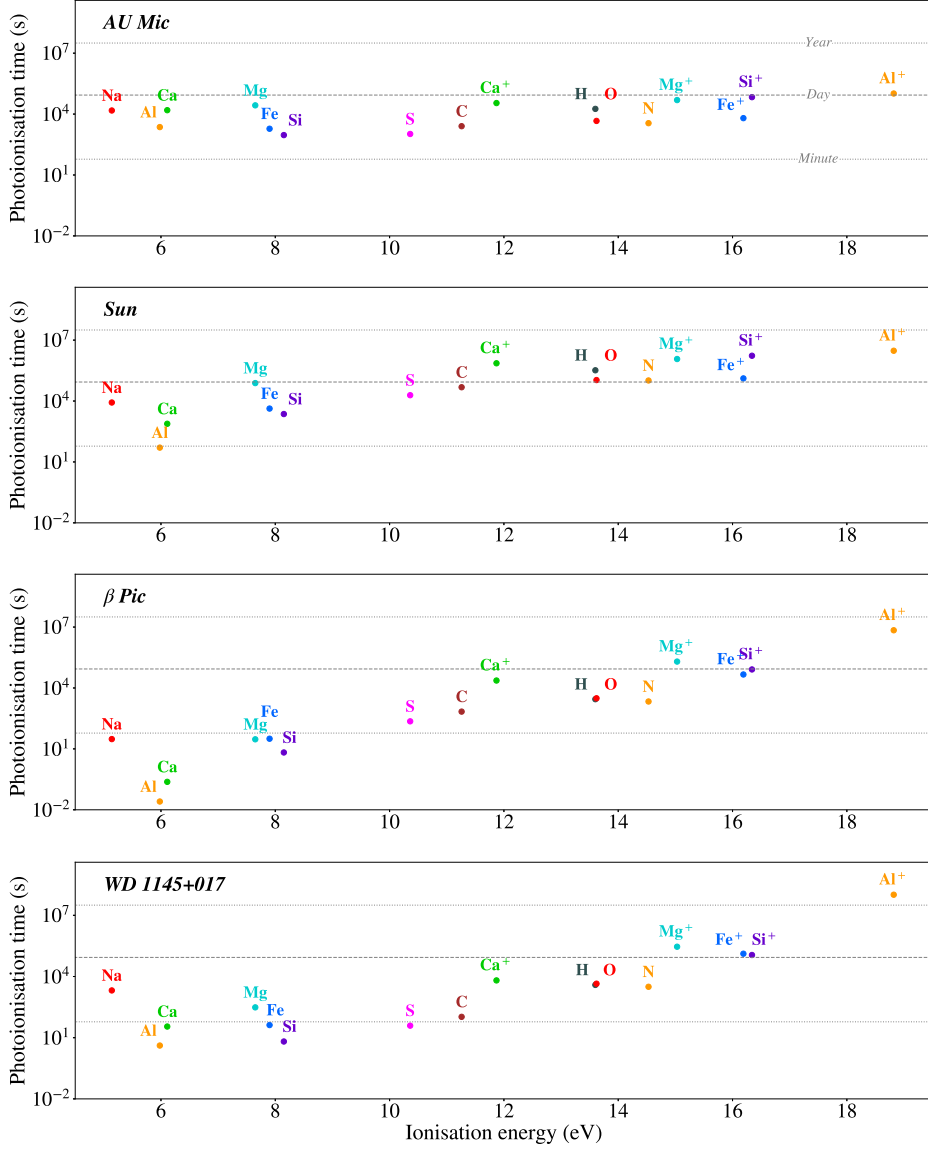


Fig. 10: Photoionization timescales of various atoms and ions around our four case-study stars, at a distance of 0.2 au. Horizontal dotted lines indicates reference times of 1 minute, 1 day and 1 year.

library (Husser et al., 2013). As for Fig. 9, the PHOENIX spectra do not include chromospheric or coronal emission in the EUV/FUV; as a result, the ionization timescales provided here should be considered as upper limits. Yet, we notice that Ca⁺, routinely detected in β Pic exocomets thanks to the 390 nm Ca II doublet, actually gets

rapidly photo-ionized into Ca^{2+} for stars hotter than $9\,000 - 10\,000\text{ K}$ ($\sim \text{A1V}$). This could considerably limit our ability to detect exocomet activity around such stars using optical spectroscopy.

Finally, we note that our calculations rely on the assumption that the atoms and ions are exposed to the unocculted stellar flux. In very young systems, however, discs may be optically thick to UV radiation (mostly due to dust absorption; e.g. [Dullemond and Monnier, 2010](#)), hence significantly suppressing photo-dissociation and photo-ionisation processes in the outer disc regions.

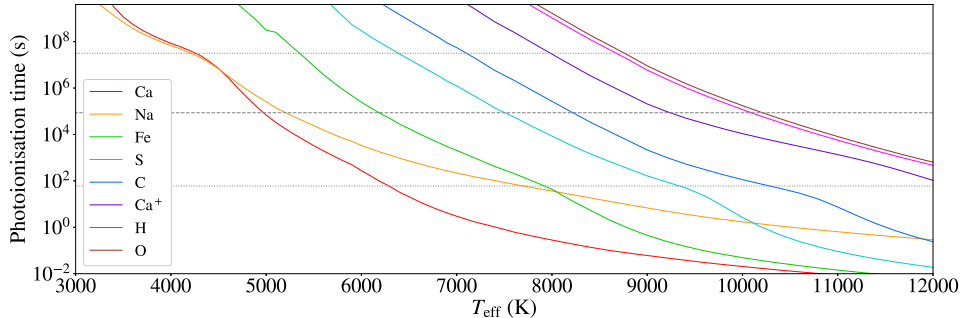


Fig. 11: Photoionization timescales of various species at 0.2 au from the host star, depending on the stellar effective temperature. Dotted horizontal lines are identical to Fig. 10. As for Fig. 9, purely photospheric fluxes were assumed.

3.3.2 Collisional ionization

The different rates of photoionization found for the Sun and β Pic (Fig. 10) explain why neutral species, such as Na, Fe and Ni, are commonly detected in Solar System comets ([Manfroid et al., 2021](#)) or planetary tails ([Wurz et al., 2022](#)), whereas in the β Pic system these elements are primarily found in their ionized form (see the review of [Strøm et al., 2020](#)). However, the presence of highly ionized species (Al^{2+} , Si^{3+} , C^{3+} , ...) in β Pic exocomets ([Deleuil et al., 1993](#)) has long been puzzling, as an A5V star like β Pic was not expected to emit sufficient EUV photons to produce species like C^{3+} . To resolve this problem, it has been proposed that these highly ionized species observed around β Pic are produced through collisional ionization processes occurring within a dense and hot plasma environment.

Collisional ionization rates of various abundant elements were calculated in [Arnaud and Rothenflug \(1985\)](#). The collisional ionization probability of a given atom or ion within dt can be written as:

$$dP_{\text{col}} = \frac{6.69 \cdot 10^7}{(k_B T_e)^{3/2}} \sum_j \frac{e^{-x_j}}{x_j} F_j(x_j) n_e dt \quad (13)$$

where the sum is performed over all the subshells j of the initial ion, and where $x_j = I_j/(k_B T_e)$ with I_j the energy of the sub-shell j . The electronic density n_e and

electronic temperature T_e are expressed in cm^{-3} and K, respectively. The function F_j is described in [Arnaud and Rothenflug \(1985\)](#); it depends on four coefficients A_j , B_j , C_j and D_j specific to the considered sub-shell.

Little literature exists on the typical temperature and density in exocometary tails. Based on the observed population of excited levels of Fe^+ around β Pic, [Vrignaud and Lecavelier des Etangs \(2024\)](#) recently showed that the electronic density in these environments must be below 10^7 cm^{-3} (see Sect. 3.4). Geometric estimates, based on the observed column density of Fe^+ and on the typical size of the transiting clouds ($\sim 1 R_*$) suggest electron densities of the order of $10^5 - 10^6 \text{ cm}^{-3}$ ([Vrignaud and Lecavelier des Etangs, 2024](#)).

Assuming an electronic density of 10^6 cm^{-3} , Fig. 12 provides the direct ionization times of a few species, as a function of the electronic temperature. We note that the various ‘highly ionized’ species (Si^{3+} , C^{3+} , ...) observed in β Pic exocometes are produced at temperatures of $\approx 100\,000$ K. Such high temperatures could be reached when the cometary gas is compressed by radiation pressure ([Beust and Tagger, 1993](#), see Sect. 4.2.4).

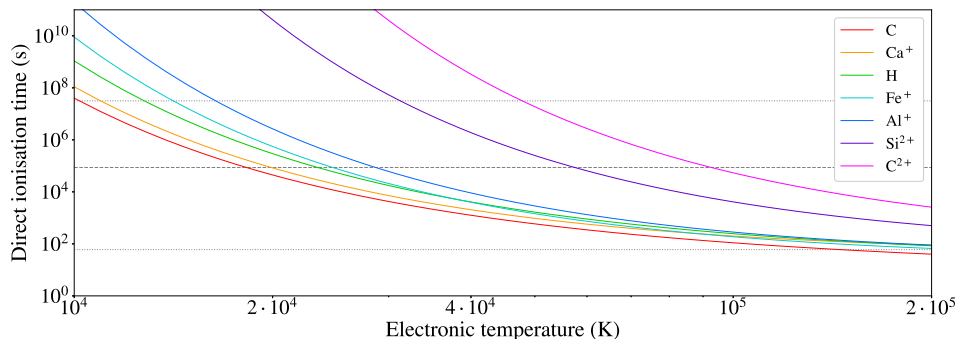


Fig. 12: Direct electron-impact ionization timescales of various species as a function of T_e , for an electron number density of 10^6 cm^{-3} . Dotted horizontal lines are identical to Fig. 10.

3.3.3 Recombination and ionization equilibrium

Ions in cometary tails can also recombine with electrons to reproduce neutral or less ionized species. Two main processes exist: radiative recombination, which is fairly homogeneous among ions, and dielectric recombination, a resonant process that can dominate the recombination rate of specific ions.

The radiative recombination probability of a given ion can be generally expressed as (see [Shull and van Steenberg, 1982](#)):

$$dP_{\text{rad}} = A \left(\frac{T_e}{10^4 \text{ K}} \right)^\eta n_e dt, \quad (14)$$

with T_e and n_e the electronic temperature and density, and (A, η) parameters specific to the considered ion. Calculations in the following will be performed using the values

of Shull and van Steenberg (1982) and Landini and Fossi (1991). On the other hand, the dielectric recombination probability can be described by the following formula (see for instance Mazzotta et al., 1998):

$$dP_{\text{dielec}} = T^{-3/2} \sum_{j=1}^4 c_j \exp\left(-\frac{E_j}{k_B T_e}\right) n_e dt, \quad (15)$$

where the parameters c_j and E_j , $j = 1 \dots 4$, are specific to the studied ion.

Using the ionization and recombination processes described above, one can estimate the ionization state of a given element at equilibrium. This ionization state depends on the distance to the host star (d), on the electronic density (n_e), and on the electronic temperature (T_e). For instance, Fig. 13 provides the ionization equilibrium of Ca, Fe, Al and Si at 0.2 au from β Pic, for temperatures in the range $3 \cdot 10^3 - 10^6$ K and an electronic density of 10^6 cm^{-3} . Due to photo-ionization, the neutral fraction of these elements is always negligible. At low temperature ($T_e \leq 30\,000$ K), the dominant state can either be the singly-ionized form (e.g. Al^+) or the doubly-ionized (Fe^{2+} , Ca^{2+} , Si^+), depending on the photoionization rate of the singly-ionized form. At higher temperatures, strongly ionized species are produced: for instance, Si^{3+} (commonly observed in β Pic exocomets) is associated with temperatures of $\sim 10^5$ K. At such temperatures, the production of many other highly ionized species – Ca^{2+} , Ca^{3+} , Fe^{2+} , Fe^{3+} , Al^{3+} , ... – is expected. However, these species cannot be directly probed in β Pic exocomets, due to the absence of optically-allowed transition at wavelengths accessible with the Hubble Space Telescope.

Note that the values shown in Fig. 13 should be regarded as rough estimates. In particular, the EUV spectrum of β Pic – which drives the photoionization of most atoms and ions – was taken from Wu et al. (2025). Their reconstruction relies on a simplified chromospheric model, constrained by observations in C III and O VI emission lines with FUSE. The reliability of this spectrum, and therefore of our calculations, remains difficult to assess.

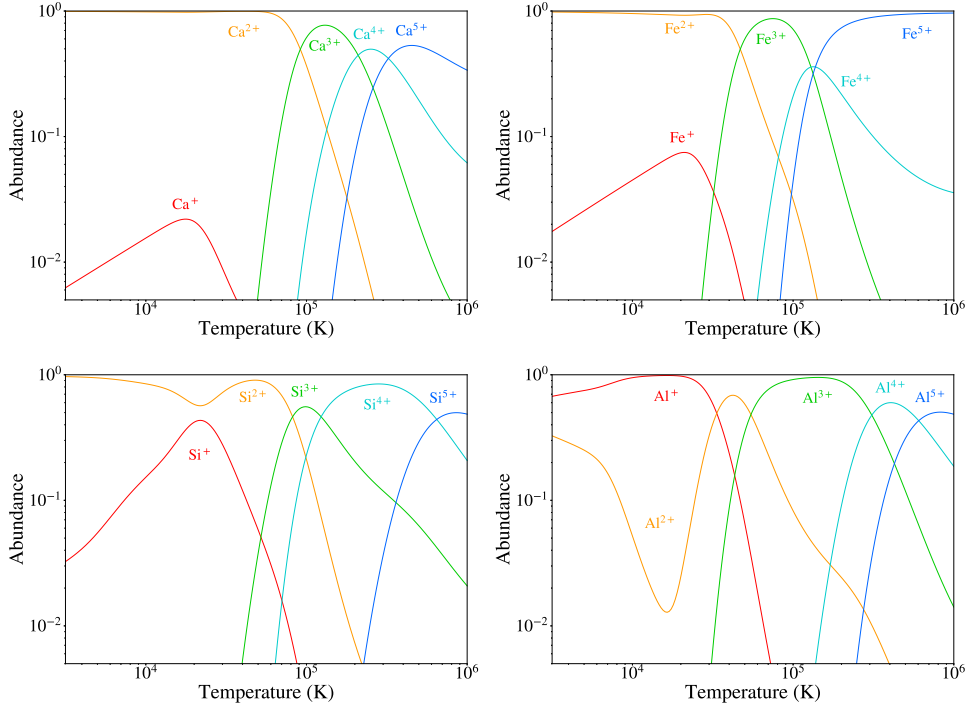


Fig. 13: Ionization equilibrium of a cometary plasma at 0.2 au from β Pic, as a function of T_e , for different elements. An electronic density $n_e = 10^6 \text{ cm}^{-3}$ was assumed.

3.4 Excitation

The various molecules, atoms, and ions that make up cometary tails can get excited. The excitation state of those particles can then be probed, using either emission lines (when observing Solar System comets) or absorption lines (when studying transiting exocomets). Fig. 14 provides two examples of excitation diagrams of species released by comets: the excitation diagram of atomic Fe in a solar comet (left), and the excitation diagram of Fe^+ in a β Pic exocomet (right).

The observed excitation diagram can be linked to the local properties of the gas. Indeed, there are two main ways of exciting a particle: by collisions (e.g. with electrons) and by photo-absorption. Collisional excitation is effective at sufficiently high densities, and tends to bring the excitation temperature of the gas close to the kinetic temperature. On the other hand, photo-excitation becomes effective at close comet-to-star distance, and tends to align the excitation temperature of the gas with the black body temperature of the radiation field.

In Solar System comets, the density of the outer coma is generally low enough that photo-absorption dominates the excitation of the gas (Bodewits et al., 2024). As a result, the excitation temperatures of atomic Ni and Fe are generally found to be close to the solar effective temperature (Manfroid et al., 2021, see also Fig. 14). However,

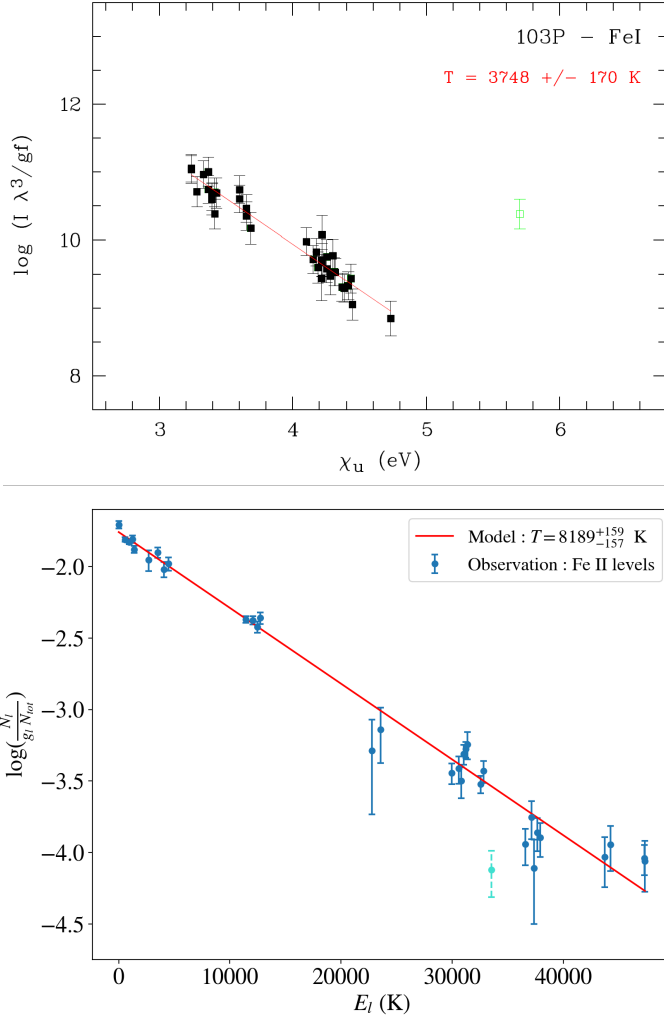


Fig. 14: Comparison of excitation diagrams of Fe and Fe⁺ in emission spectra of comets and absorption spectra of β Pic exocomets. For both diagrams, the y-axis shows the level abundance, and the x-axis shows the level energy. The slopes (red lines) are inversely proportional to the excitation temperature. **Left :** Excitation diagram of atomic Fe in 103P/Hartley 2, obtained through the analysis of the comet’s emission lines (taken from [Manfroid et al., 2021](#)). **Right :** Excitation diagram of Fe⁺ in a β Pic exocomet observed in 1997, derived from the exocomet’s absorption signatures in β Pic spectrum (taken from [Vrignaud and Lecavelier des Etangs, 2024](#)).

in the case of Solar comets, the gas excitation is strongly affected by the gas radial velocity relative to the Sun. Comets with heliocentric radial velocities near 0 km s^{-1} generally show lower excitation temperatures and weaker emission lines, because the deep Fe I and Ni I absorption lines in the solar spectrum reduce the flux available to

excite the main transitions of Fe and Ni (Swings effect; see also [Swings et al., 1941](#); [McKellar, 1944](#); [Furusho et al., 2005](#)). On the other hand, for redshifted or blueshifted comets the flux received in Fe I and Ni I lines is higher, and the gas therefore tends to be more excited and to have stronger emission lines.

A similar behavior is found in β Pic exocomets ([Vrignaud and Lecavelier des Etangs, 2024](#); [Vrignaud et al., 2025](#)): the excitation temperature is generally found to be close to 8000 K (see Fig. 14), which corresponds to the stellar effective temperature. In this case, the Swings effect is not important, because the stellar spectrum is smoothed by the rapid rotation of the star (130 km s^{-1}).

The predictability of the excitation state in cometary atmospheres is very useful for estimating the total abundances of atoms and ions, as the population of all the excited levels of a given particle can then be inferred from measurements in a small subset of levels. As an example, [Manfroid et al. \(2021\)](#) analyzed the emission spectra of a large set of Solar System comets to measure the abundance of Fe and Ni in their atmospheres, and deduce their Ni/Fe ratios. For comets at $\geq 1 \text{ au}$, this ratio is generally found to be super-solar, indicating that the nickel and iron atoms are not produced by direct sublimation of minerals, but instead by the dissociation of nickel carbonyls (e.g., $\text{Ni}(\text{CO})_4$) and iron carbonyls (e.g., $\text{Fe}(\text{CO})_5$), or by releasing Ni and Fe connected to PAHs ([Manfroid et al., 2021](#); [Bromley et al., 2021](#)). By contrast, refractory ions (e.g. Fe^+ , Ni^+ , Si^+ ...) are generally found in solar abundances in β Pic exocomets ([Vrignaud et al., 2025](#)), hinting that the refractories are produced from the complete sublimation of dust grains with solar composition.

Finally, it should be emphasized that probing the excitation state of a comet relies on different approaches whether the comet is observed in our own Solar System (using emission spectroscopy) or around another star (using absorption spectroscopy). In the first case, only the abundance of excited, unstable levels (with very short lifetimes and thus strong emissivity) can be directly probed, allowing to build the excitation diagram of the gas only above a few eV (see for instance the left panel of Fig. 14). Absorption spectroscopy, however, is sensitive to the abundance of little excited, metastable states with long radiative lifetimes. In this case, only the low-energy part of the excitation diagram can be recovered (see the right panel of Fig. 14), which has the advantage of directly probing the column densities of the most populated levels.

Detecting emission lines from exocomets appears to be difficult. To investigate what the spectra of neutral and ionized iron and nickel would look like around a given star, we used the photo-fluorescence model by [Bromley et al. \(2021\)](#). Results for AU Mic, the Sun and β Pic are provided in Fig. 15 (using again synthetic spectra from the PHOENIX library, and assuming a stellocentric distance of 0.1 au). For Fe II and β Pic, fluxes per particles as high as 10^{-18} J/s can be expected. Multiplying this value by the typical number of Fe^+ ions in a β Pic exocomet ($\sim 10^{37}$ [Vrignaud and Lecavelier des Etangs, 2024](#)) and assuming that the gas is observed from a distance of 19 pc (Sun - β Pic distance), this translates into maximum intensities of $10^{-14} \text{ erg/s/cm}^2/\text{\AA}$, or about 10^{-4} of the β Pic continuum in the Near-UV. This value is much below the typical noise level (1 %) obtained with the STIS spectrograph (*Space Telescope Imaging Spectrograph*, onboard the HST). In addition, emission features

from exocomets close to the star would very likely be mixed with absorption features of exocomets transiting the star, making it difficult to distinguish between the two.

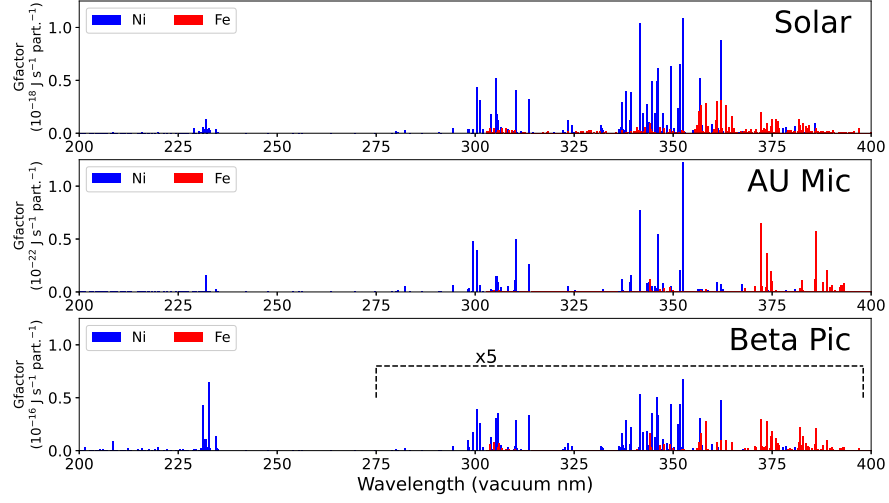


Fig. 15: Simulated photofluorescence emission spectra of Fe (red) and Ni (blue) for excitation by a solar spectrum (top), AU Mic (middle), and β Pic (bottom). Fluorescence model by Bromley et al. (2021).

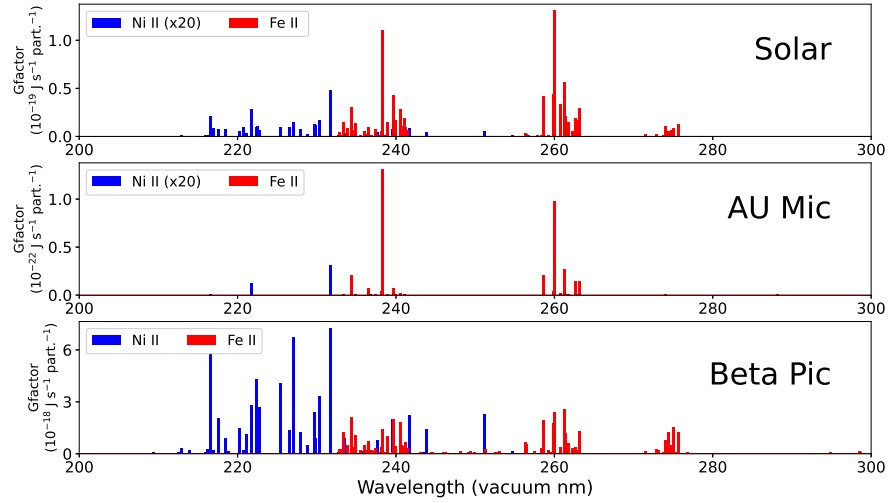


Fig. 16: Same as Fig. 15 for Fe II and Ni II. The line intensities of Ni II were multiplied by 20 around the Sun and AU Mic. Fluorescence model by Bromley et al. (2021).

4 Particle dynamics

Gas and dust particles in cometary atmosphere and tails are subject to various forces that influence their trajectories, in addition to the gravitational attraction from the star. This section reviews the main mechanisms that affect the dynamics of dust (Sect. 4.1) and gas (Sect. 4.2) released by exocomets, and how these mechanisms depend on the stellar environment.

4.1 Dust grain dynamics

4.1.1 Radiation pressure

Once liberated from the comet nucleus's gravity, and decoupled from the cometary gas, radiation pressure and gravity are the two main forces acting on dust grains in the tails of Solar System comets. The two forces are given by:

$$F_r = \frac{Q_{pr}}{c} \left(\frac{L_\odot}{4\pi r^2} \right) \pi R^2, \quad (16)$$

and

$$F_g = \frac{4}{3} \frac{GM_\odot}{r^2} \pi R^3 \rho, \quad (17)$$

where Q_{pr} is the radiation pressure scattering efficiency factor, r the heliocentric distance, R the dust grain radius, ρ the grain density, L_\odot the solar luminosity, M_\odot the solar mass, and G the gravitational constant (Finson and Probstein, 1968).

The ratio of radiation pressure to gravitational forces ($1 - \mu = F_r/F_g$, also often denoted β ; Finson and Probstein, 1968) determines whether a dust grain will remain on a bound orbit ($1 - \mu = \beta < 1$) or is swept out onto hyperbolic trajectories ($\beta > 1$). Since $F_r \propto R^2$ and $F_g \propto R^3$ for solid spherical grains, the β value of a dust grain scales as R^{-1} , meaning that smaller grains are more easily pushed away anti-sunward by radiation pressure than larger grains. For typical Solar System comets with visible dust tails, the radiation pressure forces acting on the grains in the tail are usually a few multiples larger than the magnitude of gravitational forces. To provide the reader with some context, the iconic comets C/2011 W3 (Lovejoy), C/2006 P1 (McNaught), and C/2014 Q1 (Pan-STARRS), which all entered the Near-Sun comet regime ($q < 0.307$ au; Jones et al., 2018), released dust grains with β values ranging from $\beta = [0.6, 2.5]$ (Sekanina and Chodas, 2012), $\beta = [0.2, 3.0]$ (Price et al., 2019), and $\beta \leq 0.2$ (Afghan et al., 2023) respectively. To estimate particle sizes, one can assume a density of 0.50 g cm^{-3} and take the reciprocal of the beta values (Burns et al., 1979). For C/2011 W3 (Lovejoy), C/2006 P1 (McNaught), and C/2014 Q1 (PanSTARRS), the observed β values correspond to estimated grain sizes $R = [0.4, 1.7] \mu\text{ m}$, $R = [0.3, 5.0] \mu\text{ m}$, and $R > 5.0 \mu\text{ m}$, respectively.

Whilst comets Lovejoy and McNaught produced visually spectacular dust tails with interesting features, comet C/1995 O1 (Hale-Bopp) could be a closer analogy to known exocomets, at least in terms of dust production. Comet Hale-Bopp was one of the most studied comets of the twentieth century and was easily visible with the naked eye, but unlike comets Lovejoy, McNaught, and PanSTARRS, Hale-Bopp's perihelion occurred much further out at $q \approx 0.9$ au. Analysis of Hale-Bopp images

when it was at heliocentric distances between 1.02 au and 1.28 au concluded that dust grain sizes ranged from $0.3 \mu\text{m}$ to $8 \mu\text{m}$ (Kharchuk et al., 2009). This corresponds to an upper limit of $\beta \approx 3$ which is comparable to the upper β values of comet McNaught. Furthermore, Hale-Bopp continued to remain active at greater distances and changes in the dust tail were observable for three years (Kramer et al., 2014). Analysis by Kramer et al. (2014) of Hale-Bopp beyond 20 au concluded that the observable dust tail consisted of grains with a typical β value of 0.3. Due to its impressive dust production, Hale-Bopp has been used in exocomet studies to model transits in photometric light curves. Luk'yanyk et al. (2024) showed that a comet similar to Hale-Bopp could be used to interpret a strong photometric transit observed in β Pic light curve (Zieba et al., 2019), assuming a transit distance of ~ 5 au and grains larger than $5 \mu\text{m}$ (see also Section 5.1).

The dependence of β on radiation pressure and gravitational forces means that this parameter will vary with stellar luminosity and mass. Assuming that physical grain properties, such as size and density, remain unchanged, the β value of a dust grain should scale as:

$$\frac{\beta_{\star}}{\beta_{\odot}} = \frac{L_{\star}}{L_{\odot}} \left(\frac{M_{\star}}{M_{\odot}} \right)^{-1}, \quad (18)$$

where β_{\star} is the β factor of the grain around a given star, and L_{\star} and M_{\star} are the stellar luminosity and mass, respectively. Applying this equation to our case study stars, we find $\beta_{\star}/\beta_{\odot} = 0.17$ for AU Mic, 4.97 for β Pic, and 0.02 for WD 1145+017. Thus, the $5 \mu\text{m}$ grains ($\beta_{\odot} \approx 0.3$) used by Luk'yanyk et al. (2024) to model β Pic exocomets would possess typical β values of $4.97 \times 0.3 \approx 1.5$ in the β Pic system.

It should also be noted that, at small astrocentric distances, a dust grain is no longer exposed to the full area of the stellar disk: stellar photons impact the dust grains with a range of incident angles. Consequently, the typical β calculation is no longer suitable for dust grains close to a star, as equation (16) assumes the star behaves as a point source for all heliocentric distances. Thus, an empirical geometric correction accounting for the deviation of radiation pressure forces from the inverse square law and the reduction in visible area of the disk is required. Such correction can be parameterized as:

$$\log_{10}(\Gamma) = \sum_{i=0}^4 a_i x^i, \quad (19)$$

where $a_0 = -0.353$, $a_1 = 0.656$, $a_2 = -0.477$, $a_3 = 0.159$, $a_4 = -0.020$ are empirically derived, and $x = \log_{10}(r_h/R_{\star})$ (Hanlon and Jones, 2025). This correction becomes necessary within $\sim 200 R_{\star}$ (~ 1 au in the Solar System). It is particularly useful when modeling the dynamics of dust grains at very small stellar-centric distances, as the Γ parameter can be multiplied by the standard β factor to produce an effective β value, given by $\beta_{\text{eff}} = \Gamma\beta$. For distances ranging from $6R_{\star}$ to $215R_{\star}$, Γ varies from 0.86 to 1.00 (Hanlon and Jones, 2025).

Modeling of Solar System cometary dust tails often implements equations 16 and 17. As radiation pressure forces and gravity operate in opposite directions, the

acceleration of a dust grain is given by:

$$a = \frac{GM_*}{r^2} (1 - \beta_{\text{eff}}). \quad (20)$$

Such an approach can provide an insight into where grains with different β values are found within the dust tail. In such cases, lines connecting grains of equal β are known as syndynes and lines connecting grains of the same age are referred to as synchrones (Finson and Probstein, 1968). Figure 17 displays the simulated dust tail of a comet with the same grain properties as C/2006 P1 (McNaught) orbiting AU Mic, the Sun, and β Pic respectively. The tails were simulated by numerically modelling grain dynamics via the RK4 method with grains being assigned the Solar System β values of Comet McNaught. For AU Mic and β Pic these were scaled using equation (18). We note that the tail length and width increases rapidly with the stellar size and luminosity. These differences in shape arise from dust grains having a variety of starting conditions when ejected from the nucleus. In general, the orbital velocity of cometary nuclei increases with stellar mass, which in turn increases the initial velocity of an ejected dust grain. Coupled with variations in radiation pressure (which increases with stellar luminosity), this means that each star imparts a unique set of motion vectors to dust grains ejected from cometary nuclei. Around low-mass and low luminosity stars such as AU Mic, orbital velocity and radiation pressure are significantly reduced compared to an exocomet at the same distance in the β Pic system. On the other hand, dust grains around more massive and luminous stars have larger initial velocities and experience greater anti-sunward acceleration.

Here, it should be noted that this form of analysis does not account for the dust production of the comet; a complete study of an exocometary dust tail would need to consider the dust production and distribution, as discussed in Sect. 2.2.2.

4.1.2 Rocket Effect

The sublimation of ices at the surface of a dust grain can produce a noticeable rocket effect that accelerates dust particles, due to the anisotropy of the vapor ejection (which is favorably released on the sunlit side of the grain). For spherical grains, the resulting acceleration is given by

$$a_{\text{rocket}} = \frac{3\mu m_H Z v_{\text{th}} f_{\text{ice}}}{4\rho_p a} = 1.1 \times 10^{-18} \frac{Z}{\rho_p a}, \quad (21)$$

where μ is the molecular weight of the sublimating ice, m_H is the mass of hydrogen, Z is the sublimation rate of the individual particle ($\text{molecules cm}^{-2} \text{s}^{-1}$), v_{th} is the mean thermal expansion speed of the gas, f_{ice} is the ice fraction of the particle, ρ_p is the particle density, and a is the particle radius (Kelley et al., 2013). All parameters are expressed in cgs units.

Similarly to how the magnitude of radiation pressure and gravitational forces are compared using a dimensionless ratio, α is used to compare the relative magnitude of rocket effect forces to gravitational forces such that (Reach et al., 2009; Kelley et al.,

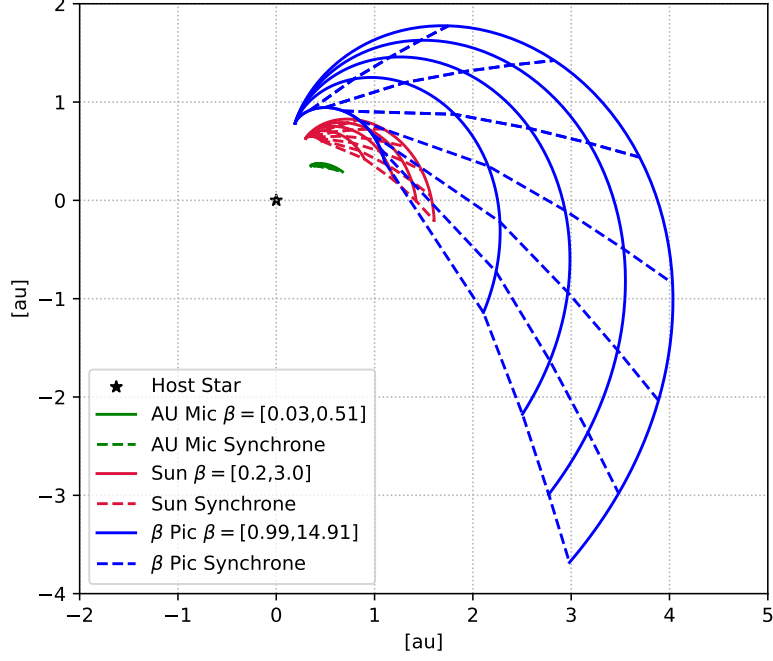


Fig. 17: The simulated shape of an exocomet dust tail viewed above the plane of the orbit in the AU Mic, Solar System, and β Pic systems. The solid lines connect grains with the same β values and the dashed lines connect grains of constant age. In each scenario the comet was simulated for 28 days and passed through a periastron of 0.50 au on day 14.

2013)

$$\alpha = 2.238 \times 10^{26} \frac{3\mu m_H Z v_{th} f_{ice}}{4GM_{\odot} \rho_p a}, \quad (22)$$

where parameters are again expressed in cgs units. For a particle with a radius of 10 cm and assuming that only water ice is ejected, Kelley et al. (2013) found that α can be as high as 0.27, which is many orders of magnitude greater than the radiation-driven β value of the dust particle ($\beta \approx 1 / (1 \times 10^4 [\mu\text{m}]) = 1 \times 10^{-4}$).

4.1.3 Charged grain motion

The Lorentz force is another force which can alter the structure of a cometary dust tail. In the Solar System, studies show correlations between the realignment of dust tail features and magnetic structures found in the solar wind (Price et al., 2019, 2023).

Since the Debye length (distance over which electrostatic effects persist) of a dust grain is significantly smaller than the typical distance between grains, charged dust grains can be considered as individual and isolated charges. As such, the Lorentz force acting on a dust grain is given by:

$$\vec{F}_L = q \left(\vec{E} + \vec{v}_d \times \vec{B} \right) \quad (23)$$

where v_d and q are grain velocity and charge and \vec{E} , and \vec{B} are the electric magnetic fields. The electric field ‘felt’ by a dust grain is dependent on the velocity of the solar wind (\vec{v}_{sw}) and its magnetic field such that $\vec{E} = -\vec{v}_{\text{sw}} \times \vec{B}$. Substituting this into equation (23) leads to:

$$\vec{F}_L = q \left(-\vec{v}_{\text{sw}} \times \vec{B} + \vec{v}_d \times \vec{B} \right) = q \left(\vec{v}_{\text{rel}} \times \vec{B} \right) \quad (24)$$

where $\vec{v}_{\text{rel}} = \vec{v}_d - \vec{v}_{\text{sw}}$. Further assuming $\vec{v}_{\text{sw}} \gg \vec{v}_d$, the relative velocity term becomes $\vec{v}_{\text{rel}} \approx -\vec{v}_{\text{sw}}$, resulting in $\vec{F}_L \approx -q \left(\vec{v}_{\text{sw}} \times \vec{B} \right)$.

From a Solar System perspective, Lorentz forces are associated with lofting (see section 2.2.2) and the realignment of fine-scale structures in the dust tails of highly active Solar System comets; these events being associated with Heliospheric Current Sheet (HCS) crossings (Price et al., 2019, 2023) where the polarity of the Interplanetary Magnetic Field (IMF) abruptly changes. Therefore, unlike plasma tails, the impact of the heliospheric magnetic field on the large-scale structure of a dust tail is relatively modest, having only been observed in few cases (Kramer et al., 2014; Price et al., 2019, 2023). In the AU Mic system, however, the magnetic environment is much stronger, with an average intensity of 550 ± 30 G (Donati et al., 2023, about 275 times more than the Sun). Even though it is difficult to fully comment on the electrostatically-driven motion of exocometary dust grains in this system, the dusty tails of hypothetical AU Mic exocomets could be severely disrupted from the interaction with their star’s magnetic field.

Regarding the β Pic system, the stellar magnetic field is poorly constrained (Zwintz et al., 2019, proposes an upper limit field strength of 300 G, or $\sim 150\times$ the solar value). In this case, interactions with magnetic fields are usually not taken into account when modeling the light curves of exocomets. Finally, about 20 % of white dwarfs have detectable magnetic fields (Ferrario et al., 2015). As a result, most studies about polluted white dwarfs don’t include magnetic fields. However, it has been suggested that the lifetime of dusty debris discs around white dwarfs could be significantly reduced if the star is magnetized (especially when $B > 10$ kG; see Hogg et al., 2021), due to an increase of the accretion rate of the grains.

4.1.4 Poynting-Robertson drag

The Poynting-Robertson (PR) effect arises when incident photons gradually decrease the angular momentum of a dust grain, causing it to spiral onto the surface of the host star (e.g. Ragoth and Kahler, 2003; Klačka et al., 2014; Klačka and Kocifaj, 2008). The acceleration of a dust grain caused by radiation pressure and the PR effect is given by:

$$\vec{a} = \Gamma \beta \frac{GM}{r^2} \left[\left(1 - \frac{\vec{v} \cdot \vec{e}}{c} \right) \vec{e} - \frac{\vec{v}}{c} \right]. \quad (25)$$

where r , \vec{v} , and \vec{e} are the distance from the Sun, the particle velocity, and the particle positional unit vector respectively (Klačka et al., 2014), β is the standard radiation pressure factor, and $\Gamma \leq 1$ is the correction factor given in Eq. 19.

This form of the acceleration can be used to derive the secular, or time-averaged, change of orbital elements of dust grains. The result is a pair of coupled ordinary differential equations for the dust grain’s semimajor axis, a and its eccentricity, e (Wyatt and Whipple, 1950):

$$\frac{da}{dt} \approx - \left(\frac{1}{c^2} \right) \frac{3(2 + 3e^2) L_\star}{16\pi R \rho a (1 - e^2)^{3/2}} \quad (26)$$

$$\frac{de}{dt} \approx - \left(\frac{1}{c^2} \right) \frac{15eL_\star}{32\pi R \rho a^2 \sqrt{1 - e^2}}, \quad (27)$$

where L_\star is the luminosity of the star, c is the speed of light, and again R and ρ are the radius and density of the dust grain. The equations are exact when $\Gamma = 1$.

Poynting-Robertson drag has a minimal effect on Solar System comets, as the timescale for a grain to spiral inward toward the Sun is significantly longer than the rapid motion changes induced by radiation pressure or solar wind interactions. However, this effect becomes more important when considering stars such as white dwarfs, which can be windless systems with minimal radiation pressure (e.g., Rafikov, 2011; Malamud et al., 2021; Veras et al., 2022; Okuya et al., 2023). In this case, dust grains will be slowly accreted towards the star, ultimately leading them to contaminate the white dwarf’s photosphere.

4.2 Gas/Ion dynamics

We now investigate the various processes that drive the dynamics of gaseous particles (molecules, atoms, or ions) in exocometary tails.

4.2.1 Radiation pressure

Like dust grains, gas particles experience radiation pressure, which push them in the anti-stellar direction as they absorb photons. This pressure depends both on the stellar spectrum - the brighter the star, the stronger the radiation pressure - and on the spectral properties of the absorbing species.

In the case where a gas particle is excited to a specific energy level and exhibits a single spectral line, its β value—defined as the ratio of radiation pressure to gravitational force—is given by (e.g., Lagrange et al., 1995):

$$\beta = \frac{R_\star^2}{GmM_\star} \frac{1}{4\pi\epsilon_0} \frac{\pi e^2}{m_e c^2} \pi I_\star(\lambda) \frac{\lambda^2}{c} f, \quad (28)$$

where m is the mass of the absorbing particle, M_\star is the stellar mass, R_\star is the stellar radius, λ is the wavelength of the transition, I_\star is the stellar specific intensity per unit wavelength, f is the oscillator strength of the line, ϵ_0 is the vacuum permittivity, m_e is the electron mass, and e is the elementary charge. The β factor can also be expressed as a function of the stellar flux ϕ_λ received on Earth (in $\text{erg/s/cm}^{-2}/\text{\AA}$) and our distance to the star d , using:

$$\phi_\star(\lambda) = \left(\frac{R_\star}{d} \right)^{-2} \pi I_\star(\lambda), \quad (29)$$

which gives:

$$\beta = \frac{d^2}{GmM_\star} \frac{1}{4\pi\epsilon_0} \frac{\pi e^2}{m_e c^2} \frac{\lambda^2}{c} \phi_\star(\lambda) f. \quad (30)$$

Numerically, Eq. 30 becomes (Lagrange et al., 1995):

$$\beta = 0.509 f \left(\frac{d}{1 \text{ pc}} \right)^2 \left(\frac{m}{m_u} \right)^{-1} \left(\frac{M_\star}{M_\odot} \right)^{-1} \left(\frac{\lambda}{2000 \text{ \AA}} \right)^2 \times \frac{\phi_\star(\lambda)}{10^{-11} \text{ erg cm}^{-2} \text{ s}^{-1} \text{ \AA}^{-1}}. \quad (31)$$

In cases where the species has multiple spectral lines, the total β value is obtained by summing Eq. 31 over all lines. If the species is also distributed over multiple excitation levels (as for instance Fe^+ , Fig. 14), an effective β value can be calculated by averaging the β values across the different levels, weighted by their relative abundances. Assuming that the gas is characterized by an excitation temperature T , this is:

$$\beta_{\text{eff}} = \frac{1}{Z(T)} \sum_{\text{lines}} \beta g e^{-\frac{E}{k_B T}}, \quad (32)$$

where g and E denote the lower level multiplicity and lower level energy of each line, k_B the Boltzmann constant, and $Z(T)$ the partition function.

Since the excitation temperature in cometary tails can be approximated by the stellar effective temperature (Sect. 3.4), Eq. 32 allows us to easily estimate the radiation pressure felt by a given atom or ion, around a given star. For instance, Fig. 18 provide the β values of neutral and ionized Ca and Fe, around our four case-study stars. For AU Mic, β Pic and 1145+017, the excitation temperature was set equal to the stellar effective temperature, following the results of Vrignaud and Lecavelier des Etangs (2024) for β Pic. For the Sun, we used an excitation temperature of 4000 K, as found in Manfroid et al. (2021).

The efficiency of radiation pressure strongly depends on the spectral type of the host star: while around AU Mic the radiation pressure felt by Ca and Fe is rather weak ($\beta < 1$, Fig. 18), it becomes significant around the Sun ($\beta \approx 1$) and largely dominant around β Pic ($\beta = 40 - 100$ for Ca^+ , 5-10 for Fe^+). Due to its small size (0.012 R_\odot), the white dwarf WD 1145+017 exerts a much weaker radiation pressure ($\beta \sim 0.1$ for Ca^+ and Fe^+). Such differences could induce strong contrasts between the dynamics of exocometary tails in those four systems, even though the motion of the most accelerated ions (e.g. Fe^+ , Ca^+) could be slowed down by drag forces induced by other species (e.g. C^+ ; see for instance Brandeker (2011) and Sect. 4.2.3).

The radiation pressure felt by a gas particle can be highly sensitive to its radial velocity, particularly in the presence of absorption lines in the stellar spectrum. These absorption lines reduce the flux at the main transitions of the considered species, reducing the radiation pressure felt by the gas when its radial velocity is low. This effect is particularly strong for slowly rotating stars (e.g., the Sun or AU Mic), where

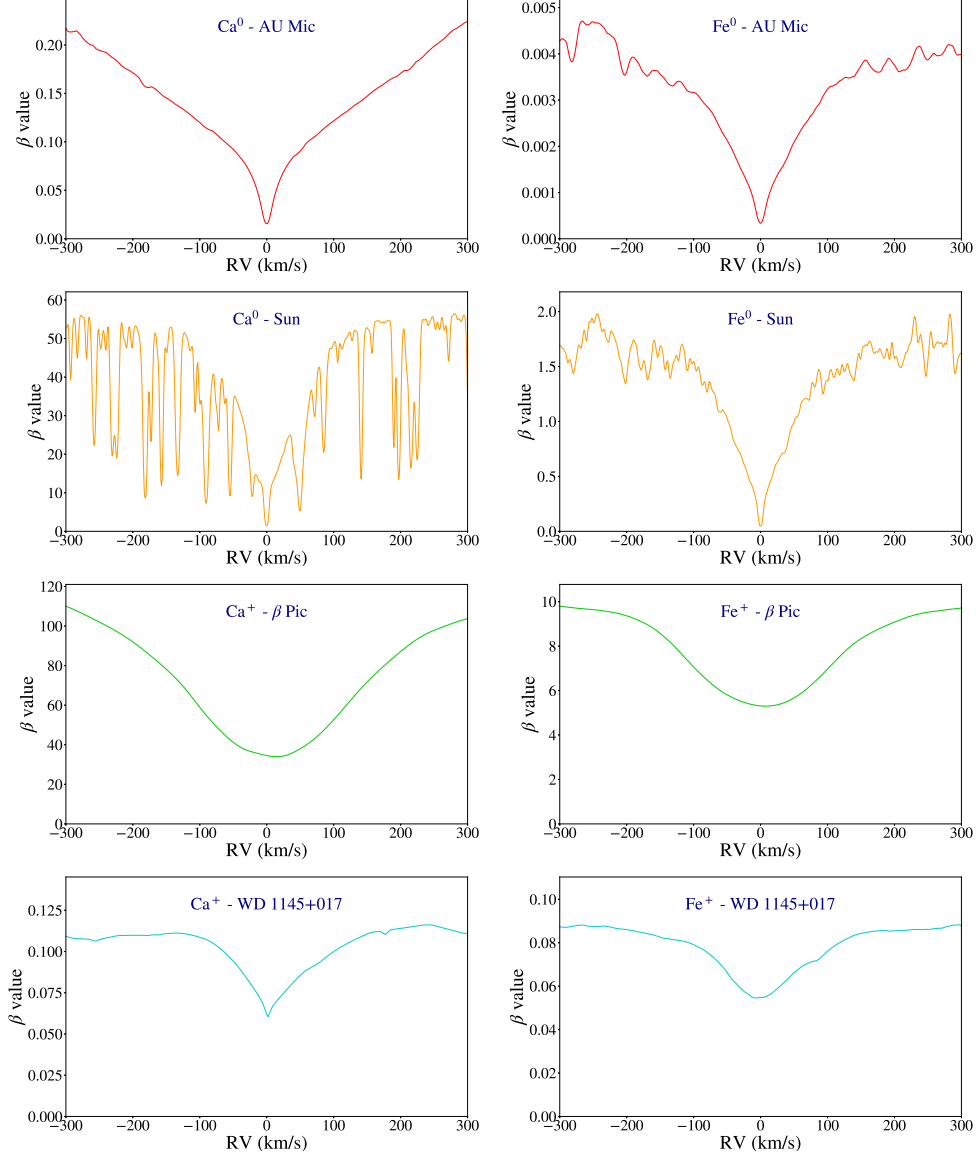


Fig. 18: Radiation pressure-to-gravity ratio of Ca and Fe around AU Mic and the Sun, and of Fe^+ and Ca^+ around β Pic and WD 1145+017, as a function of the radial velocity.

photospheric lines are very deep. For instance, the β value of neutral Fe around the Sun can range from 0.05 to 1.5, depending on the radial velocity of the gas. A similar effect is observed for atomic sodium (Spinrad and Miner, 1968; Brown et al., 1998). In contrast, this effect is less important in the β Pic system due to the fast rotation

of the host star (130 km s^{-1}), even though the β value of Ca^+ still varies from ~ 35 at 0 km s^{-1} to ~ 100 for highly red or blue-shifted gas.

Finally, it should be noted that the radiation pressure acting on a given particle depends significantly on the location of its main spectral lines: species with lines further in the UV will generally feel a weaker radiation pressure than species with allowed transitions in the optical or NUV. This explains, for instance, the very weak radiation pressure felt by Si^+ around $\beta \text{ Pic}$ ($\beta = 0.05 - 0.1$): the main Si II lines are all located below 1500 \AA , where the flux of $\beta \text{ Pic}$ is rather weak. On the contrary, Fe^+ ions experience a much larger pressure ($\beta = 5 - 10$) thanks to the strong Fe II transitions in the NUV ($2300\text{--}2800 \text{ \AA}$).

4.2.2 Impact of stellar winds

Stellar winds are continuous radial outflows emanating from the atmospheres of stars. In many cases, they play a significant role in the production and shaping of exocomet tails. The nature of these winds vary greatly in terms of density, speed, dynamic pressure ($10^{-10} - 10^1 \text{ Pa}$ across all systems), and magnetic field, which in the Solar System is referred to as the interplanetary or heliospheric magnetic field. We refer the reader to [Bennett \(2010\)](#) and [Vidotto \(2021\)](#), and references therein, for relevant reviews of this research field. In brief, stellar winds in extrasolar systems can differ dramatically from the collisionless solar, and the expansive studies undertaken of ion tails' formation and interactions with the solar wind are therefore not always readily comparable with all exocomet systems, e.g. [Strøm et al. \(2020\)](#).

Stellar winds affect the dust and gas around exocomets in multiple ways. First, the wind interacts with the atmosphere of these bodies by picking up charged ions. Second, in the Solar System, the solar wind ($\sim 2 \times 10^{-14} \text{ M}_\odot/\text{yr}$) contributes a few percent to the production of ion tails in comets: charge exchange between solar wind protons and neutral gas species from the comae produces new ions (CO^+ , H_2O^+), which are then accelerated in the anti-solar direction (the rest of the ion tails are produced from photo-ionization, [Combi et al., 2004](#)). In addition, coronal mass ejections (CME) can strongly increase the dissociation rates in comae, mostly through electron impact (e.g., [Noonan et al., 2018](#), for 67P/Churyumov–Gerasimenko). Third, charge exchange between highly charged ions in the solar wind and neutral gases surrounding comets results in highly characteristic X-ray emission. In the Solar System, comets produce up to 1 GW in X-rays ([Dennerl et al., 2012](#)), and similar interactions between stellar wind ions and interstellar neutrals have been detected around three main-sequence stars ([Kislyakova et al., 2024](#))

Around $\beta \text{ Pic}$, studies indicate that the effect of the stellar wind ($\sim 10^{-14} \text{ M}_\odot/\text{yr}$, [Bruhweiler et al., 1991](#)) on ionic clouds is negligible, as their shape is primarily sculpted by radiation pressure ([Beust et al., 2001](#)). Some other young stars, however, can exhibit strong mass loss rates. This is the case of Herbig stars (pre-main sequence stars younger than 10 Myr, with stellar type A or B), which exhibit stellar winds in the range $10^{-9} - 10^{-7} \text{ M}_\odot/\text{yr}$. Some of these stars have been hypothesized to host exocomets based on variable absorption signatures observed in refractory species (e.g. HD 100546, [Grady et al., 1997](#)). However, [Beust et al. \(2001\)](#) predicted that objects in such systems would be very difficult to detected, as their gaseous tails would be

confined to compact regions by the intense stellar wind and would therefore cover only small fractions of the stellar disc. [Beust et al. \(2001\)](#) provided a maximum loss rate of $10^{-10} M_{\odot}/\text{yr}$ for the stellar wind above which no exocomets can be detected using absorption spectroscopy (e.g. in Mg II h & k lines).

Another interesting case is AU Mic, a young (23 Myr) M-dwarf surrounded by an edge-on debris disc. Although the star has a relatively moderate stellar wind ($1 - 2 \times 10^{-13} M_{\odot}/\text{yr}$, [Alvarado-Gómez et al., 2022](#)), it exhibits highly energetic flares and frequent coronal mass ejections, which release large amount of material at a daily frequency ($10^{18} \text{ g} = 10^{-15} M_{\odot}$ or 10^{35} erg for typical CME events, e.g. [Alvarado-Gómez et al., 2022](#)). The effect of such events on potential exocomets has not been studied yet, but it is likely that they would significantly affect the shape and composition of comae and tails, by increasing the ionization rate and rapidly blowing the produced ions in the anti-stellar direction.

As stars evolve beyond the main sequence, their mass loss rates increase dramatically during certain evolutionary phases. The red giant branch and asymptotic giant branch (AGB) phases are particularly significant, as mass loss rates can rise by several orders of magnitude. During the AGB phase, stellar winds can reach peak rates of $10^{-5} M_{\odot}/\text{yr}$, a value which is approximately 8 orders of magnitude higher than the current solar wind. Such stellar winds would probably have a dramatic effect on exocomets, by rapidly sweeping away the evaporated material. Yet, the gas/ion interactions in this violent environment, coupled with orbital shifts of exocomets due to the stellar mass loss, not only could help explain nebular structures around young white dwarfs ([Marshall et al., 2023](#)), but also help determine the distribution of reservoirs of planetary material which may eventually pollute the white dwarf (see the accompanying chapter [Bannister et al., 2025](#))).

4.2.3 Drag forces in atomic and plasma tails

The various forces detailed above (radiation pressure, ion pick-up, stellar wind pressure, magnetic forces) are generally specific to the atom or ion they act on: two different ions will usually undergo different accelerations, depending on their masses, charges or spectral lines. Consequently, one may expect to observe a wide range of dynamics among the species released by exocomets, with, for example, species subject to greater radiation pressure expanding over larger distances. However, the motion of ions and atoms in cometary tails is also influenced by collisions with other particles, which induce drag forces and tend to couple their dynamics. These drag forces have been studied in previous studies of β Pic exocomets, in particular [Beust et al. \(1989\)](#), [Beust et al. \(1990\)](#) and [Beust et al. \(2001\)](#), where further information on some of the effects below may be found.

Motion of particles in neutral gas: A particle (of mass m_1) evolving in a field of neutral atoms of mass m_2 experiences a drag force, due to collisions with the field particles. This drag force can be described as (see for instance [Kwok, 1975](#); [Lagrange et al., 1998](#)):

$$\vec{f}_{\text{col}} = \left. \frac{d\vec{p}_1}{dt} \right|_{\text{col}} = -k_{\text{col}}\vec{v}_1, \quad (33)$$

with \vec{v}_1 and \vec{p}_1 the velocity and momentum of the considered particle relative to the neutral gas, and k_{col} the drag coefficient, given by:

$$k_{\text{col}} = \pi a_2^2 \mu n_2 \sqrt{v_T^2 + v_1^2}, \quad (34)$$

where a_2 is the radius of the field atoms, n_2 their volume density, $\mu = \frac{m_1 m_2}{m_1 + m_2}$, and v_T the sound speed in the gas.

If the considered particle is an ion, it will also induce a dipole on the field atoms, increasing the dragging coefficient. This additional drag force can be expressed as (McDaniel, 1964; Beust et al., 1990):

$$\vec{f}_{\text{dip}} = \frac{d\vec{p}_1}{dt} = -k_{\text{dip}}\vec{v}_1, \quad (35)$$

with:

$$k_{\text{dip}} = n_2 \pi \sqrt{\frac{4\mu q_1^2 \alpha_2}{4\pi\epsilon_0}}, \quad (36)$$

and where q_1 is the charge of the ion and α_2 the polarizability of the field atoms. For a gas with an arbitrary density, the total drag coefficient is obtained by summing Eqs. 33 and 35 over all the different species making up the gas.

The intensities of the two drag forces are illustrated in Fig. 19 for Ca^+ (top panel), assuming a surrounding fluid of neutral hydrogen with densities of 10^4 or 10^8 cm^{-3} . We note that, for typical thermal or orbital velocities ($\sim \text{km s}^{-1}$), the contributions of 33 and 35 are generally comparable, although dipole-induced interaction dominate for velocities below 50 km s^{-1} . We also note that at low densities (e.g. 10^4 cm^{-3}), dragging forces are rather weak, allowing the particles to accelerate to large velocities ($> 100 \text{ km s}^{-1}$) when undergoing strong radiation pressure (see for instance Beust et al., 1989, for the motion of Ca^+ ions in atomic hydrogen gas).

Motion of ions in plasma: The motion of an ion in a dense, ionized exocometary tail was studied by Beust et al. (1990). The interaction between a charged particle #1 (of charge q_1 and mass m_1) and a field of particles #2 (of charge q_2 and mass m_2) is described by the Coulomb potential. This interaction induces a drag force on particle #1, which can be expressed as (see Beust et al., 1989, 2001):

$$\vec{f}_{\text{coul}} = \frac{d\vec{p}_1}{dt} = -2\pi n_2 \mu \frac{C^2}{v_1^2} \ln\left(\frac{\lambda_D^2 v_1^4}{C^2} + 1\right) \frac{\vec{v}_1}{v_1}, \quad (37)$$

where v_1 is the velocity of the considered ion relative to the plasma, n_2 the volume density of particle #2, $\mu = \frac{m_1 m_2}{m_1 + m_2}$, $C = \frac{1}{4\pi\epsilon_0} \frac{q_1 q_2}{\mu}$, and where $\lambda_D = \sqrt{\epsilon_0 k_B T_e / (n_e e^2)}$ is the Debye length of the plasma, with T_e the electronic temperature and n_e the electronic density.

Fig. 19 (bottom panel) provides the norm of the drag force undergone by Ca^+ ions in a plasma of ionized hydrogen of various densities, as a function of the Ca^+ velocity relative to the plasma. The drag force is generally very strong, exceeding by several orders of magnitude the radiation pressure (which itself is very strong compared to other exocometary species). For typical thermal velocities ($\sim \text{km s}^{-1}$), the radiation pressure can overcome the drag force only if the local density is very low ($n_{\text{H}^+} < 10^2 \text{ cm}^{-3}$). Above this density, the dynamics of all ions in the plasma are coupled, and the plasma behaves as a single fluid. The effective radiation pressure acting on the gas is then the average of the radiation pressures felt by individual species (Ca^+ , Fe^+ ...).

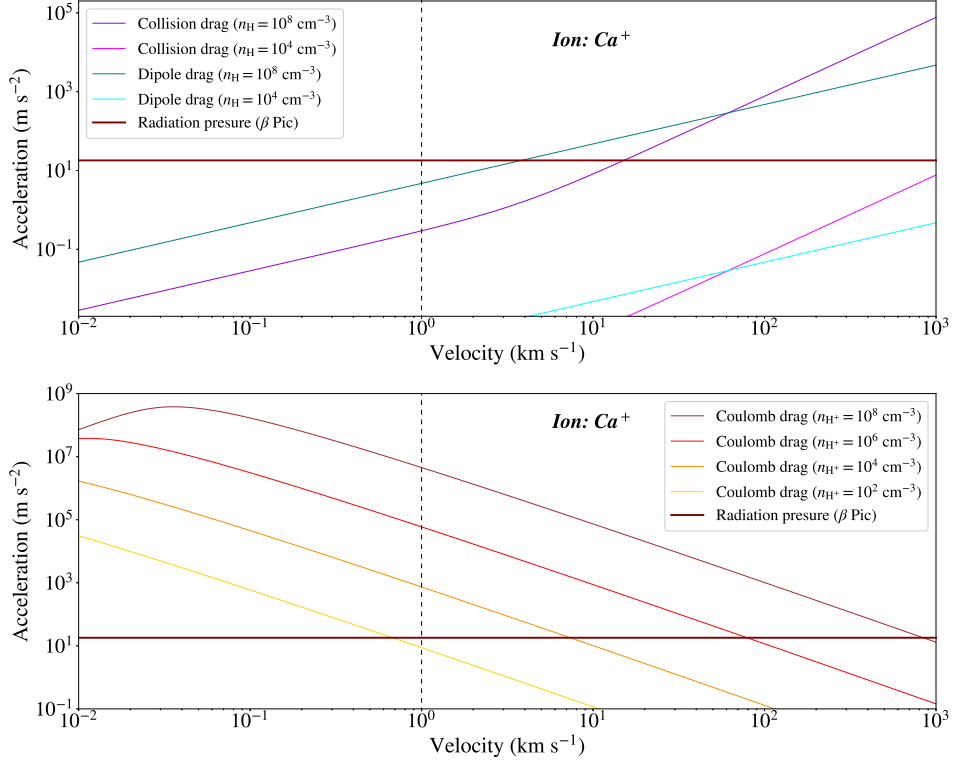


Fig. 19: Top: Drag forces acting on Ca^+ ions in a neutral gas of hydrogen, as a function of the Ca^+ velocity relative to the gas. The black, brown line shows the radiation pressure felt by Ca^+ ions at $20 R_{\star}$ from $\beta \text{ Pic}$, using a β value of 35 (zero-velocity gas). The vertical, dashed line indicates a velocity of 1 km s^{-1} , typical of thermal movements. Note that only the norm of the acceleration is shown: for drag forces, the acceleration is opposed to the motion of the ion relative to the surrounding medium, and for radiation pressure the acceleration is directed in the anti-stellar direction.

Bottom: Coulomb drag force acting of Ca^+ ions in a plasma of ionized hydrogen, as a function of the Ca^+ velocity relative to the plasma. An electronic temperature of 1000 K was assumed. The electronic density (n_e) was taken to be equal to the hydrogen density (n_{H^+}). Horizontal and vertical lines are identical to the top panel.

The ionization state and density of a cometary tail/atmosphere are thus key properties that influence the dynamics of individual particles. If the gas is neutral or diluted, drag forces are weak, and the dynamics of individual species rapidly decouple as they expand away from the nucleus. In this case, the motion of particles is set by their own radiation pressure and/or by the forces induced by the stellar wind. This is typically the case for the thin plasma tails of Solar System comets. On the contrary, in dense, ionized tails, drag forces efficiently couple the dynamics of all ionized species, maintaining them within the same fluid over large distances. This behavior has been observed for β Pic exocomets (Vrignaud and Lecavelier des Etangs, 2024): cometary signatures in Fe II, Ni II, Mn II and Si II lines are very well correlated, showing that these ions can remain well-mixed over distances of several stellar radii despite undergoing different radiation pressures.

4.2.4 Gas compression

The detection of highly ionized species (Al^{2+} , Si^{3+} , C^{3+}) in β Pic exocomets has long remained puzzling, since the production of those ions is not expected from photo-ionization (Sect. 3.3). Much work has been conducted (Beust et al., 1989, 1990; Beust and Tagger, 1993) to explain their presence in exocometary tail. The main conclusion of these studies is that highly ionized species are produced from collisional ionization in a dense, hot 'bow shock', located at the front of the comae. This shock is created by a combined effect of radiation pressure — which accelerates the gas in the anti-stellar direction, Sect. 4.2.1 — and drag forces with a neutral medium — which resist to the movement of ions, Sect. 4.2.3. These mechanisms strongly compress the gas, allowing it to reach high temperatures ($> 30\,000$ K; Beust and Tagger, 1993) at which Al^+ is rapidly ionized into Al^{2+} .

In Beust and Tagger (1993), the dynamics of cometary ions is controlled by radiation pressure and drag forces. The drag forces are assumed to be induced by a surrounding cloud of neutral hydrogen (see Eqs. 33, 35, and the first panel of Fig. 19). An estimate for the size of the bow shock (which depend on the considered ion, e.g. Ca^+) is then given by:

$$r = \sqrt{\frac{Fv_e}{\beta g} \left(1 + \frac{a_2}{a_1}\right)}, \quad (38)$$

with F a factor characterizing the sensitivity of the studied ion to collisions with neutral hydrogen, v_e the expansion velocity of the hydrogen cloud, β the radiation pressure to gravity ratio (Sect. 4.2.1), g the stellar gravity acting on the comet, and a_1 , a_2 the sizes of the two layers used to model the shock front. This formula was used by Kiefer et al. (2014) to infer basic properties of β Pic cometary nuclei from their covering factor in Ca II lines.

It should be noted, however, that the model proposed by Beust and Tagger (1993) could be refined. In particular, the assumption that ion trajectories (Ca^+ , Mg^+ , ...) are primarily slowed by collisions with neutral hydrogen is debatable, as observations indicate that most of the gas in β Pic exocomets is ionized, implying significantly stronger drag forces than previously considered (Sect. 4.2.3). In fact, the observed tendency of ions to remain well-mixed in exocometary tails (Vrignaud and Lecavelier des Etangs,

2024) suggests that ion-ion interactions play a dominant role in the dynamics of cometary tails. In addition, the role of photoionisation was probably under-estimated in the study of [Beust and Tagger \(1993\)](#), as our calculations showed that this mechanism can also produce Al^{2+} if the comet is sufficiently close to the star. Despite these limitations, the [Beust and Tagger \(1993\)](#) model provides a valuable foundation for developing more accurate descriptions of the physics of β Pic exocomets.

5 Case studies

This section provides a comparative analysis of comet-like activity in four different stellar environments: the Sun, AU Mic, β Pic, and WD 1145+017. A summary of the main properties of (exo)comets in the four systems is also presented in [Table 6](#), allowing for a direct comparison.

5.1 Solar System comets

The observable characteristics of comets in our own Solar System are readily discussed in many works, notably in *Comets III* (see also the reviews of [Biver et al., 2022](#); [Bodewits et al., 2024](#); [Engrand et al., 2023](#); [Knight et al., 2024](#)). Here, we consider them from a different perspective: if we were to study the Sun from another Solar System, what would be the potential observable signatures of our comets and other small bodies?

The most obvious candidates for consideration are the various populations of near-Sun comets (cf. reviews by [Marsden, 2005](#); [Jones et al., 2018](#)), since these are nominally most analogous to the β Pic exocomets: they share similar periastron distance (a few 1 – 10 stellar radii) and produce large amounts of refractory gas through dust sublimation (e.g., [Iseli et al., 2002](#)). More than 5000 near-Sun comets have been discovered to date; however, nearly all are thought to be 10s of meters in size or smaller (e.g., [Sekanina, 2003](#); [Knight et al., 2010](#)), far too small for remote detection. The vast majority of these comets are members of the Kreutz group ([Battams and Knight, 2017](#)), a group of sungrazing comets created by hierarchical fragmentation of a single parent body near the Sun, likely within the last few millenia (e.g., [Marsden, 1989](#)). Over the last two centuries, several spectacularly bright members of the group have been detected whose brightness implied radii of order 1 km or more, such as Ikeya-Seki ([Preston \(1967\)](#); see also [Sekanina, 2002](#); [Knight et al., 2010](#)), suggesting that the progenitor body may have been of order 10 km in radius.

Among comets with perihelion distances near Earth, C/1995 O1 (Hale-Bopp) offers the most optimistic test case for what might be detectable as an exocomet. Hale-Bopp’s 37 km radius ([Szabó et al., 2012](#)) is among the largest known (see review by [Knight et al., 2024](#)) and it had the highest measured activity near 1 au, reaching production rates of $\sim 10^{31}$ molecules/s of H_2O and $\sim 10^{30}$ molecules/s of CO (e.g., [Biver et al., 2002](#); [Schleicher et al., 2024](#)) and $Af\rho > 10^6$ cm ([Womack et al., 2021](#)). The quantity $Af\rho$ is physically meaningless but is widely used as a proxy for dust production. It is measured within a circular aperture of radius ρ , and is the product of the albedo, A , of grains in the coma, the filling factor, f , of grains in the aperture, and ρ ([A’Hearn et al., 1984](#)). Given that an $Af\rho$ value of 1000 cm is approximately

equivalent to one metric ton of dust production per second (C. Arpigny as quoted by [A’Hearn et al., 1995](#)), this translates into a dust production rate of $> 10^6$ kg/s for Hale-Bopp.

In an early investigation of photometric transit detection capability, [Lecavelier Des Etangs et al. \(1999\)](#) found that comets with dust production rates as low as $\sim 10^3$ kg/s could be detectable from highly favorable viewing geometry due to the optical depth along their tail (which must exceed $\sim 10^{-4}$ for detection). Below, we briefly consider a different criterion: what could be detectable from any viewing geometry? [Lecavelier des Etangs et al. \(2022\)](#) identified exocomet transits in the β Pic system using the Transiting Exoplanet Survey Telescope (TESS) with transit depths shallower than 2×10^{-4} . Taking this as a representative detection threshold and multiplying by πR_{\odot}^2 yields the cross-section of dust along a column towards the Sun that a comet would need to produce in order to potentially be detected as a transit. Approximating comet dust as spheres of radius $1 \mu\text{m}$ and assuming a grain density of 500 kg/m^3 (consistent with Rosetta’s measurement of 67P’s bulk nucleus; [Jorda et al., 2016](#)), this would require $\sim 2 \times 10^{11}$ kg of dust, or about ~ 9 hr of Hale-Bopp’s peak activity. Assuming that grains remain within the column for 24 hr (likely an underestimate given that the column would have the diameter of the Sun), Hale-Bopp would have been detectable within ~ 1.5 au of the Sun for a duration of ~ 5 months. Alternatively, this mass of dust is equivalent to the complete dissolution of a nucleus of radius ~ 600 m (assuming a dust-to-gas mass ratio of 1), implying that many of the brightest Kreutz comets might have been detectable as single events. This argument is obviously an over simplification, but demonstrates that it is at least plausible that some comets in our current Solar System could be detected as exocomets. More realistic models (e.g., [Lecavelier Des Etangs et al., 1999](#)) might include a grain size distribution, different densities for grains versus the nucleus, variable dust-to-gas ratio, radiation pressure, forward-scattering, grain composition, etc. but are beyond the scope of this paper. See [Kálmán et al. \(2024\)](#) for a discussion of recent modeling efforts.

Since detection of exocomets by pollution of the star’s atmosphere has only been detected for white dwarfs, it can be expected that this mechanism would be irrelevant for extra-solar detection of our system’s comets. In the interest of completeness, we note that such an event would be extremely rare in the current Solar System. No comets or asteroids have been observed to impact the Sun, although a few of the poorly observed, tiny Kreutz sungrazers have had nominal orbits with perihelion distance below $1 R_{\odot}$ but none appeared to survive to this point. See Section 1.3.3 of [Jones et al. \(2018\)](#) for additional discussion of these so-called “sundivers.”

The current distribution of comet orbits makes extra-solar detection less favorable. The majority of comets are thought to be isotropically distributed throughout the Oort cloud (see the recent review by [Kaib and Volk, 2022](#)). When perturbed into the inner Solar System, they generally retain their near-random inclination distribution. Thus, no view of the Solar System would yield a preferred orientation for transits of comets arriving from the Oort cloud. Since most short period comets have orbits with inclinations below 20° ([Kaib and Volk, 2022](#)) and these comets have much shorter orbital periods than Oort cloud comets, there is a clear preference for edge-on observations. However, there are no current short-period comets with activity anywhere near

that of Hale-Bopp; 1P/Halley, itself an outlier in the population, is about an order of magnitude less active (e.g., [Schleicher et al., 1998](#)). There are a small number of known Centaurs with sizes comparable to Hale-Bopp (e.g., 29P/Schwassmann-Wachmann 1; [Schambeau et al., 2015](#)). Centaurs are objects currently orbiting on low inclination orbits in the outer planet region, but which may evolve into or have already been on orbits that reach the inner Solar System (cf. [Sarid et al., 2019](#)). Thus, at certain times in the Solar System’s history, there might be a regularly detectable object, but such periods are likely infrequent. Furthermore, many of these objects will be thermally processed during their long dynamical evolution into such an orbit ([Gkotsinas et al., 2022](#)), potentially suppressing activity as compared to a comparably sized Oort cloud comet reaching the same perihelion distance.

5.2 β Pictoris

β Pic was the first star discovered to be an exocomet system, using observations of variable features in Ca II H&K lines ([Ferlet et al., 1987](#)) attributed to the transit of large cometary-like tails in front of the star. Since then, many studies (e.g. [Beust et al., 1990](#); [Beust and Tagger, 1993](#); [Beust et al., 1998](#)) have tried to model and simulate these exocomets, in order to demonstrate that they are a valid scenario to explain the observed events, and to better constrain what physical properties these objects should have. A full review on this system is provided in the accompanying chapter [Lu et al. \(submitted\)](#).

The main differences between Solar System comets and those observed around β Pic lie in (1) the very high production rates and (2) the high level of ionization of the surrounding gas. Concerning the production rates of β Pic exocomets, studies ([Beust et al., 1989](#)) have shown that comets in the β Pic system could release hydrogen at rates of $\sim 10^{33}$ atoms/s, or about $1000\times$ higher than Solar System comets. This is mostly due to the higher luminosity ($\sim 9 L_{\odot}$) and temperature (~ 8000 K) of β Pic compared to the Sun, as well as the close proximity ($10 - 20 R_{\star}$, [Kiefer et al., 2014](#)) at which the comets are observed (the production rate of a comet typically scales as r^{-2} , see Sect. 2). As a result, the total amount of gas found in a β Pic cometary tail typically corresponds to the full evaporation of a $\sim \text{km}^3$ solid body ([Lagrange et al., 1996](#); [Vignaud et al., 2024](#)). Dust production rates are also significant. [Lecavelier des Etangs et al. \(2022\)](#) analyzed 30 photometric events over a five-month observation period with the TESS satellite (average of 1 event every 5 days), and found dust production rates at 1 au ranging between 10^5 and 10^6 kg/s. As discussed in the previous subsection, these rates compare with that of Hale-Bopp, which was an exceptionally active comet by Solar System standards.

Such high production rates may appear contradictory with the dynamical mechanisms proposed to explain the presence of star-grazing comets around β Pic (i.e., orbital perturbation from β Pic b and c that slowly elongate the orbits of minor bodies; see the accompanying chapter [Mustill et al. \(submitted\)](#)), which act over long timescales. However, recent simulations by [Beust et al. \(2024\)](#), incorporating planetary perturbations and estimates of mass loss at each periastron passage, have helped resolve this apparent contradiction. The study suggested that a likely reservoir of exocomets exists at $\sim 1\text{au}$ from the star, corresponding to high-order mean motion

resonances with β Pic c (see the accompanying chapter [Bannister et al., 2025](#), for further details)).

The ionization level of the gas in the β Pic system also distinguishes these comets from Solar System comets. As discussed in Sect. 3.3, photo-ionization occurs rather slow for Solar System comets; for instance, at 1 au, the typical timescale for atomic photoionization is approximately 10 days ([Huebner et al., 1992b](#)), allowing Fe and Ni to be detected ([Manfroid et al., 2021](#)). In contrast, around β Pic, many abundant elements (e.g., Fe, Na, Ca) are photo-ionized almost instantaneously, within seconds or minutes. The ionization can also be enhanced by electronic collisions, producing highly charged species such as Al^{2+} , Si^{3+} , and C^{3+} . As a result, nearly all the gas that is released by β Pic exocomets is in the form of a dense plasma ($n_e \sim 10^6 \text{ cm}^{-3}$ for the most active cases). This leads to a markedly different dynamical behavior compared to Solar System comets: instead of distinct, radiation-driven ion tails, the plasma in β Pic cometary tails undergoes self-braking. Species subject to weaker radiation pressure (e.g., O^+ , C^+) act to slow down those experiencing stronger acceleration (e.g., Ca^+ , Fe^+). Consequently, the various ions remain well-mixed rather than separating by mass or charge. This behavior, which is illustrated on Fig. 20, was highlighted in [Vrignaud and Lecavelier des Etangs \(2024\)](#) and is discussed further in Section 4.2.3.

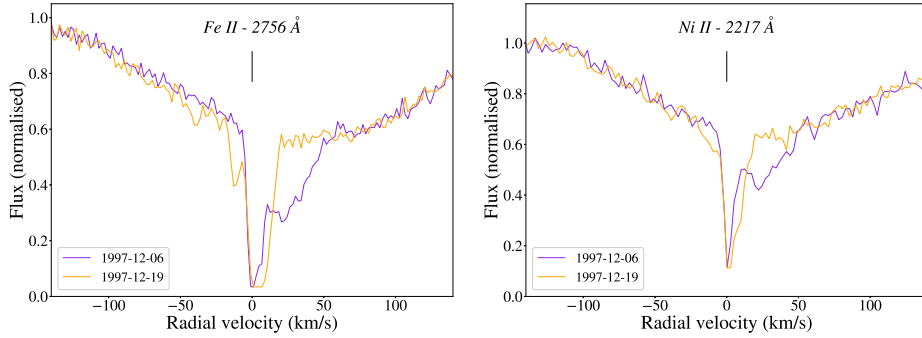


Fig. 20: Comparison of a Fe II line (2756 Å, left) and Ni II line (2217 Å, right) in β Pic spectrum, as observed at two epochs in 1997 with HST (program 7512; [Lagrange, 1997](#)). A red shifted absorption (between roughly +10 and +50 km s^{-1}) attributed to a transiting exocomet is detected in the December 6, 1997 observation, in both lines. The similarity of the two absorption features suggests that Fe^+ and Ni^+ are well-mixed in the gaseous tail, despite undergoing different radiation pressure.

Future models of ion dynamics around β Pic will aim to incorporate key physical processes discussed in this paper. These models should account for sublimation rates (Sect. 3.1), the effects of radiation pressure (Sect. 4.2.1), and drag forces within the plasma environment (Sect. 4.2.3). Additionally, upcoming HST observations planned for 2025 ([Vrignaud et al., 2024](#)) will offer new perspective on β Pic exocomets, helping to refine theoretical predictions and improve our understanding of their behavior.

5.3 AU Mic

AU Mic is a nearby (≈ 10 pc; Gaia Collaboration et al., 2018), young ($18_{-2.4}^{+2.0}$ Myr; Miret-Roig et al., 2020) M1 dwarf, known for its planetary system, which consists of two confirmed warm Neptunes and two other planetary candidates (Donati et al., 2023). The mass estimates for the two confirmed planets range from $10.2 - 14.3 M_{\oplus}$ and $14.2 - 34.9 M_{\oplus}$ (Donati et al., 2023; Plavchan et al., 2020; Klein et al., 2022; Wittrock et al., 2023) and orbit at a distance of 0.07 au (Plavchan et al., 2020) and 0.11 au (Zicher et al., 2022), respectively. The system also hosts an edge-on debris disk which extends from 50 to 210 au (Kalas et al., 2004) and an inner dusty belt between 8.8 and 43 au (MacGregor et al., 2013). As one of the most extensively studied debris disks around an M dwarf (e.g., Grady et al., 2020; Arnold et al., 2022; Lawson et al., 2023; Boccaletti et al., 2018), AU Mic presents a compelling target for future searches for cometary activity (Janson et al., 2023). The system’s edge-on orientation, similar to that of β Pic, could facilitate the detection of transiting or spectroscopically identifiable comet-like bodies. However, AU Mic’s low luminosity ($L = 0.10 L_{\odot}$) would limit the dust production compared to a Solar System comet, and liberated dust grains would experience smaller radiation pressure than its Solar System counterpart (see Table 1). The shape of a hypothetical AU Mic comet dust tail is displayed in Fig. 17. Here, it can be seen the dust tail is significantly smaller in size than the Solar System and β Pic counterparts. This suggests that the photometric detection of transiting exocomet dust tails in the AU Mic system could be elusive.

M dwarf stars are known to be highly active and TESS light curve data of AU Mic shows frequent flares occurring regularly (Gilbert et al., 2022). Space weather modeling suggested it is unlikely planetary atmospheres could survive in such conditions (Alvarado-Gómez et al., 2022). Given that even coronal mass ejections have been observed to disrupt the plasma and dust environments of Solar System comets (e.g., Edberg et al., 2016; Jia et al., 2009; Jian-chun et al., 2011; Kuchar et al., 2008), it is reasonable to suggest AU Mic comets would also be altered by extreme space weather events. Consequently, the combination of relatively low β values, poor dust production, and intense space weather would probably undermine the possibility of cometary tails to form and become detectable in the AU Mic system.

5.4 WD 1145+017

Cometary bodies in white dwarf planetary systems have likely already been detected, both directly and indirectly, with more discoveries expected in the future. These exocomets, however, are observed during the late stages of their destruction, or after they have been completely destroyed. Hence, when compared to main-sequence stars, the observational signatures of exocomets around white dwarfs are fundamentally different, as these objects are observed through active tidal breakup and chemical signatures in the stellar photosphere, rather than through the transit of sublimation-driven tails.

One method of detecting exocomets around white dwarfs is by looking in the atmospheres of the white dwarfs themselves. Because of these stars’ crushingly high density, the photospheres of most white dwarfs could support only primordial hydrogen and

helium. Consequently, any metals detected are transient features from remnant planetary systems (Bonsor, 2024; Williams et al., 2024; Xu et al., 2024). Most of these accreted materials resemble dry, carbon-poor asteroidal material. However, certain detections include elevated levels of carbon and volatile elements—key ingredients for water-rich bodies—suggesting contributions from icy or more primitive objects and highlighting the diverse compositions of small bodies that once orbited the star (Farahi et al., 2013; Raddi et al., 2015; Gentile Fusillo et al., 2017; Xu et al., 2017; Hoskin et al., 2020; Izquierdo et al., 2021).

An alternative and indirect method to detect exocomets within white dwarf atmospheres is to consider their hydrogen budget as a function of time: as exocomets deposit hydrogen in their atmospheres, this hydrogen cannot escape through winds or sink into the core. Therefore, a model for exocometary accretion as a function of time (e.g. O’Connor et al., 2023; Pham and Rein, 2024), combined with a large enough observational sample of hydrogen in white dwarfs (e.g. Raddi et al., 2015), could pose a statistical argument for the detection of these exocomets (Veras et al., 2014).

Despite the above considerations, perhaps the most striking observational manifestation of an exocomet orbiting a white dwarf is a photometric transit curve shaped by active sublimation. The first minor planet found to be disrupting around a white dwarf broke up around WD 1145+017 (Vanderburg et al., 2015). The minor planet’s orbital period was approximately 4.5 hours, and broke up over the course of about 7 years (since first detection in 2015); activity around that star has now, as of 2024, largely ceased (Aungwerojwit et al., 2024b). The breakup was observed through complex and dynamic photometric transit curves, which differ significantly from those produced by exoplanets transiting their stars and instead resemble exocomet transits. The photometric curves for WD 1145+107 (e.g. Fig. 21) are full of structures which indicate ongoing breakup and a potential collisional cascade. How exactly this breakup is linked to sublimation (similarly to comets) as opposed to tidal fragmentation remains an outstanding question, and requires further modeling (Veras et al., 2017; Xu et al., 2018; Duvvuri et al., 2020), especially as many additional systems like WD 1145+017 are now increasing our sample of disrupted exo-minor planets (whether they be exo-asteroids or exocomets) (Guidry et al., 2021; Malamud, 2024).

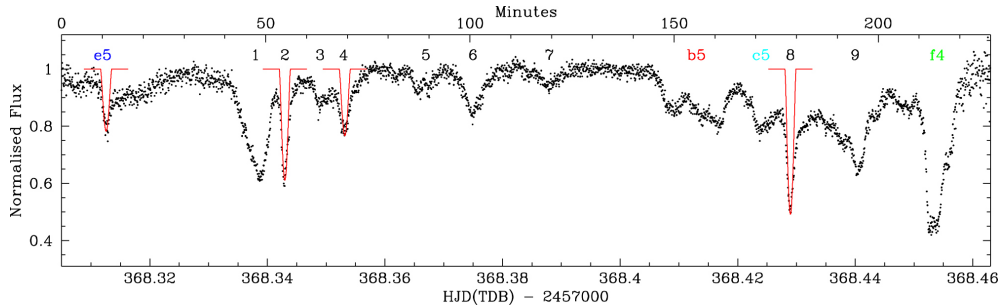


Fig. 21: Photometry of WD 1145+017 obtained with the TNT/ULTRASPEC camera (reproduction of Fig. 2 of Gänsicke et al., 2016). The light curve shows the transit of numerous debris over a single night. The alphanumeric labels specify features of interest. These features change shape with subsequent observations, and showcase intricate substructure which is likely associated with active and complex breakup and sublimation of a parent body which may be an exocomet, exo-asteroid, or some hybrid of the two.

5.5 A bias towards A-type stars?

As seen in the previous sections, the physical processes influencing comets can vary greatly depending on the type of stellar environment to which they are exposed. The stellar properties therefore determine the ability of a minor body to produce tails on close approach to its host star, and of these tails to become detectable (either in spectroscopy or photometry) from Earth.

The primary technique for detecting exocometes is **spectroscopy**, which is sensitive to gaseous and ionized species. The simplest method involves searching for time variable absorption in optically allowed transitions in the visible spectrum, such as Ca I, Ca II, or Na I lines. However, this technique has proven to be heavily biased toward A-type stars, such as β Pic. This bias can be attributed to several factors.

On the one hand, exocometes around cool stars will tend to have less activity, due to a lower stellar flux. Indeed, the production rate of a comet (for a given stellar distance) typically scales as L_* , meaning that comets around the Sun and AU Mic will generally produce $10\times$ and $100\times$ (respectively) less material than β Pic exocometes. In addition, sublimation lines around cool stars are further in: while refractory dust starts sublimating at ~ 0.2 au around β Pic (Sect. 3.1), this limit falls down to ~ 0.06 au around the Sun - a region that is rarely reached by large Solar System comets. This considerably limits our ability to detect exocometes around cool stars, at least when the targeted species are Ca or Na. If we assume that the sublimation lines of refractories have to be located sufficiently far way from the star, say 0.1 au, for exocometes to produce significant amounts of refractory gas, we find that the minimum effective temperature above which exocometes can be detected in optical spectroscopy is around 7000 K, corresponding to a \sim F1V type.

On the other hand, strong stellar luminosities may undermine the detectability of potential exocometes. In particular, we saw in Sect. 3.3 that, above ~ 9500 K (\approx A1V), the photospheric flux starts to quickly photo-ionize Ca^+ into Ca^{2+} , limiting our ability to detect exocometes using optical spectral lines like Ca II. Detecting exocometes

System	Dust grains	Volatiles	Refractory atoms & ions
Sun	Released by volatile sublimation Dust tails shaped by radiation pressure Power-law size distribution	Dominant species : H ₂ O, CO, CO ₂ Slow photo-dissociation (≈ 1 day at 1 au) Ionization by solar EUV photons and solar wind (H ₂ O ⁺ , CO ⁺ ...)	Complex production mechanisms: carbonyls sublimation (≥ 1 au), dust sublimation (≤ 0.1 au) Slow photoionization ($\approx 1 - 100$ day at 1 au)
β Pic	Large production ($\dot{M}_{1 \text{ au}} \geq 10^5 \text{ kg/s}$) Rapid sublimation below 0.2 au Large radiation pressure ($\beta > 1$)	High loss rate ($\sim 10^{33}$ atoms/s) Rapid dissociation: CO, H ₂ O... are not detected in the variable gas (although CO is present in the disc)	Rapid production from grain sublimation Rapid ionization of neutrals (Fe, Ni, Mg...) High plasma density: species remain well-mixed
AU Mic	Weaker volatile sublimation could induce smaller dust activity Smaller radiation pressure : more compact dust tails	Smaller volatile outgassing Higher photo-ionization rates due to stronger EUV flux Stellar flares accelerate ionization and affects tail structure	Low production from dust sublimation Photoionisation of neutrals and ions is quicker than in the Solar System Tail structure affected by flare events
WD 1145+17	Observations at the last stages of destruction Dust release from tidal disruption Low radiation pressure ; grain dynamics affected by Poyting-Roberston drag	Volatiles are quickly dissociated, and accreted to the surface of the WD. Gas detected from atmospheric pollution (e.g. C, N, O)	Detected from atmospheric pollution (e.g. Fe II, Si II...) Observations suggest that the accreted material is mostly rocky

Table 6: Recapitulation of the main properties of exocomets in our four case-study systems. The three columns discuss the observed or expected behavior of dust grains, volatiles (e.g. H₂O, CO₂, ...) and refractory species (e.g. Fe, Fe⁺, ...).

around O-B stars would therefore require targeting lines from more resistant species in the UV (e.g C II, Al III, Si IV, C IV...), which is observationally challenging. As pointed out by [Rebollido \(2020\)](#), another limitation of O-B stars is that ice lines are located at very large stellocentric distances (≥ 100 au, Fig. 3). Exocomets in those systems would thus start to show activity very far from the star, where the transit probability is extremely low, and could be fully destroyed before reaching the ~ 1 au region (where the transit - and thus detection - probability becomes significant).

Even though the proposed thresholds are only approximate, they suggest that the favored T_{eff} for detecting exocomets in visible-light spectroscopy is $\sim 7000 - 9500$ K, or F1V - A1V. A-type stars thus naturally appear to be the most favored systems for exocomet observations, explaining why most previous detections - or hints of detection - have been obtained around such stars ([Rebollido, 2020](#)).

Detecting exocometary gas around cooler stars may instead require focusing on spectral lines other than Ca II or Na I, since these are mainly produced from dust sublimation. For instance, the infrared bands of H₂O or CO₂ may represent better targets, in the case where the gas is not strongly dissociation nor ionized. These bands are accessible with the JWST, which could allow us to detect exocomets around Sun-like stars.

The other primary method for detecting exocomets is **photometry**, which relies on observing the transit of the dust tail. This technique could, a priori, allow for the detection of exocomets across a broader range of stellar effective temperatures, as dust activity can be triggered even around cool stars. For instance, we saw in Sect. 5.1 that the transit of a Hale-Bopp-like comet around a Sun-like star would be detectable in photometry, if the observation conditions are favorable. Yet, very little photometric detections of exocomets have been made, the clearest being β Pic (A5V, $T_{\text{eff}} = 8000$ K; see [Zieba et al., 2019](#)) and KIC 3542116 & 11084727 (F2V, $T_{\text{eff}} = 6800$ K; see [Rappaport et al., 2018](#)). The existence of some bias regarding photometric detections thus remains uncertain. It is however possible that hotter stars, such as A-type stars, are also favored, as their higher luminosities would naturally trigger larger dust productions.

6 Conclusion

Exocomets provide a direct means of probing the composition and dynamical evolution of planetary systems beyond our own. Their activity, likely driven by sublimation, desorption, sputtering, or impacts, reveals how small bodies respond to stellar irradiation, winds, and magnetic fields under conditions far more diverse than those in the Solar System. These processes, when viewed across different stellar environments, reveal not only the diversity of small-body evolution but also the shared physical mechanisms that shape planetary systems throughout the Galaxy.

By comparing the Sun, β Pic, AU Mic, and WD 1145+017, we highlight that stellar luminosity and activity fundamentally govern the onset and efficiency of mass loss. Around hot A-type stars like β Pic, high radiation pressure and elevated temperatures shift the ice lines outward, allowing CO- and CO₂-driven activity far from the star. Around active M dwarfs like AU Mic, strong stellar winds and flares may dominate

material erosion and dust removal. Around white dwarfs such as WD 1145+017, the remnants of small bodies accrete onto the stellar surface, producing the metal-polluted atmospheres that reveal the composition of disrupted planetary material.

The morphology and composition of exocometary tails can reveal valuable diagnostics of the local environment. The interplay between radiation pressure, stellar winds, and magnetic fields determines the balance between gas and dust, the ionization structure of the coma, and the persistence of charged species. In systems like β Pic, the dense, ionized plasma tails exhibit strong coupling between ions of differing radiation pressure, leading to self-braking and compositional mixing—behaviors unseen in Solar System comets. Around low-luminosity M-dwarfs, faint dust emission and intense space weather may render transiting tails nearly undetectable.

Future progress will depend on coordinated, multi-wavelength observations coupled with advances in thermophysical and dynamical modeling. UV and optical spectroscopy will continue to constrain gas composition and plasma behavior, while infrared measurements with facilities such as JWST and Ariel will probe volatile release and dust-grain properties. High-resolution time-domain surveys will expand the census of exocometary systems and allow direct measurements of variability and mass-loss rates. By linking these observations with detailed modeling of sublimation, ion dynamics, and radiative transfer, we can reconstruct how small bodies evolve under different stellar conditions and how their material is redistributed into circumstellar environments.

Acknowledgements. We gratefully acknowledge the International Space Science Institute, ISSI, Bern, for supporting and hosting the workshop on “Exocomets: Bridging our Understanding of Minor Bodies in Solar and Exoplanetary Systems”, during which this work was initiated in July 2024.

We would like to thank Dr. Carl Schmidt (BU) for valuable discussions and feedback on release mechanisms.

We thank Dr. Yankin Wu for kindly sharing the panchromatic spectral model of β Pic presented in [Wu et al. \(2025\)](#).

We thank Dr. Steven Bromley for sending the fluorescence spectra of Fe and Ni around our case study stars.

T.V. acknowledges funding from the Centre National d’Études Spatiales (CNES).

D.Z.S. is supported by an NSF Astronomy and Astrophysics Postdoctoral Fellowship under award AST-2303553. This research award is partially funded by a generous gift of Charles Simonyi to the NSF Division of Astronomical Sciences. The award is made in recognition of significant contributions to Rubin Observatory’s Legacy Survey of Space and Time.

T.D.P. is supported by a UKRI Stephen Hawking Fellowship.

J.H. acknowledges support by the UK Science and Technology Facilities Council (STFC) through grant number ST/Y509784/1.

The views expressed in this article are those of the authors and do not reflect the official policy or position of the U.S. Naval Academy, Department of the Navy, the Department of Defense, or the U.S. Government.

Conflict of interest/Competing interests. Not applicable.

References

- Asphaug, E., Benz, W.: Size, Density, and Structure of Comet Shoemaker-Levy 9 Inferred from the Physics of Tidal Breakup. *Icarus* **121**(2), 225–248 (1996) <https://doi.org/10.1006/icar.1996.0083>
- Alvarado-Gómez, J.D., Cohen, O., Drake, J.J., Fraschetti, F., Poppenhaeger, K., Garraffo, C., Chebly, J., Ilin, E., Harbach, L., Kochukhov, O.: Simulating the Space Weather in the AU Mic System: Stellar Winds and Extreme Coronal Mass Ejections. *Astrophys. J.* **928**(2), 147 (2022) <https://doi.org/10.3847/1538-4357/ac54b8> [arXiv:2202.07949](https://arxiv.org/abs/2202.07949) [astro-ph.SR]
- Alvarado-Gómez, J.D., Cohen, O., Drake, J.J., Fraschetti, F., Poppenhaeger, K., Garraffo, C., Chebly, J., Ilin, E., Harbach, L., Kochukhov, O.: Simulating the Space Weather in the AU Mic System: Stellar Winds and Extreme Coronal Mass Ejections. *The Astrophysical Journal* **928**, 147 (2022) <https://doi.org/10.3847/1538-4357/ac54b8> . Publisher: IOP ADS Bibcode: 2022ApJ...928..147A. Accessed 2024-10-02
- Aungwerojwit, A., Gänsicke, B.T., Dhillon, V.S., Drake, A., Inight, K., Kaye, T.G., Marsh, T.R., Mullen, E., Pelisoli, I., Swan, A.: Long-term variability in debris transiting white dwarfs. *Mon. Not. Roy. Astron. Soc.* **530**(1), 117–128 (2024) <https://doi.org/10.1093/mnras/stae750> [arXiv:2404.04422](https://arxiv.org/abs/2404.04422) [astro-ph.EP]
- Aungwerojwit, A., Gänsicke, B.T., Dhillon, V.S., Drake, A., Inight, K., Kaye, T.G., Marsh, T.R., Mullen, E., Pelisoli, I., Swan, A.: Long-term variability in debris transiting white dwarfs. *Mon. Not. Roy. Astron. Soc.* **530**(1), 117–128 (2024) <https://doi.org/10.1093/mnras/stae750> [arXiv:2404.04422](https://arxiv.org/abs/2404.04422) [astro-ph.EP]
- Afghan, Q., Jones, G.H., Price, O., Coates, A.: Observations of a dust tail gap in comet C/2014 Q1 (PanSTARRS). *Icarus* **390**, 115286 (2023) <https://doi.org/10.1016/j.icarus.2022.115286> . Accessed 2023-09-25
- Absil, O., Marion, L., Ertel, S., Defrère, D., Kennedy, G.M., Romagnolo, A., Le Bouquin, J.-B., Christiaens, V., Milli, J., Bonsor, A., Olofsson, J., Su, K.Y.L., Augereau, J.-C.: A near-infrared interferometric survey of debris-disk stars. VII. The hot-to-warm dust connection. *Astron. Astrophys.* **651**, 45 (2021) <https://doi.org/10.1051/0004-6361/202140561> [arXiv:2104.14216](https://arxiv.org/abs/2104.14216) [astro-ph.EP]
- A’Hearn, M.F., Millis, R.C., Schleicher, D.O., Osip, D.J., Birch, P.V.: The ensemble properties of comets: Results from narrowband photometry of 85 comets, 1976-1992. *Icarus* **118**(2), 223–270 (1995) <https://doi.org/10.1006/icar.1995.1190>
- Arnaud, M., Rothenflug, R.: An Updated Evaluation of Recombination and Ionization Rates. *Astron. Astrophys. Supp.* **60**, 425 (1985)

- A'Hearn, M.F., Schleicher, D.G., Millis, R.L., Feldman, P.D., Thompson, D.T.: Comet Bowell 1980b. *Astron. J.* **89**, 579–591 (1984) <https://doi.org/10.1086/113552>
- Arnold, J.A., Weinberger, A.J., Videen, G., Zubko, E.S.: Stumbling over Planetary Building Blocks: AU Microscopii as an Example of the Challenge of Retrieving Debris-disk Dust Properties. *The Astrophysical Journal* **930**, 123 (2022) <https://doi.org/10.3847/1538-4357/ac63a9> . Publisher: IOP ADS Bibcode: 2022ApJ...930..123A. Accessed 2024-10-02
- Bahr, D.A., Baragiola, R.A.: Photodesorption of Solid CO₂ by Ly α . *Astrophys. J.* **761**(1), 36 (2012) <https://doi.org/10.1088/0004-637X/761/1/36>
- Bockelée-Morvan, D., Biver, N.: The composition of cometary ices. *Philosophical Transactions of the Royal Society of London Series A* **375**(2097), 20160252 (2017) <https://doi.org/10.1098/rsta.2016.0252>
- Biver, N., Bockelée-Morvan, D., Colom, P., Crovisier, J., Henry, F., Lellouch, E., Winnberg, A., Johansson, L.E.B., Gunnarsson, M., Rickman, H., Rantakyö, F., Davies, J.K., Dent, W.R.F., Paubert, G., Moreno, R., Wink, J., Despois, D., Benford, D.J., Gardner, M., Lis, D.C., Mehringer, D., Phillips, T.G., Rauer, H.: The 1995–2002 Long-Term Monitoring of Comet C/1995 O1 (HALE–BOPP) at Radio Wavelength. *Earth Moon and Planets* **90**(1), 5–14 (2002) <https://doi.org/10.1023/A:1021599915018>
- Bodewits, D., Bonev, B.P., Cordiner, M.A., Villanueva, G.L.: Radiative Processes as Diagnostics of Cometary Atmospheres. In: Meech, K.J., Combi, M.R., Bockelée-Morvan, D., Raymond, S.N., Zolensky, M.E. (eds.) *Comets III*, pp. 407–432 (2024). https://doi.org/10.2458/azu_uapress_9780816553631-ch013
- Brown, M.E., Bouchez, A.H., Spinrad, H., Misch, A.: Sodium Velocities and Sources in Hale-Bopp. *Icarus* **134**(2), 228–234 (1998) <https://doi.org/10.1006/icar.1998.5941>
- Bottke, W.F., Durda, D.D., Nesvorný, D., Jedicke, R., Morbidelli, A., Vokrouhlický, D., Levison, H.: The fossilized size distribution of the main asteroid belt. *Icarus* **175**(1), 111–140 (2005) <https://doi.org/10.1016/j.icarus.2004.10.026>
- Biver, N., Dello Russo, N., Opitom, C., Rubin, M.: Chemistry of comet atmospheres. arXiv e-prints, 2207–04800 (2022) <https://doi.org/10.48550/arXiv.2207.04800> [astro-ph.EP]
- Bennett, P.D.: Chromospheres and Winds of Red Supergiants: An Empirical Look at Outer Atmospheric Structure. In: Leitherer, C., Bennett, P.D., Morris, P.W., Van Loon, J.T. (eds.) *Hot and Cool: Bridging Gaps in Massive Star Evolution*. *Astronomical Society of the Pacific Conference Series*, vol. 425, p. 181 (2010). <https://doi.org/10.48550/arXiv.1004.1853>

- Battams, K., Knight, M.M.: SOHO comets: 20 years and 3000 objects later. *Philosophical Transactions of the Royal Society of London Series A* **375**(2097), 20160257 (2017) <https://doi.org/10.1098/rsta.2016.0257> arXiv:1611.02279 [astro-ph.EP]
- Bruhweiler, F.C., Kondo, Y., Grady, C.A.: Mass Outflow in the Nearby Proto-Planetary System beta Pictoris. *Astrophys. J. Lett.* **371**, 27 (1991) <https://doi.org/10.1086/185994>
- Beust, H., Karmann, C., Lagrange, A.-M.: Falling Evaporating Bodies around Herbig stars. A theoretical study. *Astron. Astrophys.* **366**, 945–964 (2001) <https://doi.org/10.1051/0004-6361:20000353>
- Bodewits, D., Kelley, M.S., Li, J.-Y., Landsman, W.B., Besse, S., A’Hearn, M.F.: Collisional Excavation of Asteroid (596) Scheila. *Astrophysical Journal Letters* **733**(1), 3 (2011) <https://doi.org/10.1088/2041-8205/733/1/13>
- Budaj, J., Kocifaj, M., Salmeron, R., Hubeny, I.: Tables of phase functions, opacities, albedos, equilibrium temperatures, and radiative accelerations of dust grains in exoplanets. *Mon. Not. Roy. Astron. Soc.* **454**(1), 2–27 (2015) <https://doi.org/10.1093/mnras/stv1711> arXiv:1505.08013 [astro-ph.EP]
- Bodewits, D., Lara, L.M., A’Hearn, M.F., La Forgia, F., Gicquel, A., Kovacs, G., Knollenberg, J., Lazzarin, M., Lin, Z.-Y., Shi, X., Snodgrass, C., Tubiana, C., Sierks, H., Barbieri, C., Lamy, P.L., Rodrigo, R., Koschny, D., Rickman, H., Keller, H.U., Barucci, M.A., Bertaux, J.-L., Bertini, I., Boudreault, S., Cremonese, G., Da Deppo, V., Davidsson, B., Debei, S., De Cecco, M., Fornasier, S., Fulle, M., Groussin, O., Gutiérrez, P.J., Güttler, C., Hviid, S.F., Ip, W.-H., Jorda, L., Kramm, J.-R., Kührt, E., Küppers, M., López-Moreno, J.J., Marzari, F., Naletto, G., Ockay, N., Thomas, N., Toth, I., Vincent, J.-B.: Changes in the Physical Environment of the Inner Coma of 67P/Churyumov-Gerasimenko with Decreasing Heliocentric Distance. *Astron. J.* **152**(5), 130 (2016) <https://doi.org/10.3847/0004-6256/152/5/130> arXiv:1607.05632 [astro-ph.EP]
- Beust, H., Lagrange, A.-M., Crawford, I.A., Goudard, C., Spyromilio, J., Vidal-Madjar, A.: The beta Pictoris circumstellar disk. XXV. The Ca II absorption lines and the Falling Evaporating Bodies model revisited using UHRF observations. *Astron. Astrophys.* **338**, 1015–1030 (1998)
- Burns, J.A., Lamy, P.L., Soter, S.: Radiation forces on small particles in the solar system. *Icarus* **40**(1), 1–48 (1979) [https://doi.org/10.1016/0019-1035\(79\)90050-2](https://doi.org/10.1016/0019-1035(79)90050-2) . Accessed 2024-11-01
- Beust, H., Lagrange-Henri, A.M., Vidal-Madjar, A., Ferlet, R.: The beta Pictoris circumstellar disk. IX. Theoretical results on the infall velocities of CA II, AI III and MG II. *Astron. Astrophys.* **223**, 304–312 (1989)
- Beust, H., Lagrange-Henri, A.M., Vidal-Madjar, A., Ferlet, R.: The beta Pictoris

- circumstellar disk. X. Numerical simulations of infalling evaporating bodies. *Astron. Astrophys.* **236**, 202 (1990)
- Bonnefoy, M., Marleau, G.-D., Galicher, R., Beust, H., Lagrange, A.-M., Baudino, J.-L., Chauvin, G., Borgniet, S., Meunier, N., Rameau, J., Boccaletti, A., Cumming, A., Helling, C., Homeier, D., Allard, F., Delorme, P.: Physical and orbital properties of β Pictoris b. *Astron. Astrophys.* **567**, 9 (2014) <https://doi.org/10.1051/0004-6361/201424041> [arXiv:1407.4001](https://arxiv.org/abs/1407.4001) [astro-ph.EP]
- Beust, H., Milli, J., Morbidelli, A., Lacour, S., Lagrange, A.-M., Chauvin, G., Bonnefoy, M., Wang, J.: Dynamics of the β Pictoris planetary system and its falling evaporating bodies. *Astron. Astrophys.* **683**, 89 (2024) <https://doi.org/10.1051/0004-6361/202348203> [arXiv:2401.00715](https://arxiv.org/abs/2401.00715) [astro-ph.EP]
- Bottke, W.F., Norman, M.D.: The Late Heavy Bombardment. *Annual Review of Earth and Planetary Sciences* **45**(1), 619–647 (2017) <https://doi.org/10.1146/annurev-earth-063016-020131>
- Bromley, S.J., Neff, B., Loch, S.D., Marler, J.P., Országh, J., Venkataramani, K., Bodewits, D.: Atomic Iron and Nickel in the Coma of C/1996 B2 (Hyakutake): Production Rates, Emission Mechanisms, and Possible Parents. *The Planetary Science Journal* **2**(6), 228 (2021) <https://doi.org/10.3847/psj/ac2dff>
- Bodewits, E.: Dynamics of highly charged ions interacting with surfaces. PhD thesis (2010). Relation: <http://www.rug.nl/> Rights: University of Groningen
- Bonsor, A.: White Dwarf Systems: the Composition of Exoplanets. arXiv e-prints, 2409–13294 (2024) <https://doi.org/10.48550/arXiv.2409.13294> [arXiv:2409.13294](https://arxiv.org/abs/2409.13294) [astro-ph.EP]
- Bryans, P., Pesnell, W.D.: The Extreme-ultraviolet Emission from Sun-grazing Comets. *Astrophys. J.* **760**(1), 18 (2012) <https://doi.org/10.1088/0004-637X/760/1/18> [arXiv:1209.5708](https://arxiv.org/abs/1209.5708) [astro-ph.SR]
- Bannister, M., Pfalzner, S., Pearce, T., Mustill, A.J., Klahr, H., Nomura, H., Ohashi, N., Kokotanekova, R., Marino, S., Bodewits, D., Marschall, R., Seligman, D.Z., Jones, G.H., Veras, D.: The Origins & Reservoirs of Exocomets. *Space Sci. Rev.* **221**(7), 90 (2025) <https://doi.org/10.1007/s11214-025-01219-w>
- Bodman, E.H.L., Quillen, A.: KIC 8462852: Transit of a Large Comet Family. *The Astrophysical Journal Letters* **819**(2), 34 (2016) <https://doi.org/10.3847/2041-8205/819/2/L34>. Publisher: The American Astronomical Society. Accessed 2024-10-01
- Brandeker, A.: Exposing the Gas Braking Mechanism of the β Pictoris Disk. *Astrophys. J.* **729**(2), 122 (2011) <https://doi.org/10.1088/0004-637X/729/2/122> [arXiv:1101.4032](https://arxiv.org/abs/1101.4032) [astro-ph.SR]

- Boccaletti, A., Sezestre, E., Lagrange, A.-M., Thébault, P., Gratton, R., Langlois, M., Thalmann, C., Janson, M., Delorme, P., Augereau, J.-C., Schneider, G., Milli, J., Grady, C., Debes, J., Kral, Q., Olofsson, J., Carson, J., Maire, A.L., Henning, T., Wisniewski, J., Schlieder, J., Dominik, C., Desidera, S., Ginski, C., Hines, D., Ménard, F., Mouillet, D., Pawellek, N., Vigan, A., Lagadec, E., Avenhaus, H., Beuzit, J.-L., Biller, B., Bonavita, M., Bonnefoy, M., Brandner, W., Cantalloube, F., Chauvin, G., Cheetham, A., Cudel, M., Gry, C., Daemgen, S., Feldt, M., Galicher, R., Girard, J., Hagelberg, J., Janin-Potiron, P., Kasper, M., Le Coroller, H., Mesa, D., Peretti, S., Perrot, C., Samland, M., Sissa, E., Wildi, F., Zurlo, A., Rochat, S., Stadler, E., Gluck, L., Origné, A., Llored, M., Baudoz, P., Rousset, G., Martinez, P., Rigal, F.: Observations of fast-moving features in the debris disk of AU Mic on a three-year timescale: Confirmation and new discoveries. *Astronomy and Astrophysics* **614**, 52 (2018) <https://doi.org/10.1051/0004-6361/201732462> . ADS Bibcode: 2018A&A...614A..52B. Accessed 2024-10-02
- Bonanno, A., Schlattl, H., Paternò, L.: The age of the Sun and the relativistic corrections in the EOS. *Astron. Astrophys.* **390**, 1115–1118 (2002) <https://doi.org/10.1051/0004-6361:20020749> [arXiv:astro-ph/0204331](https://arxiv.org/abs/astro-ph/0204331) [astro-ph]
- Beust, H., Tagger, M.: A Hydrodynamical Model for Infalling Evaporating Bodies in the β Pictoris Circumstellar Disk. *Icarus* **106**(1), 42–58 (1993) <https://doi.org/10.1006/icar.1993.1157>
- Brasser, R., Wang, J.-H.: An updated estimate of the number of Jupiter-family comets using a simple fading law. *Astron. Astrophys.* **573**, 102 (2015) <https://doi.org/10.1051/0004-6361/201423687> [arXiv:1412.1198](https://arxiv.org/abs/1412.1198) [astro-ph.EP]
- Collings, M.P., Anderson, M.A., Chen, R., Dever, J.W., Viti, S., Williams, D.A., McCoustra, M.R.S.: A laboratory survey of the thermal desorption of astrophysically relevant molecules. *Mon. Not. Roy. Astron. Soc.* **354**(4), 1133–1140 (2004) <https://doi.org/10.1111/j.1365-2966.2004.08272.x>
- Combi, M.R., Harris, W.M., Smyth, W.H.: Gas dynamics and kinetics in the cometary coma: theory and observations. *Comets II*, p. 523. University of Arizona Press (2004). http://adsabs.harvard.edu/cgi-bin/nph-data_query?bibcode=2004come.book..523C&link_type=ABSTRACT Accessed 0
- Cassidy, T.A., Johnson, R.E.: Monte carlo model of sputtering and other ejection processes within a regolith. *Icarus* **176**(2), 499–507 (2005) <https://doi.org/10.1016/j.icarus.2005.02.013>
- Cravens, T.E., Korosmezey, A.: Vibrational and rotational cooling of electrons by water vapor. *Planetary and Space Science* **34**(10), 961–970 (1986) [https://doi.org/10.1016/0032-0633\(86\)90005-x](https://doi.org/10.1016/0032-0633(86)90005-x)
- Cochran, A.L., Lvasseur-Regourd, A.-C., Cordiner, M., Hadamcik, E., Lasue, J., Gicquel, A., Schleicher, D.G., Charnley, S.B., Mumma, M.J., Paganini, L.,

- Bockelée-Morvan, D., Biver, N., Kuan, Y.-J.: The Composition of Comets. *Space Sci. Rev.* **197**(1-4), 9–46 (2015) <https://doi.org/10.1007/s11214-015-0183-6> [arXiv:1507.00761](https://arxiv.org/abs/1507.00761) [astro-ph.EP]
- Combi, M.: Hale-Bopp: What Makes a Big Comet Different? Coma Dynamics: Observations and Theory. *Earth Moon and Planets* **89**, 73–90 (2002) <https://doi.org/10.1023/A:1021534117319>. Publisher: Springer ADS Bibcode: 2002EM&P...89...73C. Accessed 2024-11-01
- Combi, M.R., Shou, Y., Fougere, N., Tenishev, V., 2020: The surface distributions of the production of the major volatile species, H₂O, CO₂, CO and O₂, from the nucleus of comet 67P/Churyumov-Gerasimenko *Icarus* **335**, 113421 (2020) <https://doi.org/10.1016/j.icarus.2019.113421>
- Collette, A., Sternovsky, Z., Horanyi, M.: Production of neutral gas by micrometeoroid impacts. *Icarus* **227**, 89–93 (2014) <https://doi.org/10.1016/j.icarus.2013.09.009>
- Cassidy, T.A., Schmidt, C.A., Merkel, A.W., Jasinski, J.M., Burger, M.H.: Detection of Large Exospheric Enhancements at Mercury due to Meteoroid Impacts. *Planet. Sci. J.* **2**(5), 175 (2021) <https://doi.org/10.3847/PSJ/ac1a19>
- Crifo, F., Vidal-Madjar, A., Lallement, R., Ferlet, R., Gerbaldi, M.: β Pictoris revisited by Hipparcos. *Star properties. Astron. Astrophys.* **320**, 29–32 (1997)
- Donati, J.-F., Cristofari, P.I., Finociety, B., Klein, B., Moutou, C., Gaidos, E., Cadieux, C., Artigau, E., Correia, A.C.M., Boué, G., Cook, N.J., Carmona, A., Lehmann, L.T., Bouvier, J., Martioli, E., Morin, J., Fouqué, P., Delfosse, X., Doyon, R., Hébrard, G., Alencar, S.H.P., Laskar, J., Arnold, L., Petit, P., Kospal, A., Vidotto, A., Folsom, C.P., collaboration, t.S.L.S.: The magnetic field and multiple planets of the young dwarf AU Mic. *Monthly Notices of the Royal Astronomical Society* **525**(1), 455–475 (2023) <https://doi.org/10.1093/mnras/stad1193>. Accessed 2024-03-19
- Deleuil, M., Gry, C., Lagrange-Henri, A.-M., Vidal-Madjar, A., Beust, H., Ferlet, R., Moos, H.W., Livengood, T.A., Ziskin, D., Feldman, P.D.: The beta Pictoris circumstellar disk. XV. Highly ionized species near beta Pictoris. *Astron. Astrophys.* **267**, 187–193 (1993)
- Dello Russo, N., Kawakita, H., Vervack, R.J., Weaver, H.A.: Emerging trends and a comet taxonomy based on the volatile chemistry measured in thirty comets with high-resolution infrared spectroscopy between 1997 and 2013. *Icarus* **278**, 301–332 (2016) <https://doi.org/10.1016/j.icarus.2016.05.039>
- Dennerl, K., Lisse, C.M., Bhardwaj, A., Christian, D.J., Wolk, S.J., Bodewits, D., Zurbuchen, T.H., Combi, M.R., Lepri, S.T.: Solar system X-rays from charge exchange processes. *Astronomische Nachrichten* **333**(4), 324–334 (2012) <https://doi.org/10.1002/asna.201211663>

- Defrère, D., Lebreton, J., Le Bouquin, J.-B., Lagrange, A.-M., Absil, O., Augereau, J.-C., Berger, J.-P., di Folco, E., Ertel, S., Kluska, J., Montagnier, G., Millan-Gabet, R., Traub, W., Zins, G.: Hot circumstellar material resolved around β Pic with VLTI/PIONIER. *Astron. Astrophys.* **546**, 9 (2012) <https://doi.org/10.1051/0004-6361/201220287> arXiv:1210.1914 [astro-ph.SR]
- Dullemond, C.P., Monnier, J.D.: The Inner Regions of Protoplanetary Disks. *Annu. Rev. Astron. Astrophys.* **48**, 205–239 (2010) <https://doi.org/10.1146/annurev-astro-081309-130932> arXiv:1006.3485 [astro-ph.SR]
- Duvvuri, G.M., Redfield, S., Veras, D.: Necroplanetology: Simulating the Tidal Disruption of Differentiated Planetary Material Orbiting WD 1145+017. *Astrophys. J.* **893**(2), 166 (2020) <https://doi.org/10.3847/1538-4357/ab7fa0> arXiv:2003.08410 [astro-ph.EP]
- Dent, W.R.F., Wyatt, M.C., Roberge, A., Augereau, J.-C., Casassus, S., Corder, S., Greaves, J.S., de Gregorio-Monsalvo, I., Hales, A., Jackson, A.P., Hughes, A.M., Lagrange, A.-M., Matthews, B., Wilner, D.: Molecular Gas Clumps from the Destruction of Icy Bodies in the β Pictoris Debris Disk. *Science* **343**(6178), 1490–1492 (2014) <https://doi.org/10.1126/science.1248726> arXiv:1404.1380 [astro-ph.SR]
- Edberg, N.J.T., Alho, M., André, M., Andrews, D.J., Behar, E., Burch, J.L., Carr, C.M., Cupido, E., Engelhardt, I.A.D., Eriksson, A.I., Glassmeier, K.-H., Goetz, C., Goldstein, R., Henri, P., Johansson, F.L., Koenders, C., Mandt, K., Möstl, C., Nilsson, H., Odelstad, E., Richter, I., Simon Wedlund, C., Stenberg Wieser, G., Szego, K., Vigren, E., Volwerk, M.: CME impact on comet 67P/Churyumov-Gerasimenko. *Monthly Notices of the Royal Astronomical Society* **462**, 45–56 (2016) <https://doi.org/10.1093/mnras/stw2112> . ADS Bibcode: 2016MNRAS.462S..45E. Accessed 2023-10-06
- Ertel, S., Defrère, D., Absil, O., Le Bouquin, J.-B., Augereau, J.-C., Berger, J.-P., Blind, N., Bonsor, A., Lagrange, A.-M., Lebreton, J., Marion, L., Milli, J., Olofsson, J.: A near-infrared interferometric survey of debris-disc stars. V. PIONIER search for variability. *Astron. Astrophys.* **595**, 44 (2016) <https://doi.org/10.1051/0004-6361/201527721> arXiv:1608.05731 [astro-ph.SR]
- Eichhorn, G.: Time-resolved temperature measurements in hypervelocity dust impact. *Planetary and Space Science* **26**(5), 463–467 (1978) [https://doi.org/10.1016/0032-0633\(78\)90006-0](https://doi.org/10.1016/0032-0633(78)90006-0)
- Engrand, C., Lasue, J., Wooden, D.H., Zolensky, M.E.: Chemical and physical properties of cometary dust. arXiv e-prints, 2305–03417 (2023) <https://doi.org/10.48550/arXiv.2305.03417> arXiv:2305.03417 [astro-ph.EP]
- Farnham, T.L.: Coma morphology of Jupiter-family comets. *Planetary and Space Science* **57**(10), 1192–1217 (2009) <https://doi.org/10.1016/j.pss.2009.02.008>

- Fulle, M., Barbieri, C., Cremonese, G., Rauer, H., Weiler, M., Milani, G., Ligustri, R.: The dust environment of comet 67P/Churyumov-Gerasimenko. *Astron. Astrophys.* **422**, 357–368 (2004) <https://doi.org/10.1051/0004-6361:20035806>
- Fortenberry, R.C., Bodewits, D., Pierce, D.M.: Knowledge Gaps in the Cometary Spectra of Oxygen-bearing Molecular Cations. *The Astrophysical Journal Supplement Series* **256**(1), 6 (2021) <https://doi.org/10.3847/1538-4365/ac0cfd>
- Feng, F., Butler, R.P., Vogt, S.S., Clement, M.S., Tinney, C.G., Cui, K., Aizawa, M., Jones, H.R.A., Bailey, J., Burt, J., Carter, B.D., Crane, J.D., Flammini Dotti, F., Holden, B., Ma, B., Ogihara, M., Oppenheimer, R., O’Toole, S.J., Shectman, S.A., Wittenmyer, R.A., Wang, S.X., Wright, D.J., Xuan, Y.: 3D Selection of 167 Substellar Companions to Nearby Stars. *Astrophys. J. Supp. Ser.* **262**(1), 21 (2022) <https://doi.org/10.3847/1538-4365/ac7e57> [arXiv:2208.12720](https://arxiv.org/abs/2208.12720) [astro-ph.EP]
- Feldman, p.D., Cochran, A.L., Combi, M.R.: Spectroscopic Investigations of Fragment Species in the Coma. *Comets II*, p. 425. University of Arizona Press (2004)
- Fillion, J.-H., Dupuy, R., Féraud, G., Romanzin, C., Philippe, L., Putaud, T., Baglin, V., Cimino, R., Marie-Jeanne, P., Jeseck, P., Michaut, X., Bertin, M.: Vacuum-UV Photodesorption from Compact Amorphous Solid Water: Photon Energy Dependence, Isotopic and Temperature Effects. *ACS Earth and Space Chemistry* **6**(1), 100–115 (2022) <https://doi.org/10.1021/acsearthspacechem.1c00302> [2103.15435](https://pubs.acs.org/doi/abs/10.1021/acsearthspacechem.1c00302)
- Ferrario, L., de Martino, D., Gänsicke, B.T.: Magnetic White Dwarfs. *Space Sci. Rev.* **191**(1-4), 111–169 (2015) <https://doi.org/10.1007/s11214-015-0152-0> [arXiv:1504.08072](https://arxiv.org/abs/1504.08072) [astro-ph.SR]
- Feinstein, A.D., France, K., Youngblood, A., Duvvuri, G.M., Teal, D.J., Cauley, P.W., Seligman, D.Z., Gaidos, E., Kempton, E.M.-R., Bean, J.L., Diamond-Lowe, H., Newton, E., Ginzburg, S., Plavchan, P., Gao, P., Schlichting, H.: AU Microscopii in the Far-UV: Observations in Quiescence, during Flares, and Implications for AU Mic b and c. *Astron. J.* **164**(3), 110 (2022) <https://doi.org/10.3847/1538-3881/ac8107> [arXiv:2205.09606](https://arxiv.org/abs/2205.09606) [astro-ph.SR]
- Farihi, J., Gänsicke, B.T., Koester, D.: Evidence for Water in the Rocky Debris of a Disrupted Extrasolar Minor Planet. *Science* **342**(6155), 218–220 (2013) <https://doi.org/10.1126/science.1239447> [arXiv:1310.3269](https://arxiv.org/abs/1310.3269) [astro-ph.EP]
- Ferlet, R., Hobbs, L.M., Vidal-Madjar, A.: The beta Pictoris circumstellar disk. V. Time variations of the Ca II-K line. *Astron. Astrophys.* **185**, 267–270 (1987)
- Farnham, T.L., Kelley, M.S.P., Bauer, J.M.: Early Activity in Comet C/2014 UN271 Bernardinelli-Bernstein as Observed by TESS. *Planet. Sci. J.* **2**(6), 236 (2021) <https://doi.org/10.3847/PSJ/ac323d>
- Furusho, R., Kawakita, H., Fujii, M., Watanabe, J.-i.: Heliocentric Dependence of

- Sodium Emission of Comet Hale-Bopp (C/1995O1). *Astrophys. J.* **618**(1), 543–546 (2005) <https://doi.org/10.1086/425953>
- Fulle, M., Leblanc, F., Harrison, R.A., Davis, C.J., Eyles, C.J., Halain, J.P., Howard, R.A., Bockelée-Morvan, D., Cremonese, G., Scarmato, T.: Discovery of the Atomic Iron Tail of Comet MCNaught Using the Heliospheric Imager on STEREO. *Astrophys. J. Lett.* **661**(1), 93–96 (2007) <https://doi.org/10.1086/518719>
- Finson, M.J., Probst, R.F.: A theory of dust comets. I. Model and equations. *The Astrophysical Journal* **154**, 327–352 (1968) <https://doi.org/10.1086/149761> . ADS Bibcode: 1968ApJ...154..327F. Accessed 2023-09-29
- Ferland, G.J., Porter, R.L., van Hoof, P.A.M., Williams, R.J.R., Abel, N.P., Lykins, M.L., Shaw, G., Henney, W.J., Stancil, P.C.: The 2013 Release of Cloudy. *Rev. Mex. Astron. Astrophys.* **49**, 137–163 (2013) <https://doi.org/10.48550/arXiv.1302.4485> [arXiv:1302.4485](https://arxiv.org/abs/1302.4485) [astro-ph.GA]
- Fink, U., Rubin, M.: The calculation of A_{frho} and mass loss rate for comets. *Icarus* **221**, 721–734 (2012) <https://doi.org/10.1016/j.icarus.2012.09.001> . ADS Bibcode: 2012Icar..221..721F. Accessed 2024-10-31
- Filacchione, G., Raponi, A., Capaccioni, F., Ciarniello, M., Tosi, F., Capria, M.T., Sanctis, M.C.D., Migliorini, A., Piccioni, G., Cerroni, P., Barucci, M.A., Fornasier, S., Schmitt, B., Quirico, E., Erard, S., Bockelée-Morvan, D., Leyrat, C., Arnold, G., Mennella, V., Ammannito, E., Bellucci, G., Benkhoff, J., Bibring, J.P., Blanco, A., Blecka, M.I., Carlson, R., Carsenty, U., Colangeli, L., Combes, M., Combi, M., Crovisier, J., Drossart, P., Encrenaz, T., Federico, C., Fink, U., Fonti, S., Fulchignoni, M., Ip, W.-H., Irwin, P., Jaumann, R., Kuehrt, E., Langevin, Y., Magni, G., McCord, T., Moroz, L., Mottola, S., Palomba, E., Schade, U., Stephan, K., Taylor, F., Tiphene, D., Tozzi, G.P., Beck, P., Biver, N., Bonal, L., Combe, J.-P., Despan, D., Flamini, E., Formisano, M., Frigeri, A., Grassi, D., Gudipati, M.S., Kappel, D., Longobardo, A., Mancarella, F., Markus, K., Merlin, F., Orosei, R., Rinaldi, G., Cartacci, M., Cicchetti, A., Hello, Y., Henry, F., Jacquino, S., Rees, J.M., Noschese, R., Politi, R., Peter, G.: Seasonal exposure of carbon dioxide ice on the nucleus of comet 67P/Churyumov-Gerasimenko. *Science* **354**(6319), 1563–1566 (2016) <https://doi.org/10.1126/science.aag3161>
- Famá, M., Shi, J., Baragiola, R.A.: Sputtering of ice by low-energy ions. *Surface Science* **602**(1), 156–161 (2008) <https://doi.org/10.1016/j.susc.2007.10.011>
- Faggi, S., Villanueva, G.L., McKay, A., Pinto, O.H., Kelley, M.S.P., Bockelée-Morvan, D., Womack, M., Chambeau, C.A., Feaga, L., DiSanti, M.A., Bauer, J.M., Biver, N., Wierzchos, K., Fernandez, Y.R.: Heterogeneous outgassing regions identified on active centaur 29P/Schwassmann–Wachmann 1. *Nature Astronomy*, 1–9 (2024) <https://doi.org/10.1038/s41550-024-02319-3>

- Farihi, J., von Hippel, T., Pringle, J.E.: Magnetospherically-trapped dust and a possible model for the unusual transits at WD 1145+017. *Mon. Not. Roy. Astron. Soc.* **471**(1), 145–149 (2017) <https://doi.org/10.1093/mnrasl/slx122> arXiv:1707.09474 [astro-ph.SR]
- Gänsicke, B.T., Aungwerojwit, A., Marsh, T.R., Dhillon, V.S., Sahman, D.I., Veras, D., Farihi, J., Chote, P., Ashley, R., Arjyotha, S., Rattanasoon, S., Littlefair, S.P., Pollacco, D., Burleigh, M.R.: High-speed Photometry of the Disintegrating Planetesimals at WD1145+017: Evidence for Rapid Dynamical Evolution. *Astrophys. J. Lett.* **818**(1), 7 (2016) <https://doi.org/10.3847/2041-8205/818/1/L7> arXiv:1512.09150 [astro-ph.EP]
- Gilbert, E.A., Barclay, T., Quintana, E.V., Walkowicz, L.M., Vega, L.D., Schlieder, J.E., Monsue, T., Cale, B.L., Collins, K.I., Gaidos, E., Mufti, M.E., Reefer, M.A., Plavchan, P., Tanner, A., Wittenmyer, R.A., Wittrock, J.M., Jenkins, J.M., Latham, D.W., Ricker, G.R., Rose, M.E., Seager, S., Vanderspek, R.K., Winn, J.N.: Flares, Rotation, and Planets of the AU Mic System from TESS Observations. *The Astronomical Journal* **163**(4), 147 (2022) <https://doi.org/10.3847/1538-3881/ac23ca>. Publisher: The American Astronomical Society. Accessed 2024-10-02
- Gaia Collaboration, Brown, A.G.A., Vallenari, A., Prusti, T., Bruijne, J.H.J., Babusaix, C., Bailer-Jones, C.A.L., Biermann, M., Evans, D.W., Eyer, L., Jansen, F., Jordi, C., Klioner, S.A., Lammers, U., Lindegren, L., Luri, X., Mignard, F., Panem, C., Pourbaix, D., Randich, S., Sartoretti, P., Siddiqui, H.I., Soubiran, C., Leeuwen, F., Walton, N.A., Arenou, F., Bastian, U., Cropper, M., Drimmel, R., Katz, D., Lattanzi, M.G., Bakker, J., Cacciari, C., Castañeda, J., Chaoul, L., Cheek, N., De Angeli, F., Fabricius, C., Guerra, R., Holl, B., Masana, E., Messineo, R., Mowlavi, N., Nienartowicz, K., Panuzzo, P., Portell, J., Riello, M., Seabroke, G.M., Tanga, P., Thévenin, F., Gracia-Abril, G., Comoretto, G., Garcia-Reinaldos, M., Teyssier, D., Altmann, M., Andrae, R., Audard, M., Bellas-Velidis, I., Benson, K., Berthier, J., Blomme, R., Burgess, P., Busso, G., Carry, B., Cellino, A., Clementini, G., Clotet, M., Creevey, O., Davidson, M., De Ridder, J., Delchambre, L., Dell’Oro, A., Ducourant, C., Fernández-Hernández, J., Fouesneau, M., Frémat, Y., Galluccio, L., García-Torres, M., González-Núñez, J., González-Vidal, J.J., Gosset, E., Guy, L.P., Halbwachs, J.-L., Hambly, N.C., Harrison, D.L., Hernández, J., Hestroffer, D., Hodgkin, S.T., Hutton, A., Jasiewicz, G., Jean-Antoine-Piccolo, A., Jordan, S., Korn, A.J., Krone-Martins, A., Lanzafame, A.C., Lebzelter, T., Löffler, W., Manteiga, M., Marrese, P.M., Martín-Fleitas, J.M., Moitinho, A., Mora, A., Muinonen, K., Osinde, J., Pancino, E., Pauwels, T., Petit, J.-M., Recio-Blanco, A., Richards, P.J., Rimoldini, L., Robin, A.C., Sarro, L.M., Siopis, C., Smith, M., Sozzetti, A., Süveges, M., Torra, J., Reeven, W., Abbas, U., Abreu Aramburu, A., Accart, S., Aerts, C., Altavilla, G., Alvarez, M.A., Alvarez, R., Alves, J., Anderson, R.I., Andrei, A.H., Anglada Varela, E., Antiche, E., Antoja, T., Arcay, B., Astraatmadja, T.L., Bach, N., Baker, S.G., Balaguer-Núñez, L., Balm, P., Barache, C., Barata, C., Barbato, D., Barblan, F., Barklem, P.S., Barrado, D., Barros, M., Barstow, M.A., Bartholomé Muñoz, S., Bassilana, J.-L., Becciani, U., Bellazzini, M., Berihuete, A.,

Bertone, S., Bianchi, L., Bienaymé, O., Blanco-Cuaresma, S., Boch, T., Boeche, C., Bombrun, A., Borrachero, R., Bossini, D., Bouquillon, S., Bourda, G., Bragaglia, A., Bramante, L., Breddels, M.A., Bressan, A., Brouillet, N., Brüsmeister, T., Brugaletta, E., Bucciarelli, B., Burlacu, A., Busonero, D., Butkevich, A.G., Buzzi, R., Caffau, E., Cancelliere, R., Cannizzaro, G., Cantat-Gaudin, T., Carballo, R., Carlucci, T., Carrasco, J.M., Casamiquela, L., Castellani, M., Castro-Ginard, A., Charlot, P., Chemin, L., Chiavassa, A., Cocozza, G., Costigan, G., Cowell, S., Crifo, F., Crosta, M., Crowley, C., Cuyppers, J., Dafonte, C., Damerджи, Y., Dapergolas, A., David, P., David, M., Laverny, P., De Luise, F., De March, R., Martino, D., Souza, R., Torres, A., Deboscher, J., Pozo, E., Delbo, M., Delgado, A., Delgado, H.E., Di Matteo, P., Diakite, S., Diener, C., Distefano, E., Dolding, C., Drazinos, P., Durán, J., Edvardsson, B., Enke, H., Eriksson, K., Esquej, P., Eynard Bontemps, G., Fabre, C., Fabrizio, M., Faigler, S., Falcão, A.J., Farràs Casas, M., Federici, L., Fedorets, G., Fernique, P., Figueras, F., Filippi, F., Findeisen, K., Fonti, A., Fraile, E., Fraser, M., Frézouls, B., Gai, M., Galleti, S., Garabato, D., García-Sedano, F., Garofalo, A., Garralda, N., Gavel, A., Gavras, P., Gerssen, J., Geyer, R., Giacobbe, P., Gilmore, G., Girona, S., Giuffrida, G., Glass, F., Gomes, M., Granvik, M., Gueguen, A., Guerrier, A., Guiraud, J., Gutiérrez-Sánchez, R., Haignon, R., Hatzidimitriou, D., Hauser, M., Haywood, M., Heiter, U., Helmi, A., Heu, J., Hilger, T., Hobbs, D., Hofmann, W., Holland, G., Huckle, H.E., Hypki, A., Icardi, V., Janßen, K., Fombelle, G., Jonker, P.G., Juhász, A.L., Julbe, F., Karampelas, A., Kewley, A., Klar, J., Kochoska, A., Kohley, R., Kolenberg, K., Kontizas, M., Kontizas, E., Koposov, S.E., Kordopatis, G., Kostrzewa-Rutkowska, Z., Koubsky, P., Lambert, S., Lanza, A.F., Lasne, Y., Lavigne, J.-B., Le Fustec, Y., Le Poncin-Lafitte, C., Lebreton, Y., Leccia, S., Leclerc, N., Lecoeur-Taibi, I., Lenhardt, H., Leroux, F., Liao, S., Licata, E., Lindstrøm, H.E.P., Lister, T.A., Livanou, E., Lobel, A., López, M., Managau, S., Mann, R.G., Mantelet, G., Marchal, O., Marchant, J.M., Marconi, M., Marinoni, S., Marschalkó, G., Marshall, D.J., Martino, M., Marton, G., Mary, N., Massari, D., Matijevič, G., Mazeh, T., McMillan, P.J., Messina, S., Michalik, D., Millar, N.R., Molina, D., Molinaro, R., Molnár, L., Montegriffo, P., Mor, R., Morbidelli, R., Morel, T., Morris, D., Mulone, A.F., Muraveva, T., Musella, I., Nelemans, G., Nicastrò, L., Noval, L., O'Mullane, W., Ordénovic, C., Ordóñez-Blanco, D., Osborne, P., Pagani, C., Pagano, I., Paillet, F., Palacin, H., Palaversa, L., Panahi, A., Pawlak, M., Piersimoni, A.M., Pineau, F.-X., Plachy, E., Plum, G., Poggio, E., Poujoulet, E., Prša, A., Pulone, L., Racero, E., Ragaini, S., Rambaux, N., Ramos-Lerate, M., Regibo, S., Reylé, C., Riclet, F., Ripepi, V., Riva, A., Rivard, A., Rixon, G., Roegiers, T., Roelens, M., Romero-Gómez, M., Rowell, N., Royer, F., Ruiz-Dern, L., Sadowski, G., Sagristà Sellés, T., Sahlmann, J., Salgado, J., Salguero, E., Sanna, N., Santana-Ros, T., Sarasso, M., Savietto, H., Schultheis, M., Sciacca, E., Segol, M., Segovia, J.C., Ségransan, D., Shih, I.-C., Siltala, L., Silva, A.F., Smart, R.L., Smith, K.W., Solano, E., Solitro, F., Sordo, R., Soria Nieto, S., Souchay, J., Spagna, A., Spoto, F., Stampa, U., Steele, I.A., Steidelmüller, H., Stephenson, C.A., Stoev, H., Suess, F.F., Surdej, J., Szabados, L., Szegedi-Elek, E., Tapiador, D., Taris, F., Tauran, G., Taylor, M.B., Teixeira, R., Terrett, D., Teyssandier, P., Thuillot, W., Titarenko, A., Torra Clotet, F., Turon,

- C., Ulla, A., Utrilla, E., Uzzi, S., Vaillant, M., Valentini, G., Valette, V., Elteren, A., Van Hemelryck, E., Leeuwen, M., Vaschetto, M., Vecchiato, A., Veljanoski, J., Viala, Y., Vicente, D., Vogt, S., Essen, C., Voss, H., Votruba, V., Voutsinas, S., Walmsley, G., Weiler, M., Wertz, O., Wevers, T., Wyrzykowski, L., Yoldas, A., Žerjal, M., Ziaeeepour, H., Zorec, J., Zschocke, S., Zucker, S., Zurbach, C., Zwitter, T.: Gaia Data Release 2. Summary of the contents and survey properties. *Astronomy and Astrophysics* **616**, 1 (2018) <https://doi.org/10.1051/0004-6361/201833051> . ADS Bibcode: 2018A&A...616A...1G. Accessed 2024-10-04
- Gray, R.O., Corbally, C.J., Garrison, R.F., McFadden, M.T., Bubar, E.J., McGahee, C.E., O'Donoghue, A.A., Knox, E.R.: Contributions to the Nearby Stars (NStars) Project: Spectroscopy of Stars Earlier than M0 within 40 pc-The Southern Sample. *Astron. J.* **132**(1), 161–170 (2006) <https://doi.org/10.1086/504637> [arXiv:astro-ph/0603770](https://arxiv.org/abs/astro-ph/0603770) [astro-ph]
- Gentile Fusillo, N.P., Gänsicke, B.T., Farihi, J., Koester, D., Schreiber, M.R., Pala, A.F.: Trace hydrogen in helium atmosphere white dwarfs as a possible signature of water accretion. *Mon. Not. Roy. Astron. Soc.* **468**(1), 971–980 (2017) <https://doi.org/10.1093/mnras/stx468> [arXiv:1702.06542](https://arxiv.org/abs/1702.06542) [astro-ph.SR]
- Gkotsinas, A., Guilbert-Lepoutre, A., Raymond, S.N., Nesvorný, D.: Thermal Processing of Jupiter-family Comets during Their Chaotic Orbital Evolution. *Astrophys. J.* **928**(1), 43 (2022) <https://doi.org/10.3847/1538-4357/ac54ac> [arXiv:2202.06685](https://arxiv.org/abs/2202.06685) [astro-ph.EP]
- Gloeckler, G., Geiss, J., Schwadron, N.A., Fisk, L.A., Zurbuchen, T.H., Ipavich, F.M., von Steiger, R., Balsiger, H., Wilken, B.: Interception of comet Hyakutake's ion tail at a distance of 500 million kilometres. *Nature* **404**(6778), 576–578 (2000) <https://doi.org/10.1038/35007015>
- Gronkowski, P.: The destruction of cometary grains and changes in the luminosity of comets. *Astronomische Nachrichten* **330**(8), 784 (2009) <https://doi.org/10.1002/asna.200711234>
- Grady, C.A., Sitko, M.L., Bjorkman, K.S., Pérez, M.R., Lynch, D.K., Russell, R.W., Hanner, M.S.: The Star-grazing Extrasolar Comets in the HD 100546 System. *Astrophys. J.* **483**(1), 449–456 (1997) <https://doi.org/10.1086/304230>
- Guilbert-Lepoutre, A.: Survival of Amorphous Water Ice on Centaurs. *Astron. J.* **144**(4), 97 (2012) <https://doi.org/10.1088/0004-6256/144/4/97>
- Galli, A., Vorburget, A., Carberry Mogan, S.R., Roussos, E., Stenberg Wieser, G., Wurz, P., Föhn, M., Krupp, N., Fränz, M., Barabash, S., Futaana, Y., Brandt, P.C., Kollmann, P., Haggerty, D.K., Jones, G.H., Johnson, R.E., Tucker, O.J., Simon, S., Tippens, T., Liuzzo, L.: Callisto's Atmosphere and Its Space Environment: Prospects for the Particle Environment Package on Board JUICE. *Earth and Space Science* **9**(5), 02172 (2022) <https://doi.org/10.1029/2021EA002172>

- Guidry, J.A., Vanderbosch, Z.P., Hermes, J.J., Barlow, B.N., Lopez, I.D., Boudreaux, T.M., Corcoran, K.A., Bell, K.J., Montgomery, M.H., Heintz, T.M., Castanheira, B.G., Reding, J.S., Dunlap, B.H., Winget, D.E., Winget, K.I., Kuehne, J.W.: I Spy Transits and Pulsations: Empirical Variability in White Dwarfs Using Gaia and the Zwicky Transient Facility. *Astrophys. J.* **912**(2), 125 (2021) <https://doi.org/10.3847/1538-4357/abee68> arXiv:2012.00035 [astro-ph.SR]
- Grady, C.A., Wisniewski, J.P., Schneider, G., Boccaletti, A., Gaspar, A., Debes, J.H., Hines, D.C., Stark, C.C., Thalmann, C., Lagrange, A.-M., Augereau, J.-C., Sezestre, E., Milli, J., Henning, T., Kuchner, M.J.: The Eroding Disk of AU Mic. *The Astrophysical Journal* **889**, 21 (2020) <https://doi.org/10.3847/2041-8213/ab65bb> . Publisher: IOP ADS Bibcode: 2020ApJ...889L..21G. Accessed 2024-10-02
- Howe, A.R., Adams, F.C., Meyer, M.R.: Survival of Primordial Planetary Atmospheres: Photodissociation-driven Mass Loss. *Astrophys. J.* **894**(2), 130 (2020) <https://doi.org/10.3847/1538-4357/ab620c> arXiv:1912.08820 [astro-ph.EP]
- Hanner, M.S.: The nature of cometary dust from remote sensing. In: Gombosi, T.I. (ed.) *Cometary Exploration*, Volume 2, vol. 2, pp. 1–22 (1983)
- Huebner, W.F., Benkhoff, J., Capria, M.T., Coradini, A., Sanctis, M.C.D., Orosei, R., Prialnik, D.: Heat and Gas Diffusion in Comet Nuclei. *International Space Science Institute*. International Space Science Institute, ??? (2006)
- Hammel, H.B., Beebe, R.F., Ingersoll, A.P., Orton, G.S., Mills, J.R., Simon, A.A., Chodas, P., Clarke, J.T., de Jong, E., Dowling, T.E., Harrington, J., Huber, L.F., Karkoschka, E., Santori, C.M., Toigo, A., Yeomans, D., West, R.A.: HST Imaging of Atmospheric Phenomena Created by the Impact of Comet Shoemaker-Levy 9. *Science* **267**(5202), 1288–1296 (1995) <https://doi.org/10.1126/science.7871425>
- Hogg, M.A., Cutter, R., Wynn, G.A.: The effect of a magnetic field on the dynamics of debris discs around white dwarfs. *Mon. Not. Roy. Astron. Soc.* **500**(3), 2986–3001 (2021) <https://doi.org/10.1093/mnras/staa3316> arXiv:2009.03444 [astro-ph.SR]
- Hughes, A.M., Duchêne, G., Matthews, B.C.: Debris Disks: Structure, Composition, and Variability. *Annu. Rev. Astron. Astrophys.* **56**, 541–591 (2018) <https://doi.org/10.1146/annurev-astro-081817-052035> arXiv:1802.04313 [astro-ph.EP]
- Hsieh, H.H., Jewitt, D.: A Population of Comets in the Main Asteroid Belt. *Science* **312**(5773), 561–563 (2006) <https://doi.org/10.1126/science.1125150>
- Hanlon, J., Jones, G.H.: An empirical radiation pressure correction for dust at small stellarcentric distances. *Monthly Notices of the Royal Astronomical Society: Letters* **543**(1), 14–19 (2025) <https://doi.org/10.1093/mnrasl/slaf087> . Accessed 2025-08-28
- Hui, M.-T., Jewitt, D., Clark, D.: Pre-discovery Observations and Orbit of Comet

- C/2017 K2 (PANSTARRS). *Astron. J.* **155**(1), 25 (2018) <https://doi.org/10.3847/1538-3881/aa9be1> arXiv:1711.06355 [astro-ph.EP]
- Hoeijmakers, H.J., Jaworska, K.P., Prinoth, B.: Exocomets of β Pictoris: I. Exocomet destruction, sodium absorption and disk line variability in 17 years of HARPS observations. *Astron. Astrophys.* **700**, 239 (2025) <https://doi.org/10.1051/0004-6361/202451594> arXiv:2505.21625 [astro-ph.EP]
- Huebner, W.F., Keady, J.J., Lyon, S.P.: Solar Photo Rates for Planetary Atmospheres and Atmospheric Pollutants. *Astrophys. Space Sci.* **195**(1), 1–294 (1992) <https://doi.org/10.1007/BF00644558>
- Huebner, W.F., Keady, J.J., Lyon, S.P.: Solar Photo Rates for Planetary Atmospheres and Atmospheric Pollutants. *Astrophys. Space Sci.* **195**(1), 1–294 (1992) <https://doi.org/10.1007/BF00644558>
- Hoskin, M.J., Toloza, O., Gänsicke, B.T., Raddi, R., Koester, D., Pala, A.F., Manser, C.J., Farihi, J., Belmonte, M.T., Hollands, M., Gentile Fusillo, N., Swan, A.: White dwarf pollution by hydrated planetary remnants: hydrogen and metals in WD J204713.76-125908.9. *Mon. Not. Roy. Astron. Soc.* **499**(1), 171–182 (2020) <https://doi.org/10.1093/mnras/staa2717> arXiv:2009.05053 [astro-ph.EP]
- Husser, T.-O., Wende-von Berg, S., Dreizler, S., Homeier, D., Reiners, A., Barman, T., Hauschildt, P.H.: A new extensive library of PHOENIX stellar atmospheres and synthetic spectra. *Astron. Astrophys.* **553**, 6 (2013) <https://doi.org/10.1051/0004-6361/201219058> arXiv:1303.5632 [astro-ph.SR]
- Harrington Pinto, O., Womack, M., Fernandez, Y., Bauer, J.: A Survey of CO, CO₂, and H₂O in Comets and Centaurs. *Planet. Sci. J.* **3**(11), 247 (2022) <https://doi.org/10.3847/PSJ/ac960d> arXiv:2209.09985 [astro-ph.EP]
- Hui, M.-T., Weryk, R., Micheli, M., Huang, Z., Wainscoat, R.: Serendipitous Archival Observations of a New Ultradistant Comet C/2019 E3 (ATLAS). *Astron. J.* **167**(3), 140 (2024) <https://doi.org/10.3847/1538-3881/ad2500>
- Hartzell, C., Zimmerman, M., Hergenrother, C.: An Evaluation of Electrostatic Lofting and Subsequent Particle Motion on Bennu. *The Planetary Science Journal* **3**(4), 85 (2022) <https://doi.org/10.3847/PSJ/ac5629> . Publisher: IOP Publishing. Accessed 2024-09-26
- Iseli, M., Küppers, M., Benz, W., Bochsler, P.: Sungrazing Comets: Properties of Nuclei and in Situ Detectability of Cometary Ions at 1 AU. *Icarus* **155**(2), 350–364 (2002) <https://doi.org/10.1006/icar.2001.6722> arXiv:astro-ph/0110091 [astro-ph]
- Itikawa, Y., Mason, N.: Cross Sections for Electron Collisions with Water Molecules. *Journal of Physical and Chemical Reference Data* **34**(1), 1–22 (2005) <https://doi.org/10.1063/1.1799251>

- Izquierdo, P., Toloza, O., Gänsicke, B.T., Rodríguez-Gil, P., Farihi, J., Koester, D., Guo, J., Redfield, S.: GD 424 - a helium-atmosphere white dwarf with a large amount of trace hydrogen in the process of digesting a rocky planetesimal. *Mon. Not. Roy. Astron. Soc.* **501**(3), 4276–4288 (2021) <https://doi.org/10.1093/mnras/staa3987> arXiv:2012.12957 [astro-ph.EP]
- Jewitt, D., Agarwal, J., Li, J., Weaver, H., Mutchler, M., Larson, S.: Disintegrating Asteroid P/2013 R3. *Astrophys. J. Lett.* **784**(1), 8 (2014) <https://doi.org/10.1088/2041-8205/784/1/L8> arXiv:1403.1237 [astro-ph.EP]
- Johnson, R.E., Baragiola, R.A.: Lunar surface: Sputtering and secondary ion mass spectrometry. *Geophysical Research Letters* **18**(11), 2063–2066 (1991) <https://doi.org/10.1029/91GL02664>
- Janches, D., Berezhnoy, A.A., Christou, A.A., Cremonese, G., Hirai, T., Horányi, M., Jasinski, J.M., Sarantos, M.: Meteoroids as One of the Sources for Exosphere Formation on Airless Bodies in the Inner Solar System. *Space Science Reviews* **217**(4), 50 (2021) <https://doi.org/10.1007/s11214-021-00827-6>
- Jian-chun, S., Chi-sheng, L., Zhong-wei, H., Hai-bin, Z., Yue-hua, M.: A Disconnection Event of Comet Lulin†. *Chinese Astronomy and Astrophysics* **35**(3), 295–303 (2011) <https://doi.org/10.1016/j.chinastron.2011.07.007> . Accessed 2024-02-06
- Jones, J.W., Chiang, E., Duchêne, G., Kalas, P., Esposito, T.M.: Giant Impacts and Debris Disk Morphology. *Astrophys. J.* **948**(2), 102 (2023) <https://doi.org/10.3847/1538-4357/acc466> arXiv:2303.10189 [astro-ph.EP]
- Jorda, L., Crovisier, J., Green, D.W.E.: The Correlation Between Visual Magnitudes and Water Production Rates (2008). http://adsabs.harvard.edu/cgi-bin/nph-data_query?bibcode=2008LPICo1405.8046J&link_type=ARTICLE Accessed 0
- Jewitt, D.: The Active Centaurs. *Astron. J.* **137**(5), 4296–4312 (2009) <https://doi.org/10.1088/0004-6256/137/5/4296> arXiv:0902.4687 [astro-ph.EP]
- Jewitt, D.: The Active Asteroids. *Astron. J.* **143**(3), 66 (2012) <https://doi.org/10.1088/0004-6256/143/3/66> arXiv:1112.5220 [astro-ph.EP]
- Jorda, L., Gaskell, R., Capanna, C., Hviid, S., Lamy, P., Ďurech, J., Faury, G., Groussin, O., Gutiérrez, P., Jackman, C., Keihm, S.J., Keller, H.U., Knollenberg, J., Kührt, E., Marchi, S., Mottola, S., Palmer, E., Schloerb, F.P., Sierks, H., Vincent, J.-B., A’Hearn, M.F., Barbieri, C., Rodrigo, R., Koschny, D., Rickman, H., Barucci, M.A., Bertaux, J.L., Bertini, I., Cremonese, G., Da Deppo, V., Davidsson, B., Debei, S., De Cecco, M., Fornasier, S., Fulle, M., Güttler, C., Ip, W.-H., Kramm, J.R., Küppers, M., Lara, L.M., Lazzarin, M., Lopez Moreno, J.J., Marzari, F., Naletto, G., Ockay, N., Thomas, N., Tubiana, C., Wenzel, K.-P.: The global shape, density and rotation of Comet 67P/Churyumov-Gerasimenko

- from preperihelion Rosetta/OSIRIS observations. *Icarus* **277**, 257–278 (2016) <https://doi.org/10.1016/j.icarus.2016.05.002>
- Jones, G.H., Knight, M.M., Battams, K., Boice, D.C., Brown, J., Giordano, S., Raymond, J., Snodgrass, C., Steckloff, J.K., Weissman, P., Fitzsimmons, A., Lisse, C.M., Opitom, C., Birkett, K.S., Bzowski, M., Decock, A., Mann, I., Ramanjooloo, Y., McCauley, P.: The Science of Sungrazers, Sunskirters, and Other Near-Sun Comets. *Space Science Reviews* **214**(1), 20 (2018) <https://doi.org/10.1007/s11214-017-0446-5>
- Johnson, R.E.: Sputtering and composition of planetary surfaces. *Reviews of Modern Physics* **85**, 801–812 (2013) <https://doi.org/10.1103/RevModPhys.85.801>
- Janson, M., Patel, J., Ringqvist, S.C., Lu, C., Rebollido, I., Lichtenberg, T., Brandeker, A., Angerhausen, D., Noack, L.: Imaging of exocomets with infrared interferometry. *Astronomy and Astrophysics* **671**, 114 (2023) <https://doi.org/10.1051/0004-6361/202245402> . ADS Bibcode: 2023A&A...671A.114J. Accessed 2024-03-07
- Jia, Y.D., Russell, C.T., Jian, L.K., Manchester, W.B., Cohen, O., Vourlidas, A., Hansen, K.C., Combi, M.R., Gombosi, T.I.: Study of the 2007 April 20 CME-Comet Interaction Event with an MHD Model. *The Astrophysical Journal* **696**, 56–60 (2009) <https://doi.org/10.1088/0004-637X/696/1/L56> . ADS Bibcode: 2009ApJ...696L..56J. Accessed 2023-10-12
- Jura, M.: A Tidally Disrupted Asteroid around the White Dwarf G29-38. *Astrophys. J. Lett.* **584**(2), 91–94 (2003) <https://doi.org/10.1086/374036> arXiv:astro-ph/0301411 [astro-ph]
- Jackson, A.P., Wyatt, M.C., Bonsor, A., Veras, D.: Debris from giant impacts between planetary embryos at large orbital radii. *Mon. Not. Roy. Astron. Soc.* **440**(4), 3757–3777 (2014) <https://doi.org/10.1093/mnras/stu476> arXiv:1403.1888 [astro-ph.EP]
- Knight, M.M., A'Hearn, M.F., Biesecker, D.A., Faury, G., Hamilton, D.P., Lamy, P., Llebaria, A.: Photometric Study of the Kreutz Comets Observed by SOHO from 1996 to 2005. *Astron. J.* **139**(3), 926–949 (2010) <https://doi.org/10.1088/0004-6256/139/3/926>
- Kuchar, T.A., Buffington, A., Arge, C.N., Hick, P.P., Howard, T.A., Jackson, B.V., Johnston, J.C., Mizuno, D.R., Tappin, S.J., Webb, D.F.: Observations of a comet tail disruption induced by the passage of a CME. *Journal of Geophysical Research: Space Physics* **113**(A4) (2008) <https://doi.org/10.1029/2007JA012603> . eprint: <https://onlinelibrary.wiley.com/doi/pdf/10.1029/2007JA012603>. Accessed 2024-02-05
- Killen, R., Cremonese, G., Lammer, H., Orsini, S., Potter, A.E., Sprague, A.L., Wurz, P., Khodachenko, M.L., Lichtenegger, H.I.M., Milillo, A., Mura, A.: Processes that Promote and Deplete the Exosphere of Mercury. *Space Sci. Rev.* **132**(2-4), 433–509

(2007) <https://doi.org/10.1007/s11214-007-9232-0>

- Kruczkiewicz, F., Dulieu, F., Ivlev, A.V., Caselli, P., Giuliano, B.M., Ceccarelli, C., Theulé, P.: Comprehensive laboratory constraints on thermal desorption of interstellar ice analogues. *Astron. Astrophys.* **686**, 236 (2024) <https://doi.org/10.1051/0004-6361/202346948> [arXiv:2404.02695](https://arxiv.org/abs/2404.02695) [astro-ph.GA]
- Kramer, E.A., Fernandez, Y.R., Lisse, C.M., Kelley, M.S.P., Woodney, L.M.: A dynamical analysis of the dust tail of Comet C/1995 O1 (Hale–Bopp) at high heliocentric distances. *Icarus* **236**, 136–145 (2014) <https://doi.org/10.1016/j.icarus.2014.03.033> . Accessed 2025-01-16
- Kislyakova, K.G., Güdel, M., Koutroumpa, D., Carter, J.A., Lisse, C.M., Boro Saikia, S.: X-ray detection of astrospheres around three main-sequence stars and their mass-loss rates. *Nature Astronomy* **8**, 596–605 (2024) <https://doi.org/10.1038/s41550-024-02222-x> [arXiv:2404.14980](https://arxiv.org/abs/2404.14980) [astro-ph.SR]
- Kelley, M.S.P., Hsieh, H.H., Bodewits, D., Saki, M., Villanueva, G.L., Milam, S.N., Hammel, H.B.: Spectroscopic identification of water emission from a main-belt comet. *Nature* **619**(7971), 720–723 (2023) <https://doi.org/10.1038/s41586-023-06152-y>
- Killen, R.M., Hurley, D.M., Farrell, W.M.: The effect on the lunar exosphere of a coronal mass ejection passage. *Journal of Geophysical Research (Planets)* **117**, 00–02 (2012) <https://doi.org/10.1029/2011JE004011>
- Killen, R.M.: Pathways for energization of Ca in Mercury’s exosphere. *Icarus* **268**, 32–36 (2016) <https://doi.org/10.1016/j.icarus.2015.12.035>
- Klačka, J., Kocifaj, M.: Times of inspiralling for interplanetary dust grains. *Monthly Notices of the Royal Astronomical Society* **390**, 1491–1495 (2008) <https://doi.org/10.1111/j.1365-2966.2008.13801.x> . Publisher: OUP ADS Bibcode: 2008MNRAS.390.1491K. Accessed 2024-07-16
- Kharchuk, S.V., Korsun, P.P., Mikuz, H.: Model analysis of the dust tail of comet Hale–Bopp. *Kinematics and Physics of Celestial Bodies* **25**(4), 189–193 (2009) <https://doi.org/10.3103/S0884591309040035> . Accessed 2025-01-20
- Kimura, H., Kunitomo, M., Suzuki, T.K., Robrade, J., Thebault, P., Mitsuishi, I.: Hot grain dynamics by electric charging and magnetic trapping in debris disks. *Plan. Spac. Sci.* **183**, 104581 (2020) <https://doi.org/10.1016/j.pss.2018.07.010>
- Knight, M.M., Kokotanekova, R., Samarasinha, N.H.: Physical and Surface Properties of Comet Nuclei from Remote Observations. In: Meech, K.J., Combi, M.R., Bockelée-Morvan, D., Raymond, S.N., Zolensky, M.E. (eds.) *Comets III*, pp. 361–404 (2024). https://doi.org/10.2458/azu_uapress_9780816553631-ch012

- Kelley, M.S., Lindler, D.J., Bodewits, D., A’Hearn, M.F., Lisse, C.M., Kolokolova, L., Kissel, J., Hermalyn, B.: A distribution of large particles in the coma of Comet 103P/Hartley 2. *Icarus* **222**(2), 634–652 (2013) <https://doi.org/10.1016/j.icarus.2012.09.037> . Accessed 2025-03-05
- Kiefer, F., Lecavelier des Etangs, A., Boissier, J., Vidal-Madjar, A., Beust, H., Lagrange, A.-M., Hébrard, G., Ferlet, R.: Two families of exocomets in the β Pictoris system. *Nature* **514**(7523), 462–464 (2014) <https://doi.org/10.1038/nature13849>
- Kalas, P., Liu, M.C., Matthews, B.C.: Discovery of a Large Dust Disk Around the Nearby Star AU Microscopii. *Science* **303**, 1990–1992 (2004) <https://doi.org/10.1126/science.1093420> . ADS Bibcode: 2004Sci...303.1990K. Accessed 2024-10-04
- Kimura, H., Mann, I., Biesecker, D.A., Jessberger, E.K.: Dust Grains in the Comae and Tails of Sungrazing Comets: Modeling of Their Mineralogical and Morphological Properties. *Icarus* **159**(2), 529–541 (2002) <https://doi.org/10.1006/icar.2002.6940>
- Kimura, H., Ohtsuka, K., Kikuchi, S., Ohtsuki, K., Arai, T., Yoshida, F., Hirata, N., Senshu, H., Wada, K., Hirai, T., Hong, P.K., Kobayashi, M., Ishibashi, K., Yamada, M., Okamoto, T.: Electrostatic dust ejection from asteroid (3200) Phaethon with the aid of mobile alkali ions at perihelion. *Icarus* **382**, 115022 (2022) <https://doi.org/10.1016/j.icarus.2022.115022> . Accessed 2023-10-09
- Kossacki, K.J.: Sublimation of porous granular ice in vacuum. *Icarus* **368**, 114613 (2021) <https://doi.org/10.1016/j.icarus.2021.114613>
- Klačka, J., Petržala, J., Pástor, P., Kómar, L.: The Poynting–Robertson effect: A critical perspective. *Icarus* **232**, 249–262 (2014) <https://doi.org/10.1016/j.icarus.2012.06.044> . Accessed 2024-07-25
- Kálmán, S., Szabó, G.M., Kiss, C.: Exocomet Models in Transit: Light Curve Morphology in the Optical—Near Infrared Wavelength Range. *Publ. Astron. Soc. Pac.* **136**(8), 084401 (2024) <https://doi.org/10.1088/1538-3873/ad4fe3> arXiv:2405.13663 [astro-ph.EP]
- Killen, R.M., Sarantos, M., Potter, A.E., Reiff, P.: The effect of solar wind variability on the mercury exosphere. *Icarus* **209**(1), 75–87 (2012) <https://doi.org/10.1016/j.icarus.2010.08.005>
- Kaib, N.A., Volk, K.: Dynamical Population of Comet Reservoirs. arXiv e-prints, 2206–00010 (2022) <https://doi.org/10.48550/arXiv.2206.00010> arXiv:2206.00010 [astro-ph.EP]
- Kirchschlager, F., Wolf, S., Krivov, A.V., Mutschke, H., Brunngräber, R.: Constraints on the structure of hot exozodiacal dust belts. *Mon. Not. Roy. Astron. Soc.* **467**(2), 1614–1626 (2017) <https://doi.org/10.1093/mnras/stx202> arXiv:1701.07271 [astro-ph.SR]

- Kwok, S.: Radiation pressure on grains as a mechanism for mass loss in red giants. *Astrophys. J.* **198**, 583–591 (1975) <https://doi.org/10.1086/153637>
- Kramida, A., Yu. Ralchenko, Reader, J., and NIST ASD Team NIST Atomic Spectra Database (ver. 5.11), [Online]. Available: <https://physics.nist.gov/asd> [2023, December 15]. National Institute of Standards and Technology, Gaithersburg, MD. (2023)
- Klein, B., Zicher, N., Kavanagh, R.D., Nielsen, L.D., Aigrain, S., Vidotto, A.A., Barragán, O., Strugarek, A., Nicholson, B., Donati, J.-F., Bouvier, J.: One year of AU Mic with HARPS – II. Stellar activity and star–planet interaction. *Monthly Notices of the Royal Astronomical Society* **512**(4), 5067–5084 (2022) <https://doi.org/10.1093/mnras/stac761> . Accessed 2024-10-04
- Lagrange, A.-M.: STIS observations of Beta Pictoris. HST Proposal ID 7512. Cycle 7 (1997)
- Lamy, P.L.: Interaction of interplanetary dust grains with the solar radiation field. *Astron. Astrophys.* **35**(2), 197–207 (1974)
- Lagrange, A.-M., Beust, H., Mouillet, D., Deleuil, M., Feldman, P.D., Ferlet, R., Hobbs, L., Lecavelier Des Etangs, A., Lissauer, J.J., McGrath, M.A., McPhate, J.B., Spyromilio, J., Tobin, W., Vidal-Madjar, A.: The beta Pictoris circumstellar disk. XXIV. Clues to the origin of the stable gas. *Astron. Astrophys.* **330**, 1091–1108 (1998)
- Lecavelier des Etangs, A., Cros, L., Hébrard, G., Martioli, E., Duquesnoy, M., Kenworthy, M.A., Kiefer, F., Lacour, S., Lagrange, A.-M., Meunier, N., Vidal-Madjar, A.: Exocomets size distribution in the β Pictoris planetary system. *Scientific Reports* **12**, 5855 (2022) <https://doi.org/10.1038/s41598-022-09021-2> [arXiv:2204.13618](https://arxiv.org/abs/2204.13618) [astro-ph.EP]
- Lecavelier Des Etangs, A.: A library of stellar light variations due to extra-solar comets. *Astronomy and Astrophysics Supplement Series* **140**, 15–20 (1999) <https://doi.org/10.1051/aas:1999114> . ADS Bibcode: 1999A&AS..140...15L. Accessed 2024-10-31
- Le Bourdais, É., Dufour, P., Xu, S.: Revisiting the Chemical Composition of WD 1145+017: Impact of Circumstellar Disks Contamination on Photospheric Abundances. *arXiv e-prints*, 2410–10948 (2024) <https://doi.org/10.48550/arXiv.2410.10948> [arXiv:2410.10948](https://arxiv.org/abs/2410.10948) [astro-ph.SR]
- Landini, M., Fossi, B.C.M.: Ion equilibrium for minor components in a thin plasma. *Astron. Astrophys. Supp.* **91**(1), 183–196 (1991)
- Luspay-Kuti, A., Hassig, M., Fuselier, S.A., Mandt, K.E., Altwegg, K., Balsiger, H., Gasc, S., Jackel, A., Roy, L.L., Rubin, M., Tzou, C.Y., Wurz, P.,

- Mousis, O., Dhooghe, F., Berthelier, J.J., Fiethe, B., Gombosi, T.t., Mall, U.A.: Composition-dependent outgassing of comet 67P/Churyumov-Gerasimenko from ROSINA/DFMS. Implications for nucleus heterogeneity? *Astronomy and Astrophysics* **583**, 4 (2015) <https://doi.org/10.1051/0004-6361/201526205>
- Löhne, T., Krivov, A.V., Rodmann, J.: Long-Term Collisional Evolution of Debris Disks. *Astrophys. J.* **673**(2), 1123–1137 (2008) <https://doi.org/10.1086/524840> [arXiv:0710.4294](https://arxiv.org/abs/0710.4294) [astro-ph]
- Luk'yanyk, I., Kulyk, I., Shubina, O., Pavlenko, Y., Vasylenko, M., Dobrycheva, D., Korsun, P.: Numerical simulations of exocomet transits: Insights from beta Pic and KIC 3542116. *Astronomy and Astrophysics* **688**, 65 (2024) <https://doi.org/10.1051/0004-6361/202348498>. ADS Bibcode: 2024A&A...688A..65L. Accessed 2024-10-31
- Luspay-Kuti, A., Mousis, O., Lunine, J.I., Ellinger, Y., Pauzat, F., Raut, U., Bouquet, A., Mandt, K.E., Maggiolo, R., Ronnet, T., Brugger, B., Ozgurel, O., Fuselier, S.A.: Origin of Molecular Oxygen in Comets: Current Knowledge and Perspectives. *Space Sci. Rev.* **214**(8), 115 (2018) <https://doi.org/10.1007/s11214-018-0541-2>
- Luspay-Kuti, A., Mousis, O., Pauzat, F., Ozgurel, O., Ellinger, Y., Lunine, J.I., Fuse-
lier, S.A., Mandt, K.E., Trattner, K.J., Petrinc, S.M.: Dual storage and release
of molecular oxygen in comet 67P/Churyumov-Gerasimenko. *Nature Astronomy* **6**,
724–730 (2022) <https://doi.org/10.1038/s41550-022-01614-1>
- Lagrange, A.-M., Plazy, F., Beust, H., Mouillet, D., Deleuil, M., Ferlet, R., Spyromilio,
J., Vidal-Madjar, A., Tobin, W., Hearnshaw, J.B., Clark, M., Thomas, K.W.: The
 β Pictoris circumstellar disk. XXI. Results from the December 1992 spectroscopic
campaign. *Astron. Astrophys.* **310**, 547–563 (1996)
- Lawson, K., Schlieder, J.E., Leisenring, J.M., Bogat, E., Beichman, C.A., Bryden,
G., Gáspár, A., Groff, T.D., McElwain, M.W., Meyer, M.R., Barclay, T., Calis-
sendorff, P., De Furio, M., Ygouf, M., Boccaletti, A., Greene, T.P., Krist, J.,
Plavchan, P., Rieke, M.J., Roellig, T.L., Stansberry, J., Wisniewski, J.P., Young,
E.T.: JWST/NIRCam Coronagraphy of the Young Planet-hosting Debris Disk AU
Microscopii. *The Astronomical Journal* **166**, 150 (2023) <https://doi.org/10.3847/1538-3881/aced08>. Publisher: IOP ADS Bibcode: 2023AJ....166..150L. Accessed 2024-10-02
- Lagrange, A.M., Vidal-Madjar, A., Deleuil, M., Emerich, C., Beust, H., Ferlet, R.:
The β Pictoris circumstellar disk. XVII. Physical and chemical parameters of the
disk. *Astron. Astrophys.* **296**, 499 (1995)
- Lecavelier Des Etangs, A., Vidal-Madjar, A., Ferlet, R.: Photometric stellar variation
due to extra-solar comets. *Astron. Astrophys.* **343**, 916–922 (1999) <https://doi.org/10.48550/arXiv.astro-ph/9812381> [arXiv:astro-ph/9812381](https://arxiv.org/abs/astro-ph/9812381) [astro-ph]

- Malamud, U.: White dwarf systems: exoplanets and debris disks. arXiv e-prints, 2403–07427 (2024) <https://doi.org/10.48550/arXiv.2403.07427> arXiv:2403.07427 [astro-ph.EP]
- Marsden, B.G.: The Sungrazing Comet Group. II. *Astron. J.* **98**, 2306 (1989) <https://doi.org/10.1086/115301>
- Marsden, B.G.: Sungrazing Comets. *Annu. Rev. Astron. Astrophys.* **43**(1), 75–102 (2005) <https://doi.org/10.1146/annurev.astro.43.072103.150554>
- Mayyasi, M., Clarke, J., Chaufray, J.-Y., Kass, D., Bougher, S., Bhattacharyya, D., Deighan, J., Jain, S., Schneider, N., Villanueva, G.L., Montmessin, F., Benna, M., Mahaffy, P., Jakosky, B.: Solar cycle and seasonal variability of H in the upper atmosphere of Mars. *Icarus* **393**, 115293 (2023) <https://doi.org/10.1016/j.icarus.2022.115293>
- McDaniel, E.W.: *Collision Phenomena in Ionized Gases*, (1964)
- McKellar, A.: Comparison of the λ 3883 CN Band in the Spectra of Comets 1940c and 1942g. *Astrophys. J.* **100**, 69 (1944) <https://doi.org/10.1086/144638>
- McClintock, W.E., Cassidy, T.A., Merkel, A.W., Killen, R.M., Burger, M.H., Vervack, R.J.: In: Solomon, S.C., Nittler, L.R., Anderson, B.J.E. (eds.) *Observations of Mercury’s Exosphere: Composition and Structure*. Cambridge Planetary Science, pp. 371–406. Cambridge University Press, ??? (2018)
- Masiero, J.R., Davidsson, B.J.R., Liu, Y., Moore, K., Tuite, M.: Volatility of Sodium in Carbonaceous Chondrites at Temperatures Consistent with Low-perihelion Asteroids. *Planet. Sci. J.* **2**(4), 165 (2021) <https://doi.org/10.3847/PSJ/ac0d02> arXiv:2108.07331 [astro-ph.EP]
- Marshall, J.P., Ertel, S., Birtcil, E., Villaver, E., Kemper, F., Boffin, H., Scicluna, P., Kamath, D.: Evidence for the Disruption of a Planetary System During the Formation of the Helix Nebula. *Astron. J.* **165**(1), 22 (2023) <https://doi.org/10.3847/1538-3881/ac9d90> arXiv:2211.02251 [astro-ph.EP]
- Malamud, U., Grishin, E., Brouwers, M.: Circularization of tidal debris around white dwarfs: implications for gas production and dust variability. *Mon. Not. Roy. Astron. Soc.* **501**(3), 3806–3824 (2021) <https://doi.org/10.1093/mnras/staa3940> arXiv:2012.07854 [astro-ph.EP]
- Manfroid, J., Hutsemékers, D., Jehin, E.: Iron and nickel atoms in cometary atmospheres even far from the Sun. *Nature* **593**(7859), 372–374 (2021) <https://doi.org/10.1038/s41586-021-03435-0>
- Meech, K.J., Kleyna, J.T., Hainaut, O.R., Micheli, M., Bauer, J., Denneau, L., Keane,

- J.V., Stephens, H., Jedicke, R., Wainscoat, R., Weryk, R., Flewelling, H., Schunova-Lilly, E., Magnier, E., Chambers, K.C.: CO-driven Activity in Comet C/2017 K2 (PANSTARRS). *Astrophysical Journal Letters* **849**(1), 8 (2017) <https://doi.org/10.3847/2041-8213/aa921f>
- Mazzotta, P., Mazzitelli, G., Colafrancesco, S., Vittorio, N.: Ionization balance for optically thin plasmas: Rate coefficients for all atoms and ions of the elements H to NI. *Astron. Astrophys. Supp.* **133**, 403–409 (1998) <https://doi.org/10.1051/aas:1998330> [arXiv:astro-ph/9806391](https://arxiv.org/abs/astro-ph/9806391) [astro-ph]
- Matrà, L., Marino, S., Wilner, D.J., Kennedy, G.M., Booth, M., Krivov, A.V., Williams, J.P., Hughes, A.M., del Burgo, C., Carpenter, J., Davies, C.L., Ertel, S., Kral, Q., Lestrade, J.-F., Marshall, J.P., Milli, J., Öberg, K.I., Pawellek, N., Sepulveda, A.G., Wyatt, M.C., Matthews, B.C., MacGregor, M.: REsolved ALMA and SMA Observations of Nearby Stars (REASONS): A population of 74 resolved planetesimal belts at millimetre wavelengths. *Astron. Astrophys.* **693**, 151 (2025) <https://doi.org/10.1051/0004-6361/202451397> [arXiv:2501.09058](https://arxiv.org/abs/2501.09058) [astro-ph.EP]
- Miret-Roig, N., Galli, P.a.B., Brandner, W., Bouy, H., Barrado, D., Olivares, J., Antoja, T., Romero-Gómez, M., Figueras, F., Lillo-Box, J.: Dynamical traceback age of the beta Pictoris moving group. *Astronomy & Astrophysics* **642**, 179 (2020) <https://doi.org/10.1051/0004-6361/202038765> . Publisher: EDP Sciences. Accessed 2024-10-04
- Meech, K.J., Svoren, J.: Using cometary activity to trace the physical and chemical evolution of cometary nuclei. In: Festou, M.C., Keller, H.U., Weaver, H.A. (eds.) *Comets II*, p. 317 (2004)
- MacGregor, M.A., Wilner, D.J., Rosenfeld, K.A., Andrews, S.M., Matthews, B., Hughes, A.M., Booth, M., Chiang, E., Graham, J.R., Kalas, P., Kennedy, G., Sibthorpe, B.: Millimeter Emission Structure in the First ALMA Image of the AU Mic Debris Disk. *The Astrophysical Journal* **762**, 21 (2013) <https://doi.org/10.1088/2041-8205/762/2/L21> . Publisher: IOP ADS Bibcode: 2013ApJ...762L..21M. Accessed 2024-10-04
- Nesvorný, D., Brož, M., Carruba, V.: Identification and Dynamical Properties of Asteroid Families. In: Michel, P., DeMeo, F.E., Bottke, W.F. (eds.) *Asteroids IV*, pp. 297–321 (2015). https://doi.org/10.2458/azu_uapress_9780816532131-ch016
- Nie, N.X., Dauphas, N., Zhang, Z.J., Hopp, T., Sarantos, M.: Lunar soil record of atmosphere loss over eons. *Science Advances* **10**(31), 7074 (2024) <https://doi.org/10.1126/sciadv.adm7074>
- Neugebauer, M., Gloeckler, G., Gosling, J.T., Rees, A., Skoug, R., Goldstein, B.E., Armstrong, T.P., Combi, M.R., Mäkinen, T., McComas, D.J., von Steiger, R., Zurbuchen, T.H., Smith, E.J., Geiss, J., Lanzerotti, L.J.: Encounter of the Ulysses Spacecraft with the Ion Tail of Comet MCNaught. *Astrophys. J.* **667**(2), 1262–1266

(2007) <https://doi.org/10.1086/521019>

- Nordheim, T.A., Jones, G.H., Halekas, J.S., Roussos, E., Coates, A.J.: Surface charging and electrostatic dust acceleration at the nucleus of comet 67P during periods of low activity. *Planetary and Space Science* **119**, 24–35 (2015) <https://doi.org/10.1016/j.pss.2015.08.008> . Accessed 2024-09-25
- Nowak, M., Lacour, S., Lagrange, A.-M., Rubini, P., Wang, J., Stolker, T., Abuter, R., Amorim, A., Asensio-Torres, R., Bauböck, M., Benisty, M., Berger, J.P., Beust, H., Blunt, S., Boccaletti, A., Bonnefoy, M., Bonnet, H., Brandner, W., Cantalloube, F., Charnay, B., Choquet, E., Christiaens, V., Clénet, Y., Coudé Du Foresto, V., Cridland, A., de Zeeuw, P.T., Dembet, R., Dexter, J., Drescher, A., Duvert, G., Eckart, A., Eisenhauer, F., Gao, F., Garcia, P., Garcia Lopez, R., Gardner, T., Gendron, E., Genzel, R., Gillessen, S., Girard, J., Grandjean, A., Haubois, X., Heißel, G., Henning, T., Hinkley, S., Hippler, S., Horrobin, M., Houllé, M., Hubert, Z., Jiménez-Rosales, A., Jocu, L., Kammerer, J., Kervella, P., Keppler, M., Kreidberg, L., Kulikauskas, M., Lapeyrère, V., Le Bouquin, J.-B., Léna, P., Mérand, A., Maire, A.-L., Mollière, P., Monnier, J.D., Mouillet, D., Müller, A., Nasedkin, E., Ott, T., Otten, G., Paumard, T., Paladini, C., Perraut, K., Perrin, G., Pueyo, L., Pfuhl, O., Rameau, J., Rodet, L., Rodríguez-Coira, G., Rousset, G., Scheithauer, S., Shangguan, J., Stadler, J., Straub, O., Straubmeier, C., Sturm, E., Tacconi, L.J., van Dishoeck, E.F., Vigan, A., Vincent, F., von Fellenberg, S.D., Ward-Duong, K., Widmann, F., Wieprecht, E., Wiezorrek, E., Woillez, J., GRAVITY Collaboration: Direct confirmation of the radial-velocity planet β Pictoris c. *Astron. Astrophys.* **642**, 2 (2020) <https://doi.org/10.1051/0004-6361/202039039> [arXiv:2010.04442](https://arxiv.org/abs/2010.04442) [astro-ph.EP]
- Newburn, R.L., Spinrad, H.: Spectrophotometry of seventeen comets. II - The continuum. *Astron. J.* **90**, 2591–2608 (1985) <https://doi.org/10.1086/113965>
- Noonan, J.W., Stern, S.A., Feldman, P.D., Broiles, T., Simon Wedlund, C., Edberg, N.J.T., Schindhelm, R., Parker, J.W., Keeney, B.A., Vervack, R.J. Jr., Steffl, A.J., Knight, M.M., Weaver, H.A., Feaga, L.M., A’Hearn, M., Bertaux, J.-L.: Ultraviolet Observations of Coronal Mass Ejection Impact on Comet 67P/Churyumov-Gerasimenko by Rosetta Alice. *Astron. J.* **156**(1), 16 (2018) <https://doi.org/10.3847/1538-3881/aac432> [arXiv:1806.06948](https://arxiv.org/abs/1806.06948) [astro-ph.EP]
- Okuya, A., Ida, S., Hyodo, R., Okuzumi, S.: Modelling the evolution of silicate/volatile accretion discs around white dwarfs. *Mon. Not. Roy. Astron. Soc.* **519**(2), 1657–1676 (2023) <https://doi.org/10.1093/mnras/stac3522> [arXiv:2211.16797](https://arxiv.org/abs/2211.16797) [astro-ph.EP]
- O’Connor, C.E., Lai, D., Seligman, D.Z.: On the pollution of white dwarfs by exo-Oort cloud comets. *Mon. Not. Roy. Astron. Soc.* **524**(4), 6181–6197 (2023) <https://doi.org/10.1093/mnras/stad2281> [arXiv:2306.10102](https://arxiv.org/abs/2306.10102) [astro-ph.EP]
- Pearce, T.D., *et al.*: Hot exozodis: cometary supply without trapping is unlikely to be the mechanism. *Mon. Not. Roy. Astron. Soc.* **517**(1), 1436–1451 (2022) <https://doi.org/10.1093/mnras/stab3000>

Plavchan, P., Barclay, T., Gagné, J., Gao, P., Cale, B., Matzko, W., Dragomir, D., Quinn, S., Feliz, D., Stassun, K., Crossfield, I.J.M., Berardo, D.A., Latham, D.W., Tieu, B., Anglada-Escudé, G., Ricker, G., Vanderspek, R., Seager, S., Winn, J.N., Jenkins, J.M., Rinehart, S., Krishnamurthy, A., Dynes, S., Doty, J., Adams, F., Afanasev, D.A., Beichman, C., Bottom, M., Bowler, B.P., Brinkworth, C., Brown, C.J., Cancino, A., Ciardi, D.R., Clampin, M., Clark, J.T., Collins, K., Davison, C., Foreman-Mackey, D., Furlan, E., Gaidos, E.J., Geneser, C., Giddens, F., Gilbert, E., Hall, R., Hellier, C., Henry, T., Horner, J., Howard, A.W., Huang, C., Huber, J., Kane, S.R., Kenworthy, M., Kielkopf, J., Kipping, D., Klenke, C., Kruse, E., Latouf, N., Lowrance, P., Mennesson, B., Mengel, M., Mills, S.M., Morton, T., Narita, N., Newton, E., Nishimoto, A., Okumura, J., Palle, E., Pepper, J., Quintana, E.V., Roberge, A., Roccatagliata, V., Schlieder, J.E., Tanner, A., Teske, J., Tinney, C.G., Vanderburg, A., Braun, K., Walp, B., Wang, J., Wang, S.X., Weigand, D., White, R., Wittenmyer, R.A., Wright, D.J., Youngblood, A., Zhang, H., Zilberman, P.: A planet within the debris disk around the pre-main-sequence star AU Microscopii. *Nature* **582**, 497–500 (2020) <https://doi.org/10.1038/s41586-020-2400-z> . ADS Bibcode: 2020Natur.582..497P. Accessed 2024-10-02

Poppe, A.R., Curry, S.M., Fatemi, S.e.a.: Solar wind interaction with the moon: A synthesis of disparate measurements. *Journal of Geophysical Research: Space Physics* **121**, 4129–4143 (2016) <https://doi.org/10.1002/2016JA022529>

Pearce, T.D.: Debris disks around main-sequence stars. arXiv e-prints, 2403–11804 (2024) [arXiv:2403.11804](https://arxiv.org/abs/2403.11804) [astro-ph.EP]

Prša, A., Harmanec, P., Torres, G., Mamajek, E., Asplund, M., Capitaine, N., Christensen-Dalsgaard, J., Depagne, É., Haberreiter, M., Hekker, S., Hilton, J., Kopp, G., Kostov, V., Kurtz, D.W., Laskar, J., Mason, B.D., Milone, E.F., Montgomery, M., Richards, M., Schmutz, W., Schou, J., Stewart, S.G.: Nominal Values for Selected Solar and Planetary Quantities: IAU 2015 Resolution B3. *Astron. J.* **152**(2), 41 (2016) <https://doi.org/10.3847/0004-6256/152/2/41> [arXiv:1605.09788](https://arxiv.org/abs/1605.09788) [astro-ph.SR]

Price, O., Jones, G.H., Battams, K., Owens, M.: Fine-scale structure in cometary dust tails II: Further evidence for a solar wind influence on cometary dust dynamics from the analysis of striae in comet C/2011 L4 Pan-STARRS. *Icarus* **389**, 115218 (2023) <https://doi.org/10.1016/j.icarus.2022.115218> . ADS Bibcode: 2023Icar..38915218P. Accessed 2023-10-06

Price, O., Jones, G.H., Morrill, J., Owens, M., Battams, K., Morgan, H., Drückmüller, M., Deiries, S.: Fine-scale structure in cometary dust tails I: Analysis of striae in Comet C/2006 P1 (McNaught) through temporal mapping. *Icarus* **319**, 540–557 (2019) <https://doi.org/10.1016/j.icarus.2018.09.013> . Accessed 2023-10-02

Pearce, T.D., Krivov, A.V., Booth, M.: Gas trapping of hot dust around main-sequence

- stars. *Mon. Not. Roy. Astron. Soc.* **498**(2), 2798–2813 (2020) <https://doi.org/10.1093/mnras/staa2514> arXiv:2008.07505 [astro-ph.EP]
- Pollack, J.B., Kasting, J.F., Richardson, S.M., Poliakoff, K.: The case for a wet, warm climate on early Mars. *Icarus* **71**(2), 203–224 (1987) [https://doi.org/10.1016/0019-1035\(87\)90147-3](https://doi.org/10.1016/0019-1035(87)90147-3)
- Pinto, O.H., Kelley, M.S.P., Villanueva, G.L., Womack, M., Faggi, S., McKay, A., DiSanti, M.A., Schambeau, C., Fernandez, Y., Bauer, J., Feaga, L., Wierzchos, K.: First Detection of CO₂ Emission in a Centaur: JWST NIRSpec Observations of 39P/Oterma. *The Planetary Science Journal* **4**(11), 208 (2023) <https://doi.org/10.3847/psj/acf928>
- Protopapa, S., Kelley, M.S.P., Yang, B., Bauer, J.M., Kolokolova, L., Woodward, C.E., Keane, J.V., Sunshine, J.M.: Icy Grains from the Nucleus of Comet C/2013 US₁₀ (Catalina). *Astrophys. J. Lett.* **862**(2), 16 (2018) <https://doi.org/10.3847/2041-8213/aad33b> arXiv:1807.08215 [astro-ph.EP]
- Phillips, E., Lee, L.C., Judge, D.L.: Absolute photoabsorption cross sections for H₂O and D₂O from lambda 180-790 Å. *J. Quantit. Spec. Rad. Trans.* **18**, 309–313 (1977) [https://doi.org/10.1016/0022-4073\(77\)90061-9](https://doi.org/10.1016/0022-4073(77)90061-9)
- Plainaki, C., Milillo, A., Mura, A., Orsini, S., Cassidy, T.: Neutral particle release from Europa’s surface. *Icarus* **210**(1), 385–395 (2010) <https://doi.org/10.1016/j.icarus.2010.06.041> arXiv:0911.4602 [astro-ph.EP]
- Plainaki, C., Milillo, A., Mura, A., Orsini, S., Massetti, S.: Exospheric o₂ at europa: The result of radiolytic, thermal, and ion-sputtering processes. *Planetary and Space Science* **88**, 42–52 (2012) <https://doi.org/10.1016/j.pss.2013.07.011>
- Parhi, A., Prialnik, D.: Combined Orbital and Thermal Evolution of Oort Cloud Comets. arXiv e-prints, 2510–26549 (2025) <https://doi.org/10.48550/arXiv.2510.26549> arXiv:2510.26549 [astro-ph.EP]
- Planes, M.B., Parisi, M.G., Millán, E.N., Bringa, E.M., Cañada-Assandri, M.: Dust-dust collisions in cometary comas: applications to comet 67P/Churyumov-Gerasimenko. *Monthly Notices of the Royal Astronomical Society* **531**, 3168–3186 (2024) <https://doi.org/10.1093/mnras/stae1078> . Publisher: OUP ADS Bibcode: 2024MNRAS.531.3168P. Accessed 2024-10-16
- Pitjeva, E.V., Pitjev, N.P., Pavlov, D.A., Turygin, C.C.: Estimates of the change rate of solar mass and gravitational constant based on the dynamics of the Solar System. *Astronomy & Astrophysics* **647**, 141 (2021) <https://doi.org/10.1051/0004-6361/202039893> 2201.09804
- Pham, D., Rein, H.: Polluting white dwarfs with Oort cloud comets. *Mon. Not. Roy. Astron. Soc.* **530**(3), 2526–2547 (2024) <https://doi.org/10.1093/mnras/stae986>

arXiv:2404.07160 [astro-ph.EP]

- Preston, G.W.: The spectrum of Ikeya-Seki (1965f). *Astrophys. J.* **147**, 718–742 (1967) <https://doi.org/10.1086/149049>
- Povich, M.S., Raymond, J.C., Jones, G.H., Uzzo, M., Ko, Y.-K., Feldman, P.D., Smith, P.L., Marsden, B.G., Woods, T.N.: Doubly Ionized Carbon Observed in the Plasma Tail of Comet Kudo-Fujikawa. *Science* **302**(5652), 1949–1952 (2003) <https://doi.org/10.1126/science.1092142>
- Probstein, R.: in *Problems of Hydrodynamics and Continuum Mechanics*, (1969)
- Pokorný, P., Sarantos, M., Janches, D.: A Comprehensive Model of the Meteoroid Environment around Mercury. *The Astrophysical Journal* **863**(1), 31 (2018) <https://doi.org/10.3847/1538-4357/aad051> 1807.02749
- Parkinson, W.H., Yoshino, K.: Absorption cross-section measurements of water vapor in the wavelength region 181–199 nm. *Chemical Physics* **294**(1), 31–35 (2003) [https://doi.org/10.1016/S0301-0104\(03\)00361-6](https://doi.org/10.1016/S0301-0104(03)00361-6)
- Rafikov, R.R.: Metal Accretion onto White Dwarfs Caused by Poynting-Robertson Drag on their Debris Disks. *Astrophys. J. Lett.* **732**(1), 3 (2011) <https://doi.org/10.1088/2041-8205/732/1/L3> arXiv:1102.3153 [astro-ph.EP]
- Rubin, M., Bekaert, D.V., Broadley, M.W., Drozdovskaya, M.N., Wampfler, S.F.: Volatile Species in Comet 67P/Churyumov-Gerasimenko: Investigating the Link from the ISM to the Terrestrial Planets. Technical report (August 2019). [message: %3C04697064-9816-46EE-B2DC-1949694A9119@gmail.com%3E](mailto:%3C04697064-9816-46EE-B2DC-1949694A9119@gmail.com%3E) Accessed 0
- Rodgers, S.D., Charnley, S.B., Huebner, W.F., Boice, D.C.: Physical processes and chemical reactions in cometary comae. In: Festou, M.C., Keller, H.U., Weaver, H.A. (eds.) *Comets II*, p. 505 (2004)
- Rebollido, I.: Exocomets: A study of the gaseous environment of A-type main sequence stars. PhD thesis, Autonomous University of Madrid, Spain (January 2020)
- Roberge, A., Feldman, P.D., Lagrange, A.M., Vidal-Madjar, A., Ferlet, R., Jolly, A., Lemaire, J.L., Rostas, F.: High-Resolution Hubble Space Telescope STIS Spectra of C I and CO in the β Pictoris Circumstellar Disk. *Astrophys. J.* **538**(2), 904–910 (2000) <https://doi.org/10.1086/309157> arXiv:astro-ph/0003446 [astro-ph]
- Rieke, G.H., Gáspár, A., Ballering, N.P.: Magnetic grain trapping and the hot excesses around early-type stars. *Astrophys. J.* **816**(2), 50 (2016) <https://doi.org/10.3847/0004-637X/816/2/50> arXiv:1511.04998 [astro-ph.EP]
- Raddi, R., Gänsicke, B.T., Koester, D., Farihi, J., Hermes, J.J., Scaringi, S., Breedt, E., Girven, J.: Likely detection of water-rich asteroid debris in a metal-polluted

- white dwarf. *Mon. Not. Roy. Astron. Soc.* **450**(2), 2083–2093 (2015) <https://doi.org/10.1093/mnras/stv701> arXiv:1503.07864 [astro-ph.SR]
- Rappaport, S., Gary, B.L., Kaye, T., Vanderburg, A., Croll, B., Benni, P., Foote, J.: Drifting asteroid fragments around WD 1145+017. *Monthly Notices of the Royal Astronomical Society* **458**, 3904–3917 (2016) <https://doi.org/10.1093/mnras/stw612> . Publisher: OUP ADS Bibcode: 2016MNRAS.458.3904R. Accessed 2024-09-03
- Raymond, J.C., Giordano, S., Mancuso, S., Povich, M.S., Bemporad, A.: Ultraviolet Observations of Comet 96/P Machholz at Perihelion. *Astrophys. J.* **926**(1), 93 (2022) <https://doi.org/10.3847/1538-4357/ac3cbd> arXiv:2111.15644 [astro-ph.EP]
- Rickman, H.: Cometary Dynamics. In: Souchay, J., Dvorak, R. (eds.) *Lecture Notes in Physics*, Berlin Springer Verlag vol. 790, pp. 341–399 (2010). https://doi.org/10.1007/978-3-642-04458-8_7
- Ragot, B.R., Kahler, S.W.: Interactions of Dust Grains with Coronal Mass Ejections and Solar Cycle Variations of the F-Coronal Brightness. *Astrophys. J.* **594**(2), 1049–1059 (2003) <https://doi.org/10.1086/377076>
- Rebollido, I., Stark, C.C., Kammerer, J., Perrin, M.D., Lawson, K., Pueyo, L., Chen, C., Hines, D., Girard, J.H., Worthen, K., Ingerbretsen, C., Betti, S., Clampin, M., Golimowski, D., Hoch, K., Lewis, N.K., Lu, C.X., van der Marel, R.P., Rickman, E., Seager, S., Soummer, R., Valenti, J.A., Ward-Duong, K., Mountain, C.M.: JWST-TST High Contrast: Asymmetries, Dust Populations, and Hints of a Collision in the β Pictoris Disk with NIRCcam and MIRI. *Astron. J.* **167**(2), 69 (2024) <https://doi.org/10.3847/1538-3881/ad1759> arXiv:2401.05271 [astro-ph.EP]
- Rappaport, S., Vanderburg, A., Jacobs, T., LaCourse, D., Jenkins, J., Kraus, A., Rizzuto, A., Latham, D.W., Bieryla, A., Lazarevic, M., Schmitt, A.: Likely transiting exocomets detected by Kepler. *Mon. Not. Roy. Astron. Soc.* **474**(2), 1453–1468 (2018) <https://doi.org/10.1093/mnras/stx2735> arXiv:1708.06069 [astro-ph.EP]
- Reach, W.T., Vaubaillon, J., Kelley, M.S., Lisse, C.M., Sykes, M.V.: Distribution and properties of fragments and debris from the split Comet 73P/Schwassmann-Wachmann 3 as revealed by *Spitzer* Space Telescope. *Icarus* **203**(2), 571–588 (2009) <https://doi.org/10.1016/j.icarus.2009.05.027> . Accessed 2025-03-05
- Sezestre, É., Augereau, J.-C., Thébault, P.: Hot exozodiacal dust: an exocometary origin? *Astron. Astrophys.* **626**, 2 (2019) <https://doi.org/10.1051/0004-6361/201935250> arXiv:1903.06130 [astro-ph.EP]
- Saki, M., Bodewits, D., Bonev, B.P., Russo, N.D., Luspay-Kuti, A., Noonan, J.W., Combi, M.R., Shou, Y.: Parent Volatile Outgassing Associations in Cometary Nuclei: Synthesizing Rosetta Measurements and Ground-based Observations. *The Planetary Science Journal* **5**(3), 70 (2024) <https://doi.org/10.3847/psj/ad118f>

- Schleicher, D.G., Birch, P.V., Farnham, T.L., Bair, A.N.: The Extreme Activity in Comet Hale-Bopp (C/1995 O1): Investigations of Extensive, Narrowband Photoelectric Photometry. arXiv e-prints, 2409–13005 (2024) <https://doi.org/10.48550/arXiv.2409.13005> arXiv:2409.13005 [astro-ph.EP]
- Shi, J., Baragiola, R.A., Grosjean, D.E., Johnson, R.E.: Sputtering of water ice surfaces and the production of extended atmospheres. *Journal of Geophysical Research: Planets* **100**, 26387–26395 (1995) <https://doi.org/10.1029/95JE02822>
- Strøm, P.A., Bodewits, D., Knight, M.M., Kiefer, F., Jones, G.H., Kral, Q., Matrà, L., Bodman, E., Capria, M.T., Cleaves, I., Fitzsimmons, A., Haghhighipour, N., Harrison, J.H.D., Iglesias, D., Kama, M., Linnartz, H., Majumdar, L., de Mooij, E.J.W., Milam, S.N., Opitom, C., Rebollido, I., Rogers, L.K., Snodgrass, C., Sousa-Silva, C., Xu, S., Lin, Z.-Y., Zieba, S.: Exocomets from a Solar System Perspective. *Publ. Astron. Soc. Pac.* **132**(1016), 101001 (2020) <https://doi.org/10.1088/1538-3873/aba6a0> arXiv:2007.09155 [astro-ph.EP]
- Sekanina, Z., Chodas, P.W.: Comet C/2011 W3 (Lovejoy): Orbit Determination, Outbursts, Disintegration of Nucleus, Dust-tail Morphology, and Relationship to New Cluster of Bright Sungrazers. *The Astrophysical Journal* **757**, 127 (2012) <https://doi.org/10.1088/0004-637X/757/2/127> . Publisher: IOP ADS Bibcode: 2012ApJ...757..127S. Accessed 2024-05-03
- Sekanina, Z., Chodas, P.W., Yeomans, D.K.: Tidal disruption and the appearance of periodic comet Shoemaker-Levy 9. *Astron. Astrophys.* **289**, 607–636 (1994)
- Steckloff, J.K., Debes, J., Steele, A., Johnson, B., Adams, E.R., Jacobson, S.A., Springmann, A.: How Sublimation Delays the Onset of Dusty Debris Disk Formation around White Dwarf Stars. *Astrophys. J. Lett.* **913**(2), 31 (2021) <https://doi.org/10.3847/2041-8213/abfd39> arXiv:2104.14035 [astro-ph.EP]
- Swings, P., Elvey, C.T., Babcock, H.W.: The Spectrum of Comet Cunningham, 1940C. *Astrophys. J.* **94**, 320 (1941) <https://doi.org/10.1086/144336>
- Sekanina, Z.: Statistical Investigation and Modeling of Sungrazing Comets Discovered with the Solar and Heliospheric Observatory. *Astrophys. J.* **566**(1), 577–598 (2002) <https://doi.org/10.1086/324335>
- Sekanina, Z.: Erosion Model for the Sungrazing Comets Observed with the Solar and Heliospheric Observatory. *Astrophys. J.* **597**(2), 1237–1265 (2003) <https://doi.org/10.1086/378192>
- Schambeau, C.A., Fernández, Y.R., Lisse, C.M., Samarasinha, N., Woodney, L.M.: A new analysis of Spitzer observations of Comet 29P/Schwassmann-Wachmann 1. *Icarus* **260**, 60–72 (2015) <https://doi.org/10.1016/j.icarus.2015.06.038> arXiv:1506.07037 [astro-ph.EP]

- Snodgrass, C., Holt, C.E., Kelley, M.S.P., Opitom, C., Guilbert-Lepoutre, A., Knight, M.M., Kokotanekova, R., Jehin, E., Mazzotta Epifani, E., Migliorini, A., Tubiana, C., Micheli, M., Farnocchia, D.: First JWST spectrum of distant activity in long-period comet C/2024 E1 (Wierzechos). *Mon. Not. Roy. Astron. Soc.* **541**(1), 8–13 (2025) <https://doi.org/10.1093/mnras/slaf046> arXiv:2503.14071 [astro-ph.EP]
- Sigmund, P.: Sputtering by ion bombardment: Theoretical concepts. *Sputtering by Particle Bombardment I*, Springer, Berlin, Heidelberg, 9–71 (1981) <https://doi.org/10.1007/3540111347>
- Su, K.Y.L., Jackson, A.P., Gáspár, A., Rieke, G.H., Dong, R., Olofsson, J., Kennedy, G.M., Leinhardt, Z.M., Malhotra, R., Hammer, M., Meng, H.Y.A., Rujopakarn, W., Rodriguez, J.E., Pepper, J., Reichart, D.E., James, D., Stassun, K.G.: Extreme Debris Disk Variability: Exploring the Diverse Outcomes of Large Asteroid Impacts During the Era of Terrestrial Planet Formation. *Astron. J.* **157**(5), 202 (2019) <https://doi.org/10.3847/1538-3881/ab1260> arXiv:1903.10627 [astro-ph.EP]
- Szabó, G.M., Kiss, L.L., Pál, A., Kiss, C., Sárneczky, K., Juhász, A., Hogerheijde, M.R.: Evidence for Fresh Frost Layer on the Bare Nucleus of Comet Hale-Bopp at 32 AU Distance. *Astrophys. J.* **761**(1), 8 (2012) <https://doi.org/10.1088/0004-637X/761/1/8> arXiv:1210.2785 [astro-ph.EP]
- Shestakova, L.I., Kenzhebekova, A.I., Serebryanskiy, A.V.: On survival of dust grains in the sublimation zone of cold white dwarfs. *Mon. Not. Roy. Astron. Soc.* **514**(1), 997–1005 (2022) <https://doi.org/10.1093/mnras/stac1405>
- Spinrad, H., Miner, E.D.: Sodium velocity fields in Comet 1965f. *Astrophys. J.* **153**, 355–366 (1968) <https://doi.org/10.1086/149672>
- Schleicher, D.G., Millis, R.L., Birch, P.V.: Narrowband Photometry of Comet P/Halley: Variation with Heliocentric Distance, Season, and Solar Phase Angle. *Icarus* **132**(2), 397–417 (1998) <https://doi.org/10.1006/icar.1997.5902> . Accessed 2024-10-31
- Strom, R.G., Malhotra, R., Ito, T., Yoshida, F., Kring, D.A.: The Origin of Planetary Impactors in the Inner Solar System. *Science* **309**(5742), 1847–1850 (2005) <https://doi.org/10.1126/science.1113544> arXiv:astro-ph/0510200 [astro-ph]
- Szalay, J.R., Poppe, A.R., Agarwal, J., Britt, D., Belskaya, I., Horányi, M., Nakamura, T., Sachse, M., Spahn, F.: Dust Phenomena Relating to Airless Bodies. *Space Sci. Rev.* **214**(5), 98 (2018) <https://doi.org/10.1007/s11214-018-0527-0>
- Seligman, D.Z., Rogers, L.A., Cabot, S.H.C., Noonan, J.W., Kareta, T., Mandt, K.E., Ciesla, F., McKay, A., Feinstein, A.D., Levine, W.G., Bean, J.L., Nordlander, T., Krumholz, M.R., Mansfield, M., Hoover, D.J., Van Clepper, E.: The Volatile Carbon-to-oxygen Ratio as a Tracer for the Formation Locations of Interstellar Comets. *Planet. Sci. J.* **3**(7), 150 (2022) <https://doi.org/10.3847/PSJ/ac75b5>

- [arXiv:2204.13211](https://arxiv.org/abs/2204.13211) [astro-ph.EP]
- Strom, R.G., Renu, M., Xiao, Z.-Y., Ito, T., Yoshida, F., Ostrach, L.R.: The inner solar system cratering record and the evolution of impactor populations. *Research in Astronomy and Astrophysics* **15**(3), 407 (2015) <https://doi.org/10.1088/1674-4527/15/3/009> [arXiv:1407.4521](https://arxiv.org/abs/1407.4521) [astro-ph.EP]
- Stern, S.A.: The lunar atmosphere: History, status, current problems, and context. *Reviews of Geophysics* **37**(4), 453–491 (1999) <https://doi.org/10.1029/1999RG900005>
- Shull, J.M., van Steenberg, M.: The ionization equilibrium of astrophysically abundant elements. *Astrophys. J. Supp. Ser.* **48**, 95–107 (1982) <https://doi.org/10.1086/190769>
- Sarid, G., Volk, K., Steckloff, J.K., Harris, W., Womack, M., Woodney, L.M.: 29P/Schwassmann-Wachmann 1, A Centaur in the Gateway to the Jupiter-family Comets. *Astrophys. J. Lett.* **883**(1), 25 (2019) <https://doi.org/10.3847/2041-8213/ab3fb3> [arXiv:1908.04185](https://arxiv.org/abs/1908.04185) [astro-ph.EP]
- Steinmeyer, M.-L., Woitke, P., Johansen, A.: Sublimation of refractory minerals in the gas envelopes of accreting rocky planets. *Astron. Astrophys.* **677**, 181 (2023) <https://doi.org/10.1051/0004-6361/202245636> [arXiv:2308.05647](https://arxiv.org/abs/2308.05647) [astro-ph.EP]
- Tenishev, V., Combi, M.R., Rubin, M.: NUMERICAL SIMULATION OF DUST IN A COMETARY COMA: APPLICATION TO COMET 67P/CHURYUMOV-GERASIMENKO. *The Astrophysical Journal* **732**(2), 104 (2011) <https://doi.org/10.1088/0004-637X/732/2/104> . Publisher: The American Astronomical Society. Accessed 2024-11-01
- Tielens, A.G.G.M.: *The Physics and Chemistry of the Interstellar Medium*. Cambridge University Press, ??? (2005). <https://doi.org/10.1017/CBO9780511810076>
- Veras, D., Birader, Y., Zaman, U.: Orbit decay of 2-100 au planetary remnants around white dwarfs with no gravitational assistance from planets. *Mon. Not. Roy. Astron. Soc.* **510**(3), 3379–3388 (2022) <https://doi.org/10.1093/mnras/stab3490> [arXiv:2111.13713](https://arxiv.org/abs/2111.13713) [astro-ph.EP]
- Veras, D., Carter, P.J., Leinhardt, Z.M., Gänsicke, B.T.: Explaining the variability of WD 1145+017 with simulations of asteroid tidal disruption. *Mon. Not. Roy. Astron. Soc.* **465**(1), 1008–1022 (2017) <https://doi.org/10.1093/mnras/stw2748> [arXiv:1610.06926](https://arxiv.org/abs/1610.06926) [astro-ph.EP]
- Vidotto, A.A.: The evolution of the solar wind. *Living Reviews in Solar Physics* **18**(1), 3 (2021) <https://doi.org/10.1007/s41116-021-00029-w> [arXiv:2103.15748](https://arxiv.org/abs/2103.15748) [astro-ph.SR]

- Vanderburg, A., Johnson, J.A., Rappaport, S., Bieryla, A., Irwin, J., Lewis, J.A., Kipping, D., Brown, W.R., Dufour, P., Ciardi, D.R., Angus, R., Schaefer, L., Latham, D.W., Charbonneau, D., Beichman, C., Eastman, J., McCrady, N., Wittenmyer, R.A., Wright, J.T.: A disintegrating minor planet transiting a white dwarf. *Nature* **526**(7574), 546–549 (2015) <https://doi.org/10.1038/nature15527> arXiv:1510.06387 [astro-ph.EP]
- Vignaud, T., Lecavelier des Etangs, A.: Population of excited levels of Fe+, Ni+ and Cr+ in exocomets gaseous tails. arXiv e-prints, 2409–15247 (2024) <https://doi.org/10.48550/arXiv.2409.15247> arXiv:2409.15247 [astro-ph.EP]
- Vignaud, T., Lecavelier des Etangs, A., Hebrard, G., Kiefer, F., Strom, P.A., Vidal-Madjar, A.: The C/Fe and dust-to-ice ratios in Beta Pictoris exocomets. HST Proposal. Cycle 32, ID. #17790 (2024)
- Vignaud, T., Lecavelier des Etangs, A., Kiefer, F., Lagrange, A.-M., Hébrard, G., Strøm, P.A., Vidal-Madjar, A.: Curves of growth for transiting exocomets: Application to Fe II lines in the β Pictoris system. *Astron. Astrophys.* **684**, 210 (2024) <https://doi.org/10.1051/0004-6361/202347588> arXiv:2402.10169 [astro-ph.EP]
- Vignaud, T., Lecavelier des Etangs, A., Strøm, P.A., Kiefer, F.: Abundances of refractory ions in Beta Pictoris exocomets. *Astron. Astrophys.* **697**, 21 (2025) <https://doi.org/10.1051/0004-6361/202453568> arXiv:2503.17346 [astro-ph.EP]
- van Lieshout, R., Min, M., Dominik, C.: Dusty tails of evaporating exoplanets. I. Constraints on the dust composition. *Astron. Astrophys.* **572**, 76 (2014) <https://doi.org/10.1051/0004-6361/201424876> arXiv:1410.3494 [astro-ph.EP]
- Veras, D., Shannon, A., Gänsicke, B.T.: Hydrogen delivery onto white dwarfs from remnant exo-Oort cloud comets. *Mon. Not. Roy. Astron. Soc.* **445**(4), 4175–4185 (2014) <https://doi.org/10.1093/mnras/stu2026> arXiv:1409.7691 [astro-ph.SR]
- Vorburger, A., Wurz, P., Barabash, S.e.a.: Energetic neutral atom imaging of surface sputtering on the moon. *Journal of Geophysical Research: Planets* **117** (2012) <https://doi.org/10.1029/2011JE004092>
- Woods, T.N., Chamberlin, P.C., Harder, J.W., Hock, R.A., Snow, M., Eparvier, F.G., Fontenla, J., McClintock, W.E., Richard, E.C.: Solar Irradiance Reference Spectra (SIRS) for the 2008 Whole Heliosphere Interval (WHI). *Geophys. Res. Lett.* **36**(1), 01101 (2009) <https://doi.org/10.1029/2008GL036373>
- Womack, M., Curtis, O., Rabson, D.A., Harrington Pinto, O., Wierzchos, K., Cruz Gonzalez, S., Sarid, G., Mentzer, C., Lastra, N., Pichette, N., Ruffini, N., Cox, T., Rivera, I., Micciche, A., Jackson, C., Homich, A., Tollison, A., Reed, S., Zilka, J., Henning, B., Spinar, M., Escoto, S.R., Erdahl, T., Goldschen-Ohm, M.P., Uhl, W.T.: The Visual Lightcurve of Comet C/1995 O1 (Hale-Bopp) from 1995 to 1999. *Planet. Sci. J.* **2**(1), 17 (2021) <https://doi.org/10.3847/PSJ/abd32c>

[arXiv:2008.06761](https://arxiv.org/abs/2008.06761) [astro-ph.EP]

- Wetherill, G.W.: Late heavy bombardment of the moon and terrestrial planets. Lunar and Planetary Science Conference Proceedings **2**, 1539–1561 (1975)
- Weaver, H.A., Feldman, P.D., A’Hearn, M.F., Arpigny, C., Brown, R.A., Helin, E.F., Levy, D.H., Marsden, B.G., Meech, K.J., Larson, S.M., Noll, K.S., Scotti, J.V., Sekanina, Z., Shoemaker, C.S., Shoemaker, E.M., Smith, T.E., Storrs, A.D., Yeomans, D.K., Zellner, B.: Hubble Space Telescope Observations of Comet P/Shoemaker-Levy 9 (1993e). *Science* **263**(5148), 787–791 (1994) <https://doi.org/10.1126/science.263.5148.787>
- Wurz, P., Fatemi, S., Galli, A., Halekas, J., Harada, Y., Jäggi, N., Jasinski, J., Lammer, H., Lindsay, S., Nishino, M.N., Orlando, T.M., Raines, J.M., Scherf, M., Slavin, J., Vorburger, A., Winslow, R.: Particles and Photons as Drivers for Particle Release from the Surfaces of the Moon and Mercury. *Space Science Reviews* **218**(3), 10 (2022) <https://doi.org/10.1007/s11214-022-00875-6>
- Williams, J., Gaensicke, B., Swan, A., O’Brien, M., Izquierdo, P., Cutolo, A.-M., Cunningham, T.: PEWDD: A database of white dwarfs enriched by exo-planetary material. arXiv e-prints, 2409–16046 (2024) <https://doi.org/10.48550/arXiv.2409.16046> [arXiv:2409.16046](https://arxiv.org/abs/2409.16046) [astro-ph.EP]
- Welsh, B.Y., Montgomery, S.: Exocomet Circumstellar Fe I Absorption in the Beta Pictoris Gas Disk. *Publ. Astron. Soc. Pac.* **128**(964), 064201 (2016) <https://doi.org/10.1088/1538-3873/128/964/064201>
- Wittrock, J.M., Plavchan, P.P., Cale, B.L., Barclay, T., Ludwig, M.R., Schwarz, R.P., Mékarnia, D., Triaud, A.H.M.J., Abe, L., Suarez, O., Guillot, T., Conti, D.M., Collins, K.A., Waite, I.A., Kielkopf, J.F., Collins, K.I., Dreizler, S., El Mufti, M., Feliz, D.L., Gaidos, E., Geneser, C.S., Horne, K.D., Kane, S.R., Lowrance, P.J., Martioli, E., Radford, D.J., Reefe, M.A., Roccagliata, V., Shporer, A., Stassun, K.G., Stockdale, C., Tan, T.-G., Tanner, A.M., Vega, L.D.: Validating AU Microscopii d with Transit Timing Variations. *Astron. J.* **166**(6), 232 (2023) <https://doi.org/10.3847/1538-3881/acfda8> [arXiv:2302.04922](https://arxiv.org/abs/2302.04922) [astro-ph.EP]
- Wyatt, M.C., Smith, R., Su, K.Y.L., Rieke, G.H., Greaves, J.S., Beichman, C.A., Bryden, G.: Steady State Evolution of Debris Disks around A Stars. *Astrophys. J.* **663**(1), 365–382 (2007) <https://doi.org/10.1086/518404> [arXiv:astro-ph/0703608](https://arxiv.org/abs/astro-ph/0703608) [astro-ph]
- Wyatt, S.P., Whipple, F.L.: The Poynting-Robertson effect on meteor orbits. *Astrophys. J.* **111**, 134–141 (1950) <https://doi.org/10.1086/145244>
- Welsh, B.Y., Wheatley, J., Browne, S.E., Siegmund, O.H.W., Doyle, J.G., O’Shea, E., Antonova, A., Forster, K., Seibert, M., Morrissey, P., Taroyan, Y.: GALEX high time-resolution ultraviolet observations of dMe flare events. *Astron. Astrophys.*

- 458(3), 921–930 (2006) <https://doi.org/10.1051/0004-6361:20065304> arXiv:astro-ph/0608254 [astro-ph]
- Wu, Y., Worthen, K., Brandeker, A., Chen, C.: Argon in β Pictoris–Entrapment and Release of Volatile in Disks. *Astrophys. J.* **982**(2), 123 (2025) <https://doi.org/10.3847/1538-4357/ada287> arXiv:2407.06035 [astro-ph.EP]
- Wyatt, M.C.: Evolution of debris disks. *Annu. Rev. Astron. Astrophys.* **46**, 339–383 (2008) <https://doi.org/10.1146/annurev.astro.45.051806.110525>
- Xu, S., Rogers, L.K., Blouin, S.: The chemistry of extra-solar materials from white dwarf planetary systems. arXiv e-prints, 2404–15425 (2024) <https://doi.org/10.48550/arXiv.2404.15425> arXiv:2404.15425 [astro-ph.EP]
- Xu, S., Rappaport, S., van Lieshout, R., Vanderburg, A., Gary, B., Hallakoun, N., Ivanov, V.D., Wyatt, M.C., DeVore, J., Bayliss, D., Bento, J., Bieryla, A., Cameron, A., Cann, J.M., Croll, B., Collins, K.A., Dalba, P.A., Debes, J., Doyle, D., Dufour, P., Ely, J., Espinoza, N., Joner, M.D., Jura, M., Kaye, T., McClain, J.L., Muirhead, P., Palle, E., Panka, P.A., Provencal, J., Randall, S., Rodriguez, J.E., Scarborough, J., Sefako, R., Shporer, A., Strickland, W., Zhou, G., Zuckerman, B.: A dearth of small particles in the transiting material around the white dwarf WD 1145+017. *Mon. Not. Roy. Astron. Soc.* **474**(4), 4795–4809 (2018) <https://doi.org/10.1093/mnras/stx3023> arXiv:1711.06960 [astro-ph.EP]
- Xu, S., Zuckerman, B., Dufour, P., Young, E.D., Klein, B., Jura, M.: The Chemical Composition of an Extrasolar Kuiper-Belt-Object. *Astrophys. J. Lett.* **836**(1), 7 (2017) <https://doi.org/10.3847/2041-8213/836/1/L7> arXiv:1702.02868 [astro-ph.EP]
- Yakshinskiy, B.V., Madey, T.E.: Photon-stimulated desorption as a substantial source of sodium in the lunar atmosphere. *Nature* **400**(6745), 642–644 (1999) <https://doi.org/10.1038/23204>
- Yakshinskiy, B.V., Madey, T.E.: Desorption induced by electronic transitions of Na from SiO₂: relevance to tenuous planetary atmospheres. *Surface Science* **451**(1-3), 160–165 (2000) [https://doi.org/10.1016/s0039-6028\(00\)00022-4](https://doi.org/10.1016/s0039-6028(00)00022-4)
- Zicher, N., Barragán, O., Klein, B., Aigrain, S., Owen, J.E., Gandolfi, D., Lagrange, A.-M., Serrano, L.M., Kaye, L., Nielsen, L.D., Rajpaul, V.M., Grandjean, A., Goffo, E., Nicholson, B.: One year of AU Mic with HARPS - I. Measuring the masses of the two transiting planets. *Monthly Notices of the Royal Astronomical Society* **512**, 3060–3078 (2022) <https://doi.org/10.1093/mnras/stac614> . ADS Bibcode: 2022MNRAS.512.3060Z. Accessed 2024-03-20
- Zhang, Q., Battams, K., Ye, Q., Knight, M.M., Schmidt, C.A.: Sodium Brightening of (3200) Phaethon near Perihelion. *The Planetary Science Journal* **4**(4), 70 (2023) <https://doi.org/10.3847/psj/acc866> 2303.17625

- Zhang, Q., Bhattams, K., Ye, Q., Knight, M.M., Schmidt, C.A.: Sodium Brightening of (3200) Phaethon near Perihelion. *Planet. Sci. J.* **4**(4), 70 (2023) <https://doi.org/10.3847/PSJ/acc866> arXiv:2303.17625 [astro-ph.EP]
- Zwintz, K., Reese, D.R., Neiner, C., Pigulski, A., Kuschnig, R., Müllner, M., Zieba, S., Abe, L., Guillot, T., Handler, G., Kenworthy, M., Stuik, R., Moffat, A.F.J., Popowicz, A., Rucinski, S.M., Wade, G.A., Weiss, W.W., Bailey, J.I., Crawford, S., Ireland, M., Lomberg, B., Mamajek, E.E., Mellon, S.N., Talens, G.J.: Revisiting the pulsational characteristics of the exoplanet host star beta Pictoris. *Astronomy and Astrophysics* **627**, 28 (2019) <https://doi.org/10.1051/0004-6361/201834744> . ADS Bibcode: 2019A&A...627A..28Z. Accessed 2025-01-13
- Zieba, S., Zwintz, K., Kenworthy, M.A., Kennedy, G.M.: Transiting exocomets detected in broadband light by TESS in the β Pictoris system. *Astron. Astrophys.* **625**, 13 (2019) <https://doi.org/10.1051/0004-6361/201935552> arXiv:1903.11071 [astro-ph.SR]